6-1998

Image Processing Based on a Fuzzy Logic Edge Detection Algorithm

Jamshid Khazaai
Western Michigan University

IMAGE PROCESSING BASED ON A FUZZY LOGIC EDGE DETECTION ALGORITHM

by

Jamshid Khazaai

A Thesis
Submitted to the
Faculty of The Graduate College
in partial fulfillment of the
requirements for the
Degree of Master of Science
Department of Electrical and Computer Engineering

Western Michigan University
Kalamazoo, Michigan
June 1998

ACKNOWLEDGEMENTS

A special note of gratitude is extended to my major thesis advisor, Dr. Frank Severance, for his continuous guidance and support throughout this project. I could not finish this work without his significant helps. I also wish to acknowledge my committee members Dr. Hossein Mousavinezhad and Dr. John Kapenga for their encouragement and taking the time to review my work.

Also, this task would not have been completed without the helps of my friends, Ann Schwindner and Ramin Monajemi for editing and providing me with a large number of articles and references.

Jamshid Khazaai

IMAGE PROCESSING BASED ON A FUZZY LOGIC EDGE DETECTION ALGORITHM

Jamshid Khazaai, M.S.E.

Western Michigan University, 1998

One of the major problems in image processing is that of efficient edge detection. This is because the automated determination of an edge requires a subjective interpretation of just what the image author intended to be an edge. By training an edge determination algorithm to be sensitive to edges in a consistent manner, efficiency can be improved. This is the central idea of this thesis in which I define edge occurrences for the intensity (monochrome) images using fuzzy sets.

Edge characteristic functions are proposed for detecting edge pixels within a desired block of an (intensity and binary) image based on quadruple child windowing and binary edge patterns. I called these functions *QCW-ECF*. Fuzzy theory has been also applied to extend the *QCW-ECF* algorithm to the *FQCW-ECF* algorithm for edge detection within a block of a fuzzy intensity image. The *(F)QCW-ECF* results in a degree of edginess concerning the middle pixel of the processing block.

Cyclic coordinate algorithm is adopted to minimize the desired performance index of the Edge Detector System (*EDS*) by tuning the input/output membership functions of the Fuzzy Logic Controller (*FLC*). This is an optimization applied to the *FQCW-ECF* algorithm of edge detection. Finally, I have all the methods simulated against classical methods. The result are very promising.

TABLE OF CONTENTS

CHAPTER

CHAPTER

CHAPTER

Table of Contents-Continued

LIST OF TABLES

LIST OF FIGURES

List of Figures-Continued

CHAPTER I

INTRODUCTION

1.1 Introduction

Edge extraction is the most significant image enhancing technique. It is a fundamental step in segmentation, object identification and motion estimation [2]. Most edge detection algorithms are implemented using block processing technique in the spatial domain by manipulation of the intensity value of each pixel and its neighborhood within a certain block of size $W \times W$ pixels. Edge detectors find edges in an intensity image by detecting pixels where the intensity values change abruptly. Using algorithms based on derivative methods, edge detection is accomplished by comparing the first derivative of the intensity to a threshold, or by checking the second derivative for a zero crossing.

Most derivative edge extraction techniques such as Sobel, Roberts, Prewitt, and Wallis methods are limited to making some non-linear manipulation of pixels over a 2×2 or 3×3 block as a means of edge enhancement before thresholding. All these mentioned methods possess the disadvantage of sensitivity to noise and dependency on the size of the block. The Roberts algorithm is sensitive to diagonal edges. The Sobel algorithm is sensitive to horizontal and vertical edges. But the edge characteristic functions based on quadruple child windowing, *QCW-ECF,* which I

introduce here, are sensitive to diagonal, vertical and horizontal edges. This follows since the generalized *QCW-ECF* is defined according to possible edge patterns illustrated in Figures 26 and 27 on pages 67 and 68. One major problem in edge detection is finding the edge in intensity images at those pixels which have the same intensity with the background [9].

Also another problem in edge extraction is that, for many cases, the intensity edge techniques depend on the appropriate choice of thresholds. I have found that Edge detection algorithms based on fuzzy logic with tunable membership functions are an effective approach to address the above mentioned problems. The *FQCW-ECF* which will be introduced here is an effective tool in fuzzy image processing for edge detection. Further, *QCW-ECF* and its fuzzy extension *FQCW-ECF* are flexible and can be applied for any desired size of block. Their sensitivities to noises are very low.

1.2 Image Processing

The term image processing generally refers to improving the visual appearance of the images or preparing the images for measurement of the features and structures present. Edge detection, which is the main part of this paper, is generally considered as a process of image feature extraction. Image processing can be generally categorized into two domains, one in frequency domain involved with the Fourier transform of images and another in the spatial domain which deals with manipulation of pixels and their neighborhoods .

1.2.1 Image Definition and Modeling

In an image processing system, the image is mathematically characterized as a deterministic or statistical model [2]. In a deterministic model, the image is functionally defined by pixel properties, such as the sum of two dimensional orthogonal functions called basis images. In a statistical model, the image is defined by statistical properties of pixels, such as mean and covariance functions.

Generally any two or higher dimensional function which carries information can be considered an image. Images can be either continuous or discrete. The continuous one is presented as a n-dimensional function $f(X_1, X_2, \ldots, X_n)$ where X_n is an independent variable and $n \geq 2$. Also a discrete image which is the result of sampling of a continuous image is represented by $f(K_1, K_2, \ldots, K_m)$ where $(K_1, K_2, \ldots, K_m)$ refers to the coordinates of a physical image pixel.

1.2.2 Digital Image Processing

Following the given definition of an image as a discrete n-dimensional function, digital image processing refers to processing of any 2-dimentional data. A digital image I of $M \times N$ dimension can be considered as an array of real or complex numbers represented by a finite number of bits [2].

In digital image processing systems, we usually deal with arrays of numbers obtained by spatially sampling points of a physical image. After processing, another array of numbers is produced and these numbers are then used to reconstruct a

continuous image for viewing. Thus, digital image processing is the sequence of digitizing (sampling and quantizing) and processing of digital data.

1.2.3 Intensity Images

A digital gray tone (monochrome) image *II* can be generally represented by a 2-dimentional intensity function $f(m,n)$ where (m,n) are the coordinates of an image pixel and $f(m,n)$ is the brightness value. A digital 2- dimensional image in spatial domain can be shown as a single $M \times N$ dimension matrix with L gray tone levels as

$$II = f(m,n) = \left[X_{mn}\right] \quad where \begin{cases} X_{mn} \in [0,1] \\ l \in \{1,2,\ldots,(L-1)\} \end{cases} \quad for \begin{cases} m = 1,2,\ldots,M \\ n = 1,2,\ldots,N \end{cases} \qquad (1.2.3-1)$$

Intensity image is represented by a single matrix of size $M \times N$ containing double precision values within continuum interval [0,1] and a crisp gray level l ranging from 0 to L-1, with L discrete gray levels. Each element of this matrix contains the information of one image pixel. The gray level of intensity *0* refers to black and L-1 refers to white , the highest intensity. A black and white photograph is the best example of intensity images.

The following 8×8 matrix *II* generated by the MATLAB image processing toolbox represents an intensity image $II = f(m,n)$ with L=16 gray levels. The normalized gray scale is considered as an intensity scale which is over the interval [0,1]. The intensity value 0 indicates the black (the gray level 0^{th}) and 1 corresponds to white (the gray level $(L\text{-}1)^{th}$). Consequently any intensity value within [0,1]

corresponds to the gray level $l \in \{0,1,...,L\text{-}1\}$. Figure 1 represents an physical intensity image, a ring. The relevant 8×8 matrix is processed in Chapter IV. This simple matrix which represents an intensity image of a ring is used as example of simulation further.

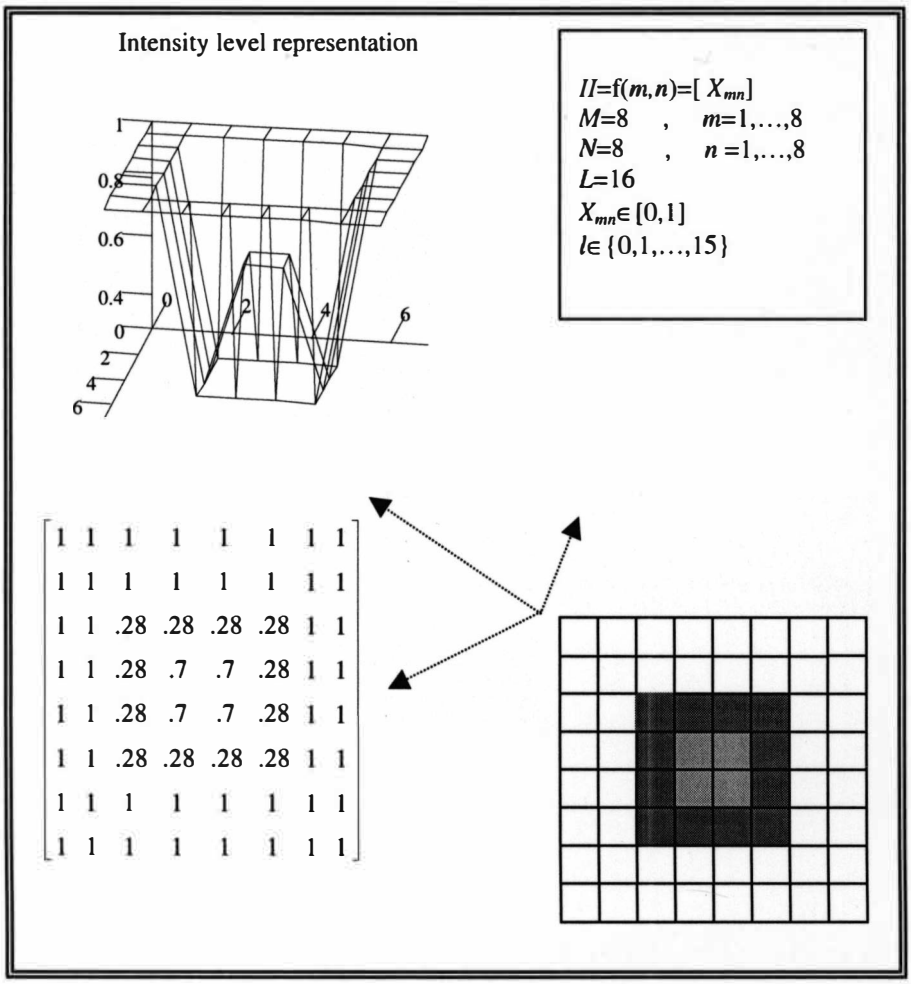

Figure 1. Illustrations of 8×8 Physical Image, 8×8 Image Matrix, and Intensity Levels.

1.2.4 Binary Images

A binary image can be considered as a special case of an intensity image. A binary image is a matrix $M \times N$ dimension with two levels, 0 (black) and 1 (white). Logical or Boolean matrices can be considered as binary images. We will see later that edge extraction from intensity image using threshold results in a binary image.

1.2.5 Enhancing Images

Image enhancement is the technique of processing an image to prepare it for further analysis or for monitoring [1]. Therefore, based on a specific application, some certain image features are accentuated for subsequent processing. Contrast stretching, smoothing and sharpening, edge extraction, noise filtering and magnifying are important image enhancing techniques.

Contrast stretching changes the intensity level of an image by mapping the gray level into another level using a single-valued transformation in order to increase the total dynamic range of gray levels. This, in turn, increases contrast.

Image smoothing is generally applied to reconstruct a noisy image. In the spatial domain, this is achieved by intensity modification of each pixel. In the frequency domain it is accomplished by applying a low pass filter, *LPF*. In this process each pixel and its neighborhood posses almost equal intensity.

Defocusing, Averaging (which is a *LPF*) and Max–Min rule algorithms are some techniques applied for the smoothing operation [1]. For example, the averaging method applied to remove the noise is based on averaging the neighboring intensities

of each pixel. If X_{mn} is the processing pixel, then the smoothed pixel X'_{mn} is computed based on N number of intensity values of neighborhoods within block B as

$$X'_{mn} = \frac{1}{N}\sum_{B} X_{ij} \qquad where \qquad (i,j) \in B - \{(m,n)\} \qquad (1.2.5-1)$$

1.2.6 Block Processing

Most algorithms of digital image processing in the spatial domain deal with modifying of an image matrix based on local algorithm. In other words, most algorithms in the spatial domain manipulate the intensity of each pixel by considering the intensities of the pixels only in immediate neighborhood. Since processing each of the $M \times N$ pixels serially is time consuming, block processing is desirable. Block processing is a suitable technique by which the image matrix is divided into some smaller matrix dimensions for processing, which can be done in parallel.

Block processing can be achieved by rectangular partitioning of whole matrix into a group of smaller matrices of $W \times W$ dimension with no component overlap or by sliding a rectangular window $W \times W$ dimension from left to right and top to bottom of an image pixel by pixel. In sliding block processing, the center pixel of the block is processed considering neighboring pixels based on an algorithm and finally replaced by the result of processing. The process is repeated pixel by pixel with its own proper $W \times W$ block until the whole image is covered.

1.2.7 Median Filtering

Median filter is a linear operation on neighboring pixels of the middle pixel in block B. Input of the filter is the intensity of the middle pixel and output is the computed intensity value from neighborhood B.

$$X'_{mn} = \underset{i,j}{median}\{X_{ij}\} \quad where \quad (i,j) \in B - \{(m,n)\} \qquad (1.2.7-1)$$

Median filtering orders the pixel values in a neighborhood and chooses the median value as the result. In this process the center pixel in the block is replaced by the median of the intensity values of neighborhoods within the block B with $W \times W$ dimension.

1.2.8 Noisy Image

Due to physical realities involved in image processing systems, there is always an additional unwanted signal, noise. For example [1], a general mathematical model for an Electro-Optical system can be expressed as

$$V(x,y) = g[w(x,y)] + n(x,y) \quad where \quad w(x,y)=h(u(x,y)) \qquad (1.2.8\text{-}1)$$

$V(x,y)$ represents the observed image, h is a linear operation on the original image $u(x,y)$ and g is a non-linear operation on w. The general model of additive noise denoted by $n(x,y)$ has application in many situations and defined as

$$n(x,y) = f[g[w(x,y)]] \cdot n_1(x,y) + n_2(x,y) \qquad (1.2.8\text{-}2)$$

Functions f and g are non-linear operation of decoder/recording mechanisms. First term of $n(x,y)$ is the image-dependent random noise and second term is independent random noise. Noise pixels distributed randomly over the image are the result of errors in image transmission and noisy components of the electronic systems. Two important types of noise are Gaussian noise with zero mean and *outliers*, extreme pixel intensity values. Median filtering is useful for removing *outliers* and Wiener filtering works best when the noise is a constant power additive noise such as Gaussian white noise.

1.2.9 Edge Definition

A pixel at which the intensity or gray level value changes abruptly is considered an edge pixel. Figure 2 illustrates one-dimensional edge model.

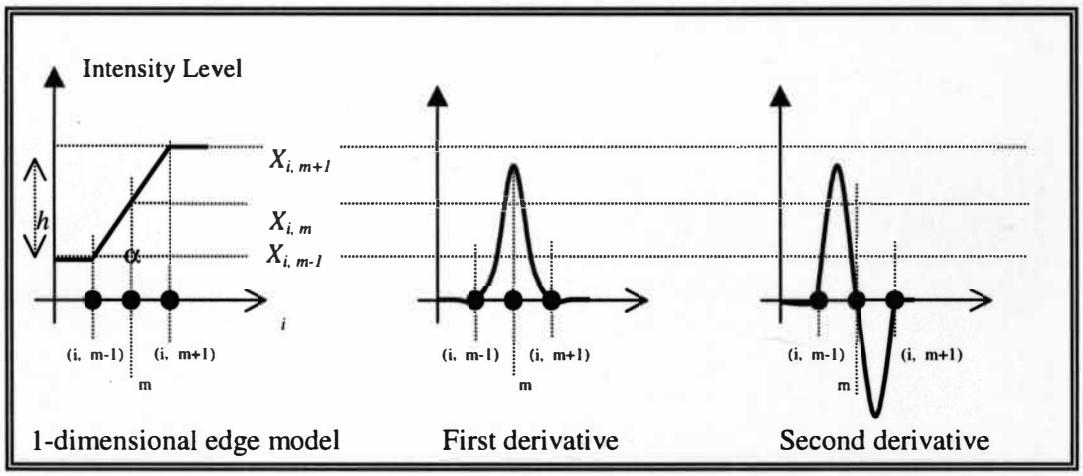

Figure 2. Edge Model Based on Intensity Transition.

Considering direction i of one dimensional edges, edge at point m on this

direction can be modeled based on one pixel wide-transition in intensity from $X_{i,m-1}$ to $X_{i,m+1}$. Above figure shows edge model as a ramp increase in intensity level. Edge is characterized by its height h, the slope angle α and m coordinate of the slope midpoint $X_{i,m}$.

According to this model we can say an edge exists if both the slope angle α and the height h are greater than specified values (thresholds). Most derivative algorithms for edge detection are based on checking the approximation of first for exceeding the threshold or the second derivative for zero crossing.

1.2.10 Edge Detectors

Edge detectors find edges in an intensity image by detecting pixels where the intensity values change abruptly. Using certain algorithms such as derivative methods, edge detection is done by comparing the first derivative of the intensity to certain thresholds, or by checking the second derivative for a zero crossing. Roberts, Sobel, Wallis, Kirsch, Marr-Hildreth and Prewitts are some possible derivative methods of non-linear edge enhancement. Most techniques are limited to making some non-linear manipulation of pixels over a 2× 2 or 3× 3 blocks illustrated in Figure 3 as a means of edge enhancement before thresholding [13].

The **Roberts method** is a simple nonlinear cross operation on a window 2×2 as a differencing method for edge sharpening and edge isolation.

$$E_R(m,n)=([f(m,n) - A_4]^2 - [A_3 - A_5]^2)^{0.5} \qquad (1.2.10\text{-}1)$$

The Roberts approximation to derivative, $E_R(m,n)$, detects edges at those pixels where the gradient of f is maximum and is also sensitive to diagonal edges.

$A_0 = f(m-1,n-1)$, $A_4 = f(m+1,n+1)$

$A_1 = f(m-1,n)$, $A_5 = f(m+1,n)$

$A_2 = f(m-1,n+1)$, $A_6 = f(m+1,n-1)$

$A_3 = f(m,n+1)$, $A_7 = f(m,n-1)$

A_0	A_1	A_2
A_7	$f(m,n)$	A_3
A_6	A_5	A_4

Figure 3. A block of 3× 3 Pixels.

The **Sobel method** is a non-linear operation on a 3 × 3 block described by pixel intensities in neighborhoods.

$$E_S(m,n) = (X + Y)^2 \qquad (1.2.10\text{-}2)$$

Where

$$X = (A_2 + 2.\, A_3 + A_4) - (A_0 + 2.\, A_7 + A_6) \qquad (1.2.10\text{-}3)$$

$$Y = (A_0 + 2.\, A_1 + A_2) - (A_6 + 2.\, A_5 + A_4) \qquad (1.2.10\text{-}4)$$

The Sobel approximation to derivative, $E_S(m,n)$, also detects edges at those pixels where the gradient of f is maximum and is sensitive to horizontal and vertical edges.

The **Wallis method** is based on the logarithm of image luminance at the center pixel and neighborhoods over a 3×3 block. According to this non-linear method an edge exists if the magnitude of the logarithm of intensity value at the center pixel exceeds the magnitude of average logarithmic intensity of its four nearest neighbors by a fixed threshold value.

$$E_w(m,n) = \frac{1}{4} \cdot \log\left[\frac{(f(m,n))^4}{A_1 \cdot A_3 \cdot A_5 \cdot A_7}\right] \qquad (1.2.10-5)$$

1.3 Fuzzy Theory

In 1965 Zadeh suggested a fuzzy set theory in which each element of a set has a degree of membership (degree of belonging to the set) which continuously ranged over [0,1], rather than being either 0 or 1. He developed all set operations such as union, intersection and complement over a fuzzy set. Today fuzzy sets and their associated fuzzy logic are widely used in many scientific and commercial problem domains.

1.3.1 Crisp Sets and Fuzzy Sets

Considering a universal set M, an ordinary crisp set A is defined by identifying those elements of M which set A contains. The characteristic function $P_A(x)$ of set A is defined so that each element of the set M has a corresponding value 1 or 0. The element x_i of M belongs to set A if and only if $P_A(x_i)=1$. Said more formally, $A=\{x \mid P_A(x)=1\}$. Fuzzy sets are based on the idea of extending the range of the characteristic function from the binary values 0 or 1 to the continuous real interval values [0,1]. Therefore, a fuzzy set A is defined by identifying its components x and their associated membership degrees $\mu_A(x)$. The membership function of fuzzy set A is defined to give each element of set A a corresponding real value within interval [0,1]. The mathematical notation of fuzzy set A is represented as

$$A = \left\{ (x, \mu_A(x)) \mid \quad \mu_A \in [0,1], \quad x \in M \right\} \qquad (1.3.1-1)$$

When the universal set M is discrete fuzzy set A is represented by Equation (1.3.1-1) where the $\sum$ referring to union operator in fuzzy set.

$$A = \sum_{i=1}^{N} \left(\mu_{x_i} / x_i \right) \qquad (1.3.1-1)$$

1.3.2 Fuzzy Logic

Logic is the study of the methods and principles of reasoning in all its possible forms [13]. Classical logic deals with propositions that yield values over set {0,1}, false or true. Boolean logic or two-valued (binary) logic has been used in traditional logic and set theory to model the world as black and white, false and true, over set T_2 = {0,1}. Two-valued logic is suitable for systems which are modeled crisply. It has the advantage of being crisp in inferences but the disadvantage of not accurately describing the analog real world.

Multi-valued logic was developed by Lukasiewicz in the 1930s. The set T_N of truth values for integer N is assumed to be evenly divided over the closed interval [0,1]. That is, N-valued logic can be extended to the case where N is countable, and the truth values are allowed correspond to the points on the interval [0,1]. This case is known as Lukaiswics L_1 logic, and provides the base logic needed for working with fuzzy sets [4].

The term fuzzy logic usually involves the manipulation of truth values such as 'nearly true' defined as fuzzy sets over the interval [0,1] of L_1 truth values. In fuzzy logic, usually the knowledge is linguistically expressed as rules in the form of *'If x is A, then y is B'* where *x* and *y* are fuzzy variables and *A* and *B* are fuzzy sets or fuzzy values. Fuzzy logic deals with propositions that possess values over interval [0,1] and also combinations of variables that stand for arbitrary propositions. These variables called fuzzy linguistic variables. The combination of truth values of these fuzzy variables is done by multi-valued logic operators such as *complement*, *max, min* operators. Table 1 illustrates the main operators used in crisp set and *N*-valued logic.

Table 1

Operator Comparison

Crisp set	Two-valued logic	N-valued logic	Fuzzy logic
A'	1 – A	1 – A	1-A
$\cup$	+, $\vee$	Max	Max, t-conorm
$\cap$	., $\wedge$	Min	Min, t-norm

Fuzzy logic processing includes fuzzification of crisp sets, decision making logic (fuzzy inferencing), knowledge base (IF – THEN rules) and defuzzification. A simple architecture of a fuzzy logic system (*FLC*) is illustrated in Figure 4. This system, which is applied in image processing, will be described in detail later.

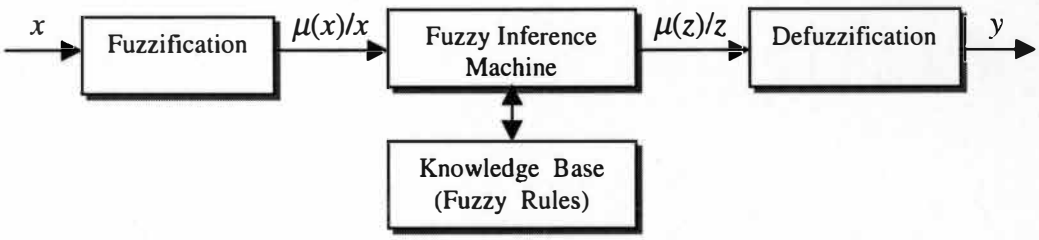

Figure 4. Illustration of a Fuzzy Processing System.

1.3.3 Fuzzy Membership Function, *FMF*

A *MF* is a curve that defines how each member x in fuzzy set A is mapped to a membership value $\mu_A(x)$ (or degree of membership) over an interval [0,1]. We mathematically represent this as

$$\mu_A(x): x \xrightarrow{\mu_A} [0,1] \qquad (1.3.3-1)$$

Membership function (*MF*) can be generated heuristically or generated by using clustering techniques, such as *c*-mean, adaptive vector quantization *AVQ*, and the self organizing map *SOM*. In this paper we simply apply a heuristic approach to generate membership function. Choosing the appropriate *MF* is application dependent. The most commonly used *MF*s are the triangular, trapezoidal, S-shaped, Z-shaped, bell-shaped, Sigmoid and Ggaussian. Following are the examples of *MF*s.

Triangular shape *MF* can be generated functionally using Equation (1.3.3-2). Parameters *a, b, c* are the parameters by which to tune the *MF* as desired to make a symmetric or anti-symmetric ***MF*.**

$$\Lambda(x;\, a, b, c) = \max\left(\min\left(\frac{x-a}{b-a} \;,\; \frac{c-x}{c-b} \right),\; 0 \right) = \begin{cases} 0 & \text{if } x \le a \\ \dfrac{x-a}{b-a} & \text{if } a \le x \le b \\ \dfrac{c-x}{c-b} & \text{if } b \le x \le c \\ 0 & \text{if } x \ge c \end{cases} \qquad (1.3.3-2)$$

Trapezoid shape *MF* can be generated functionally using Equation (1.3.3-3). Parameters *a, b, c, d* are also the tuning parameters by which to make a symmetric or anti-symmetric *MF*.

$$\Pi(x;\, a, b, c) = \max\left(\min\left(\frac{x-a}{b-a} \;,\; 1 \;,\; \frac{d-x}{d-c} \right),\; 0 \right) = \begin{cases} 0 & \text{if } x \le a \\ \dfrac{x-a}{b-a} & \text{if } a \le x \le b \\ 1 & \text{if } b \le x \le c \\ \dfrac{d-x}{d-c} & \text{if } c \le x \le d \\ 0 & \text{if } d \le x \end{cases} \qquad (1.3.3-3)$$

S-shaped *MF*, the Zadeh's *MF*, is defined as Equation (1.3.3-4). Parameters *a, b, c* are also the tuning parameters for this *MF*.

$$S(x;\, a, b, c) = \begin{cases} 0 & \text{if } x \le a \\ 2\left(\dfrac{x-a}{b-a} \right)^2 & \text{if } a \prec x \le b \\ 1 - 2\left(\dfrac{x-c}{x-a} \right)^2 & \text{if } b \prec x \le c \\ 0 & \text{if } c \prec x \end{cases} \qquad (1.3.3-4)$$

Bell-shaped *MF* is defined by Equation (1.3.3-5). Parameters *a, b, c* can be used to tune this *MF* as desired to make a symmetric or anti-symmetric *MF*.

$$\Pi(x;\ a,\ b,\ c) = \begin{cases} S\left(x; c-b, c-\frac{b}{2}, c\right) & \text{if} \quad x \le c \\ 1 - S\left(x; c+\frac{b}{2}, c+b, c\right) & \text{if} \quad x \succ c \end{cases} \qquad (1.3.3-5)$$

The generalized bell *MF* is represented in Equation (1.3.3-6). The parameters *a, b, c* are used to tune *MF* centered at point *c* over the *x*-axis.

$$\Pi(x;\ a,\ b,\ c) = \frac{1}{1+\left|\frac{x-c}{a}\right|^{2b}} \qquad (1.3.3-6)$$

Consider the case of triangular *MF*. The most significant points in *MF* are the left and right points, peak point and the cross-point level. The peak point is the point X_{peak} for which the value of the *MF* is equal to 1. Left and right points are respectively the least and the greatest value of fuzzy set *A* in which the value of *MF* is equal to *0*. The peak value is an interval for membership function. Now we can define the left and right width based on the above mentioned points. The left width, W_{left} is the length of the interval $[X_{left}, X_{peak}]$ that is $W_{left} = X_{peak} - X_{left}$. Similarly the right width, W_{right} is the length of the interval $[X_{peak}, X_{right}]$ that is $W_{right} = X_{right} - X_{peak}$. Figure 5 illustrates the triangular *MF* and its corresponding parameters.

In case of overlap between two *MF*s *A* and *B*, the cross-point X_{cross} and the cross point level are parameters which are useful in defining the percentage of

overlap. A cross-point X_{cross} is the point at which both membership functions have the same value (level). Cross-point level, which is the same on both *MF*, is the membership degree of X_{cross}. Two *MF*s *A* and *B* may have more than one cross-point. Now we can define percentage of overlap of *A* in *B* as a ratio of the length of interval $[X_{cross}, X_{right}]$ and W_{right} in membership function *A* that is

$$P_{ovl,A} = \frac{X_{right,A} - X_{cross}}{X_{right,A} - X_{peak}} = \frac{X_{right,A} - X_{cross}}{W_{right,A}} \qquad (1.3.3-7)$$

And consequently the percentage of overlap of *B* in *A* can be defined as

$$P_{ovl,B} = \frac{X_{cross} - X_{left,B}}{X_{peak} - X_{left,B}} = \frac{X_{cross} - X_{left,B}}{W_{left,B}} \qquad (1.3.3-8)$$

Figure 5 represents the triangular membership functions *A* and *B* and their corresponding parameters.

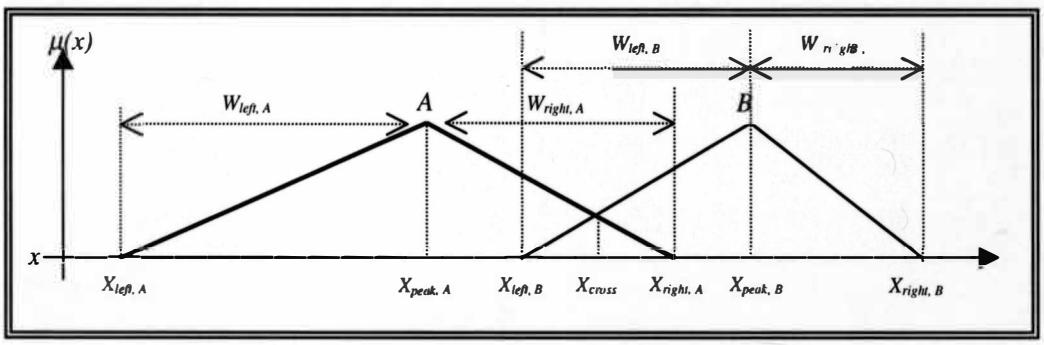

Figure 5. Illustration of Triangular *MF*.

1.3.4 Fuzzification

Fuzzification is the process of producing a fuzzy set from a crisp set as illustrated by Figure 4. Using the fuzzy logic system to process any data, we have to

first convert the crisp data to the fuzzy data in order to apply fuzzy operators for any computation in rule-based inferencing stage. Fuzzification is done by associating the membership degree for inputs to the fuzzy logic system using certain membership functions. Fuzzification requires (a) identifying relevant input and output variables of the fuzzy logic system and ranges of their values, (b) selecting meaningful linguistic states for each variables and expressing them by appropriate fuzzy sets and (c) defining membership functions for each input variable to express the associated membership degrees.

In this paper (Chapter IV) inputs to the fuzzy system range over gray levels scaled from 0 (Black) to 255 (White). We have applied fuzzification methods by first partitioning the intensity scale [0,1] (or the discrete gray scale 0-255) into 5 individual ranges, and second by defining linguistic variables Dark, Dark Gray, Bright Gray and Bright for these 5 ranges. Finally we have applied the fuzzy quantization over the range [0,1] using 5 membership functions. We have used two trapezoid-shaped *MF*s for left and right ranges, and three triangular-shaped *MF*s for the other three ranges. You will see further, Figure 7 on page 27 represents the fuzzy plane applied for fuzzification over intensity scale [0,1] or discrete gray scale 0-255.

1.3.5 Fuzzy Inference Rules

Fuzzy rules, which are often expressed in the form of **IF-THEN** statement, are essentially fuzzy relations or fuzzy implications [4]. In this step, the knowledge pertaining to the given problem is expressed in terms of fuzzy inference rules and

stored in fuzzy rule base. Figure 6 represents a rule base containing the 25 fuzzy rules applied in a fuzzy control system. Then the rule 25^{th} is expressed as follows.

Rule 25^{th}: **IF** (X_{mn} is G) and (Y is G), **THEN** (d is Z)

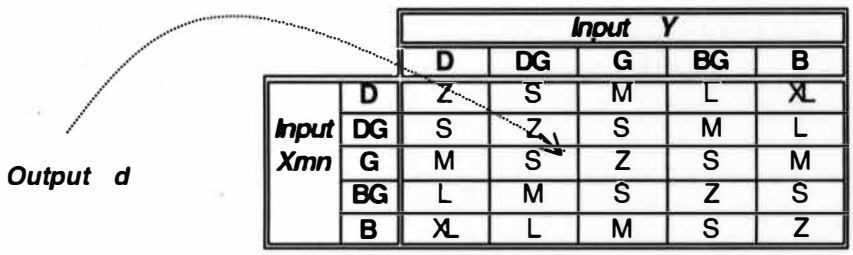

Figure 6. Illustration of the Rules for Fuzzy Logic Controller.

The module consisting a number of fuzzy rules called fuzzy knowledge-base or fuzzy rule-base. In fuzzy knowledge-base all the possible rules can conveniently be represented in a matrix form.

1.3.6 Fuzzy Reasoning

Fuzzified input variables of fuzzy logic system are taken to fuzzy inference machine to be processed by relevant fuzzy information rules to make inferences regarding the output variables. This process is called fuzzy reasoning. There are various techniques to combine inputs with relevant rule in order to infer an appropriate fuzzy output. The most commonly applied are *Max-Min* and *Max-Dot* fuzzy inference methods. Assume we have n rules in knowledge base as

Rule 1: IF (x is A_1 and y is B_1), THEN z is Z_1

.....

.....

Rule n: IF (x is A_n and y is B_n), THEN z is Z_n

For two fuzzy input variables x_o and y_o, assume only two rules 2 and 4 are active as

Rule 2: IF (x_0 is A_2 and y_0 is B_2), THEN z is C2
Rule 4: IF (x_0 is A_4 and y_0 is B_4), THEN z is C4

Then, The corresponding fire strength parameters for rules 2 and 4 are respectively defined as

$$\alpha_2 = \min\left[\mu_{A_2}(x_0), \mu_{B_2}(y_0)\right] \quad and \quad \alpha_4 = \min\left[\mu_{A_4}(x_0), \mu_{B_4}(y_0)\right] \qquad (1.3.6-1)$$

Then for Max-Min reasoning, Mamadani's minimum operation is used for fuzzy implication and the output membership function for consequent C can be inferred as

$$\mu_C(z) = \max\left[\min\left(\alpha_2, \mu_{C_2}(z)\right), \min\left(\alpha_4, \mu_{C_4}(z)\right)\right] \qquad (1.3.6-2)$$

In Max-Dot reasoning, Larsen's product operation is used as fuzzy implication function [4]. The membership degree of the inferred consequence is obtained as

$$\mu_C(z) = \max\left[\left(\alpha_2 \cdot \mu_{C_2}(z)\right), \left(\alpha_4 \cdot \mu_{C_4}(z)\right)\right] \qquad (1.3.6-3)$$

Note that in both methods, if x_0 and y_0 are crisp values then the above mentioned operations result in fuzzy singleton.

1.3.7 Defuzzification

The conclusion resulting from a certain fuzzy reasoning technique in fuzzy

inference machine is expressed in terms of fuzzy set. This must be converted to a real crisp value. This process of converting a fuzzy set to a single real number is called defuzzification. There are some defuzzification methods each of which leads to a different result. Assume the fuzzy set resulting from a fuzzy inference machine is a discrete fuzzy set C as

$$C = \sum_{k=1}^{n} \mu_k / z_k \qquad \text{where} \quad \mu_k \in [0,1] \qquad (1.3.7-1)$$

The most commonly used techniques are center of area *COA*, center of maxima *COM*, and mean of maxima *MOM*. These are defined as follows

Center Of Maxima, *COM*, Consider fuzzy set M given by Equation (1.3.7-2), where $h(c)$ is the height of C (maximum membership degree in C).

$$M = \{z_i \mid \mu_i = h(c)\} \qquad (1.3.7-2)$$

COM is defined as the average of the smallest value and the largest value of C with the same membership degree equal to $h(c)$. This is represented as

$$d_{com}(c) = \frac{\min\{z_i \mid z_i \in M\} + \max\{z_i \mid z_i \in M\}}{2} \qquad (1.3.7-3)$$

Mean Of Maxima, *MOM*, method which is the average of all members of above defined set M, is defined as

$$d_{mom}(c) = \frac{\sum_{z_i \in M} z_i}{|M|} \qquad (1.3.7-4)$$

Center Of Area, *COA*, method indicates the value within the range of z_i in which the area under membership function C is partitioned into two equal sub-areas. This is represented as

$$d_{com}(c) = \frac{\sum_{i=1}^{n}(\mu_i \cdot z_i)}{\sum_{i=1}^{n}\mu_i} \qquad (1.3.7-5)$$

The results obtained from the above methods are application dependent. For example in our approach to edge detection which is explained further in Chapter IV, the concluded fuzzy set from the inference machine is

$$D = \left\{ \mu_1/d_1, \mu_2/d_2, \mu_3/d_3, \mu_4/d_4 \right\} \qquad (1.3.7-6)$$

While the *COA* technique gives a better result than the *MOM* and *COM* techniques, using one of the edge characteristic functions (*ECF*) given in section (3.1.4) results in a better value as a defuzzification technique.

$$d_{ecf}(D) = E_{qcw}(D) = \frac{\left\{(\mu_1 \cdot d_1 + \mu_4 \cdot d_4) \cdot (\mu_2 \cdot d_2 + \mu_3 \cdot d_3)\right\}}{4} \qquad (1.3.7-7)$$

1.3.8 Membership Function Tuning Technique

As we will see, tuning of membership functions is important to optimize parameters. By reforming the membership function both the conclusion obtained from the fuzzy inference machine and, consequently the value resulting from the

defuzzification stage, change considerably.

The shape of each *MF* depends on parameters *a, b, c, d* involved in constructing the *MF*. Thus, the variation of parameters *a, b, c, d* in membership functions has an effects on the resulting output of fuzzy logic system. We take an advantage of this effect to tune *MF* in order to obtain the desired result in output. The gradient decent and neural network algorithms are two of the most commonly used approaches to tuning membership functions. In this paper we use the multidimensional vector optimization technique called the cyclic coordinate algorithm. This technique is used to tune membership functions and consequently to optimize the defuzzification parameters simultaneously.

Assume we have triangular-shaped *MF* defined by Equation (1.3.3-2) with W_{left} and W_{right}. Then the variable vector used for tuning *MF* is a 3-dimensional vector as $V = [W_{left}, b, W_{right}]$. In our approach to optimal edge detection using fuzzy logic system, we have applied the percentage of overlap P_{ovl} (the same one for all membership functions), as well as peak points of membership functions, as the variables to tune the input/output *MF*s of fuzzy logic controller (*FLC*). This *FLC* has been designed to lead the edge detector system (*EDS*) toward an optimal output using cyclic coordinate algorithm. You will see further in Figure 7 on page 27, there are five *MF*s assigned for five input linguistic variables to the fuzzy logic system. The variable vector applied for tuning input *MF* has been chosen as $V_{in} = [P_{ovl}, b_1, b_2, b_3, b_4, b_5]$. If $|X_{cross} - X_{right}| = |X_{left} - X_{cross}|$, then $(P_{ovl})_A = (P_{ovl})_B$. The cyclic coordinate algorithm is explained in section 1.5 in detail.

In Chapter IV, the variable vector pertaining to the optimal fuzzy edge detection problem consists of the overlap percentages and peak points belonging to input/output membership functions. This variable vector is used to tune membership functions to obtain the optimal edge based on minimizing the error *e* between the desired edge trace and the actual resulting edge trace from *EDS* as the objective function.

1.4 Fuzzy Image Processing

Fuzzy logic has been applied to gray tone image processing such as gray level thresholding, edge detection, image enhancement, segmentation and so on. Several fuzzy operators have been used in fuzzy image processing which include *max, min, INT* [1]. Further, as we see, the use of fuzzy logic system (controller) is a significant choice in optimization of image processing. A gray tone image possesses some ambiguity within the pixels due to the pixel multi-valued levels of brightness. Therefore it is justifiable to apply the logic of fuzzy set rather than ordinary set to image processing problems.

1.4.1 Fuzzy Intensity Image Definition

In the spatial domain, a fuzzy intensity image *FII* of dimension $M \times N$ with L gray tone levels is an array of fuzzy singletons that can mathematically be represented as Equation (1.4.1-1), for $m=1,2,\ldots,M$ and $n=1,2,\ldots,N$. X_{mn} denotes the intensity value of pixel $(m,n)^{th}$ and μ_{mn} is its associated membership degree.

$$FII = f(m,n) = \left[\mu_{mn} / X_{mn} \right] \equiv [FX_{mn}] \quad where \begin{cases} X_{mn} \in [0,1] \\ l \in \{0,1,\ldots,L-1\} \quad Gray\ level \\ \mu_{mn} \in [0,1] \end{cases} \qquad (1.4.1-1)$$

Similarly, the definition of an intensity image given by Equation (1.2.3-1), the normalized gray scale is also considered here as an intensity scale over the interval [0,1]. That is, $X_{mn} \in [0,1]$. Depending on the membership function(s) used for fuzzificatin of digital image we define the fuzzy plane as

$$\mu_{mn} = P(X_{mn}) \qquad (1.4.1-2)$$

P refers to membership function(s) defined over the intensity value range [0,1] (or gray level scale 0 to L-1). FX_{mn} is a fuzzy singleton denoting the fuzzified intensity image pixel (m,n). X_{mn} is the intensity value (or gray level l) at this pixel and $P(X_{mn})$ defined by Equation (1.4.1-2) is the corresponding membership degree of having grayness relating to some gray level l. Membership function(s) applied in the fuzzy plane P can be selected as one of the functions explained in section 1.3.3. The membership degree μ_{mn} takes a value between interval [0,1].

In Chapter IV for fuzzy approach to edge detection, we apply triangular and trapezoidal membership functions, defined by Equations (1.3.3-2) and (1.3.3-3) in the fuzzy plane illustrated in Figure 7 to fuzzify the digital image array. As this Figure shows, the fuzzy plane consists of three triangular membership functions concerning linguistic variables *DG*, *G*, *BG* and two trapezoidal membership functions relevant to

linguistic variables *D, B*. These five membership functions quantize the gray level *0-255* within interval [0,1] as fuzzification. The positive constants *a, b, c, d* which are the tools for tuning membership functions, consequently have the effects of altering the ambiguity in the fuzzy plane by changing the cross-over point and slope of transformation function.

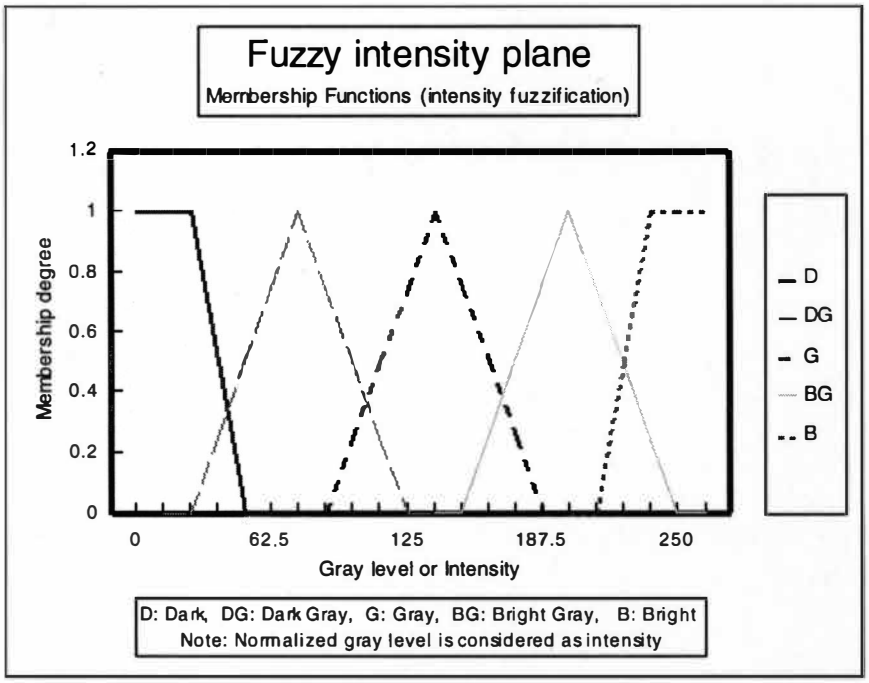

Figure 7. Fuzzy Intensity Plane.

1.4.2 Fuzzy Image Enhancement

As discussed in section 1.2.5, the purpose of enhancing an image is the modification of that image in such a way that the result is more suitable than original for a specific application. This modification is implemented by some manipulations

on pixel intensities in the fuzzy property domain. Figure 8 illustrates a block of image enhancement. The fuzzy operator *INT*, which is actually a contrast intensification function, is taken as an image enhancing tool. This function is defined as

$$T_1 = INT(\mu_{mn}) = \begin{cases} 2 \cdot \mu_{mn}^{\,2} & for \quad 0 \le \mu_{mn} \le 0.5 \\ 1 - 2 \cdot \left(1 - \mu_{mn}\right)^2 & for \quad 0.5 \le \mu_{mn} \le 1 \end{cases} \qquad (1.4.2-1)$$

This function enhances the membership value of those elements whose membership is above 0.5 and diminishes that of those elements with membership below 0.5. This function is recursively applied for better contrast enhancement as

$$T_s = INT(T_{s-1}) \qquad (1.4.2-2)$$

The subscript s represents the number of composites of *INT* function [1]. Assume $P(X_{mn})$ defines a fuzzy plane such as Figure 7. The block diagram illustrated in Figure 8 is considered as a block of image enhancement using intensification function in the fuzzy property domain. The parameters *a, b, c, d* are fuzzifiers and defuzzifiers and s in function T_s is used as an intensity tuner.

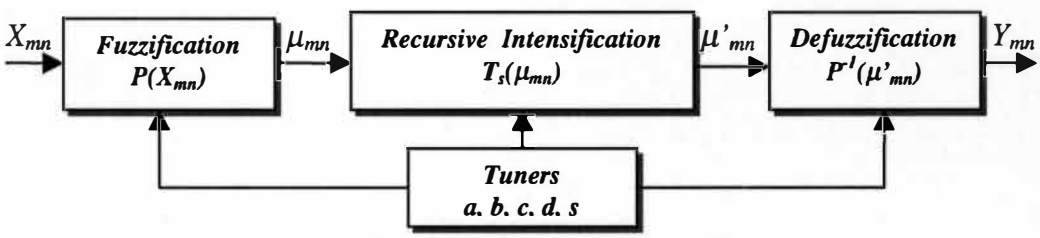

Figure 8. Image Enhancement Using Fuzzy Theory.

1.4.3 Fuzzy Image Smoothing Algorithms

Image smoothing, which is classified as an image enhancing algorithm, is achieved by intensity modification of pixels in the spatial domain. Each pixel and its neighborhood possess equal brightness or gray level. The technique used for fuzzy image enhancement [1] is presented in Figure 9.

Figure 9. Fuzzy Image Enhancement Sequence.

The sequence consists of pre-enhancement of an image using the method described in section 1.4.2, block E followed by the smoothing process through block S and a post –enhancing of the smoothed image through block E again. All smoothing processes blur the images by removing the abrupt changes in intensity or gray level and consequently smooth the edges. Therefore, the post-enhancement is used to improve the intensity contrast in order to obtain sharp images. There are some methods to smooth an image which can be applied as tools in block S.

Defocusing technique is used as a smoothing algorithm using a linear non-recursive filter. It is defined as

$$Y'_{mn} = a_0 \cdot Y_{mn} + a_1 \cdot \sum_{Q_1} Y_{ij} + a_2 \cdot \sum_{Q_2} Y_{ij} + \cdots\cdots\cdots + a_s \cdot \sum_{Q_s} Y_{ij} \qquad (1.4.3-1)$$

$$\text{where} \quad \begin{cases} a_0 + N_1 \cdot a_1 + N_2 \cdot a_2 + \cdots\cdots\cdots + N_s \cdot a_s = 1 \\ 0 \le a_1 \le a_2 \le \cdots\cdots\cdots \le a_s \le 1 \\ (i,j) \ne (m,n) \quad , \quad m = 1,2,\cdots M \quad , \quad n = 1,2,\cdots N \end{cases}$$

Y_{mn} represents the $(m,n)^{th}$ pixel intensity of the pre-enhanced image to smoother S. It is also in the center of s circles $Q_1, \ldots Q_s$ with radii $R_1,\ldots,R_s$. Each circle Q_s contains N_s number of pixels (ignoring the middle pixel) on or within the circle but out of Q_{s-1}. While the radius R_s of circle Q_s decreases, the coefficient a_s also decreases and consequently the portion of intensity added to the middle pixel Y_{mn} decreases.

Averaging technique is considered as the special case of a single circle in the defocusing technique. Since $a_i = a_j$ for $i=j=0,1,\ldots,s$, then

$$Y'_{mn} = \frac{1}{N_1} \cdot \sum_{Q_1} Y_{ij} \quad for \quad (i,j) \in Q_1 - \{(m,n)\} \qquad (1.4.3-2)$$

The other method called the *max-min* rule [1] is not explained here. As the name "defocusing algorithm" implies, smoothing algorithms also have the disadvantage of blurring the images.

1.4.4 Edge Detection

Edge detection can be applied as a final enhancement in the spatial domain. This is represented in Figure 10. As you observe block *'ED'* is added to sequence processing illustrated in Figure 9 for edge enhancement as a final process. The edge enhancing algorithm can be achieved by the algorithms introduced in section 1.2.10 or by our approach to edge detection discussed in Chapter II. Edge detection using *min* and *max* operators [1] is given in following equations. These equations can be applied for the block *ED* in sequence illustrated by Figure 10.

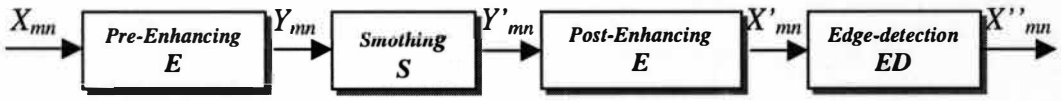

Figure 10. Smoothing and Edge Detection Sequence.

$$X''_{mn} = \left| X'_{mn} - \min_{Q}\{X'_{ij}\} \right| \qquad (1.4.4-1)$$

or

$$X''_{mn} = \left| X'_{mn} - \max_{Q}\{X'_{ij}\} \right| \qquad (1.4.4-2)$$

or

$$X''_{mn} = \left| \max_{Q}\{X'_{ij}\} - \min_{Q}\{X'_{ij}\} \right| \qquad (1.4.4-3)$$

$$for \quad \begin{cases} (i,j) \neq (m,n) \\ (i,j) \in Q \end{cases}$$

Q is a circle of radius R centered at the pixel (m,n) and contains N pixels (i,j) located on/within circle. According to this set of equations, the better edge enhancement with high intensity trace will be achieved when the intensity contrast increases. These three equations have been examined on some different gray tone images and the results indicate that equation (1.4.4.2) generates better edge trace compared to two others. Generally the edge obtained by any desired methods can be mathematically represented as

$$E_{II}(m,n) = [X''_{mn}] \qquad where \begin{cases} m = 1,2,\ldots,M \\ n = 1,2,\ldots,N \end{cases} \qquad (1.4.4-4)$$

X''_{mn} is the detected or computed intensity value of an edge pixel. The subscript *II* denotes original (or smoothed and contrast intensified) image to edge detector.

Briefly, the edge enhancing algorithm can be implemented in four stages: (1) pre-enhancing which consists of contrast intensification in the fuzzy domain; (2) Smoothing; (3) post-enhancing which consists of redoing the contrast intensification in the fuzzy domain; and (4) Edge detection by applying the appropriate algorithm.

1.5 System Optimization

The object of system optimization is to specify an input vector $V(t)$, which drives a system to a specified target state in such a way that during the process a predefined performance index is minimized or maximized.

Some different optimizations for linear and non-linear systems exist such as linear optimal quadratic control, switching curve strategy and dynamic programming which are most commonly used in control problems. They are all categorized as derivative methods involved with analytical solution (direct solution for differential equations) or numerical solution (approximation of differential equations, like Euler's method). Also there are some non-derivative methods such as sequential line searches, golden ratio sequential line search and cyclic coordinate applied in multi-dimensional optimization.

1.5.1 Discrete Nonlinear System Optimization

A discrete non-linear system can be mathematically expressed as Equation

(1.5.1-1), where S_k, S_{k+1}, U_k represent respectively the present state, next state and input variables. The term g denotes the system function at time k. This function as well as the aforementioned variables can be scalar or vector.

$$S_{k+1} = g(k, S_k, U_k) \qquad (1.5.1-1)$$

To optimize the above system, the performance index PI is defined by

$$PI(U_k) = f_k(k, S_k, U_k) \qquad (1.5.1-2)$$

The term f denotes the cost function at time k. Usually cost function during the optimization time is constant and can be denoted by f. At the optimal point the system function is optimum, $g(k^*, S_k^*, U_k^*)$. And consequently the performance index is max or min, $PI^* = f(k^*, S_k^*, U_k^*)$. In Chapter IV, we consider image enhancement system as a discrete nonlinear system and will optimize the enhanced image using a multidimensional optimization, cyclic coordinate algorithm.

1.5.2 Non-Derivative Methods

The function f aimed to be optimized is called objective function. To find an explicit formula for an objective function can sometimes be so complicated or impossible, then a non-derivative method is adopted to optimization problem, such as sequential line search algorithm.

1.5.3 Sequential Line Search Algorithm

Assume objective function f is convex meaning the concavity does not

change, or is at least locally convex in the neighborhood of the optimal value. Without loss of the generality assume that one-dimensional function f is concave up within interval $[a_i,b_i]$ during iteration i of the algorithm . Then Equations (1.5.3-1) and (1.5.3-2) define two evaluation points lep_i and rep_i for thirds algorithm of sequential line search as

$$lep_i = \frac{2 \cdot a_i + b_i}{3} \qquad (1.5.3-1)$$

$$rep_i = \frac{a_i + 2 \cdot b_i}{3} \qquad (1.5.3-2)$$

Terms lep_i and rep_i are evaluations representing left-side and right-side evaluation points respectively for objective function f at iteration i, that is, $f_{left} = f(lep_i)$ and $f_{right} = f(rep_i)$. The Figure 11 illustrates evaluation points within interval $[a_i, b_i]$.

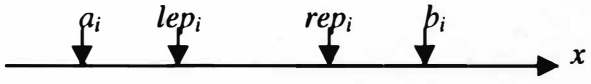

Figure 11. Sequential Line Search on Direction x.

The length of interval $[a_i,b_i]$ is called length of uncertainty and denoted by $l_i = b_i - a_i$. According to convexity theorem [16], the uncertainty interval, $[a_{i+1},b_{i+1}]$, in iteration $i+1$ can be computed as

If $f(lep_i) < f(rep_i)$ then $a_{i+1} = a_i$, $b_{i+1} = rep_i$
If $f(lep_i) > f(rep_i)$ then $a_{i+1} = lep_i$, $b_{i+1} = b_i$
If $f(lep_i) = f(rep_i)$ then $a_{i+1} = lep_i$, $b_{i+1} = rep_i$

For a given initial interval $[a,b]$ and the length of uncertainty l, the thirds

sequential search is given by the algorithm shown in Figure 12.

```
INPUT   L , a , b
lep  = (2.a + b)/3
rep  = (a + 2.b)/3
CALCULATE  f(lep)
CALCULATE  f(rep)
DO WHILE  b-a > l
    IF   f(lep) < f(rep)   THEN     b = rep
    IF   f(lep) > f(rep)   THEN     a = lep
    IF   f(lep) = f(rep)   THEN     a = lep   ,   b = rep
    lep  = (2.a + b)/3
    rep  = (a + 2.b)/3
    CALCULATE  f(lep)
    CALCULATE  f(rep)
END DO
PRINT   (a+b)/2  ,  f((a+b)/2)
```

Figure 12. Third Sequential Line Search Algorithm.

1.5.4 Golden Ratio Line Search Algorithm

Let the evaluation points in line search algorithms be defined in terms of uncertainty boundary points a_i , b_i as

$$lep_i = \alpha \cdot a_i + (1- \alpha) \cdot b_i \qquad (1.5.4\text{-}1)$$

$$rep_i = (1- \alpha) \cdot b_i + \alpha \cdot b_i \qquad (1.5.4\text{-}2)$$

If constant α is equal to 1, then the evaluation points fall on end points. If α is equal 0.5, then the evaluation points are identical and finally for $0.5 < \alpha < 1$, these points locate between boundary points a_i , b_i. The famous golden ratio from Greek antiquity is obtained approximately as $\alpha = 0.618$, [16]. The golden ratio line search algorithm is given for one-dimensional objective function as shown in Figure 13.

```
INPUT   L , a , b
lep  = (0.618).a + (0.382).b
rep  = (0.382).a + (0.618).b
CALCULATE   f_left = f(lep)
CALCULATE   f_right = f(rep)
DO WHILE  b-a > l
    IF  f_left < f_right  THEN
                    b = rep
                    rep = lep
                    lep =  (0.618).a + (0.382).b
                    CALCULATE  f(lep)
                   f_right = f_left
                   f_left = f(lep)
    IF  f_left >= f_right  THEN
                    a = lep
                    lep = rep
                    rep =  (0.382).a + (0.618).b
CALCULATE  f(rep)
                    F_left = f_right
                    F_right = f(rep)
END  DO
PRINT   (a+b)/2  ,  f((a+b)/2)
```

Figure 13. Golden Ratio Sequential Line Search Algorithm.

1.5.5 Multidimensional Optimization

Line search algorithms are techniques for optimization of a one-dimensional objective function. In system optimization, for many problems higher dimension is necessary to model system function as objective to optimize. In cases where there are no analytic means available, numerical methods are adopted for optimization. These methods may involve derivatives, but more often that not, the problems will require non-derivatives.

Assume that the two-dimensional system function $g(x,y)$ is considered to be optimized subject to the constraint $f(x,y)$. Sequential search methods adopted for one-

dimensional line search in sections 1.5.3 and 1.5.4, are also applicable in higher dimensions. This is done in multidimensional optimization by choosing a direction, then looking for the min/max along this line. In general this will require a line search. Once the minimum is found along this line a new direction is chosen and the procedure repeats. This continues until a reasonable approximation to min/max is achieved. This approach to optimum point from origin is generally illustrated on contour lines of the surface $f(x,y)$ in Figure 14.

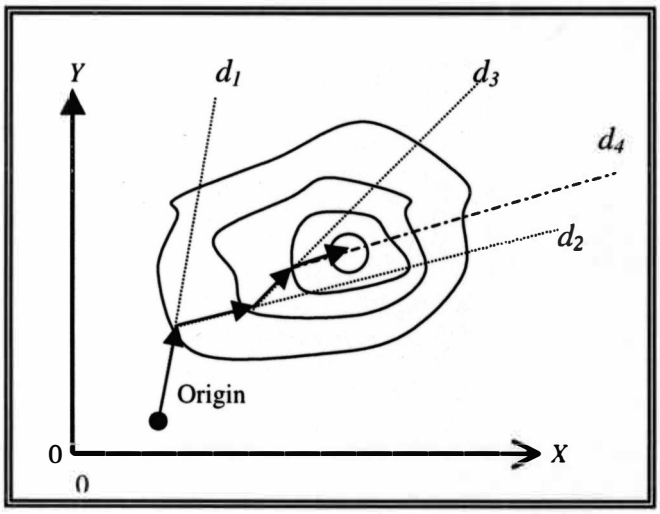

Figure 14. Sequential Line Search Illustration.

As can be seen, the line search algorithm starts from origin and by sequentially choosing line d_1, d_2, d_3 and finally d_4 ends at an optimal point. The best directions can be found by gradient of f (that is, the partial derivations of f). This is called steepest decent algorithm, [16].

1.5.6 Cyclic Coordinate Algorithm

As we told before the directions in the line search algorithm can be obtained by the gradient of function *f*. In case there is no explicit formula for gradient, non-derivative methods are helpful by cycling through a protocol of directions, independent of function *f*. In this technique of optimization directions are adopted parallel to the coordinate axis. For example, in the case of a two dimension *x*-*y*, first try the *x*-axis and then the *y*-axis, again repeating this process. Extension to higher degree systems is obvious.

To show this algorithm, consider a two-dimensional optimization problem for a function $f(c_1, c_2)$. The main structure for the cyclic coordinate algorithm is given in Figure 15.

```
INPUT  c1, c2
INPUT  ε, l, d
DO WHILE  || (c1 – c'1)^2 + (c2 – c'2)^2 || >= ε
            c'1 = c1
            c'2 = c2
          FOR  dir = 1 to 2
                 CALL     golden(c1, c2, dir, d, l ; c1, c2)
           END
END DO
c*1 = c1
c*2 = c2
f* = f(c*1, c*2)

PRINT  c*1 ,  c*2 , f*
```

Figure 15. Cyclic Coordinate Algorithm.

This main program, called cyclic, requires the initial point $c = (c_1, c_2)$, the

tolerance ε (by which we can tune the amount of closeness to optimal point) and l (the length of uncertainty during a line search). The sub-algorithm GOLDEN (golden ratio sequential line search) is shown in Figure 16.

```
GOLDEN(c1 , c2 , dir , d , l ; c1 , c2)

IF dir = 1 THEN  a = c1 - d ,  b = c1 + d
IF dir = 2 THEN  a = c2 - d ,  b = c2 + d

lep  = (0.618).a + (0.382).b
rep  = (0.382).a + (0.618).b

IF dir = 1 THEN CALCULATE  fleft = f(lep , c2),  CALCULATE  fright = f(rep , c2)
IF dir = 2 THEN CALCULATE  fleft = f(c1 , lep),  CALCULATE  fright = f(c1 , rep)

DO WHILE  b-a > l
   IF  fleft < fright  THEN
                  b = rep
                  rep = lep
                  lep =  (0.618).a + (0.382).b
                     fright = fleft
                     IF  dir = 1  THEN   CALCULATE   fleft = f(lep , c2)
                     IF  dir = 2  THEN   CALCULATE   fleft = f(c1 , lep)

   IF  fleft >= fright  THEN
                  a = lep
                  lep = rep
                  rep =  (0.382).a + (0.618).b
                  Fleft = fright
                  IF  dir = 1  THEN   CALCULATE   fright = f(rep , c2)
                  IF  dir = 2  THEN   CALCULATE   fright = f(c1 , rep)

END DO

IF  dir = 1  THEN    RETURN  c1 = ( a+b)/2 ,  c2 = c2
IF  dir = 2  THEN    RETURN  c1 = c1  ,  c2 =  (a+b)/2
```

Figure 16. Golden Ratio as a Sub-Algorithm of Cyclic Coordinate Algorithm.

In order for a line search be initiated, it is necessary to know just where to place the interval of uncertainty, $[a,b]$. This is done using a fixed distance d as

$a=c_1 - d$, $b= c_1+ d$ on direction V=(1,0) or flag *dir* =1 and $a=c_2 - d$, $b= c_2+ d$ on direction V=(0,1) or flag *dir*=2. The output from the cyclic is simply the final, min, point found by the algorithm.

The cyclic must call a line search algorithm such as golden ratio line search, considered as the best sequential line search approach, to perform the actual line search. Parameters c_1 , c_2 , l , d are passed from cyclic to golden and also flag *dir* is specified in cyclic to indicate which coordinate in golden is to be subjected to the line search algorithm. At the end, golden will pass the best point $c=(c_1 , c_2)$ back to cyclic as well. The golden ratio line search algorithm is given as sequentially follows.

The following chart, Figure 17, illustrates the inter-module communication requires for the cyclic coordinate algorithm. c^* and f^* represent respectively the optimal point (or vector) and optimal value as the output of algorithm. The block *FUNCTION* represents the calculation of f_{left} *and* f_{right} in an individual module. The given algorithm which is for a two-dimensional system can be simply extended to a higher dimension.

This algorithm is just for directions parallel to c_1 and c_2 axis. Choosing a diagonal direction may help to reach the minimal point faster. However for a n-dimensional we can consider n directions parallel to the main axis and 2^n-n-1 diagonal directions. In the case of a two-dimensional function there are two directions (1,0) and (0,1) parallel to main axis, and one diagonal direction (1,1). This algorithm is applied in Chapter IV to minimize the performance index of edge detector system by tuning a vector V (with 12 components) as an input to this algorithm.

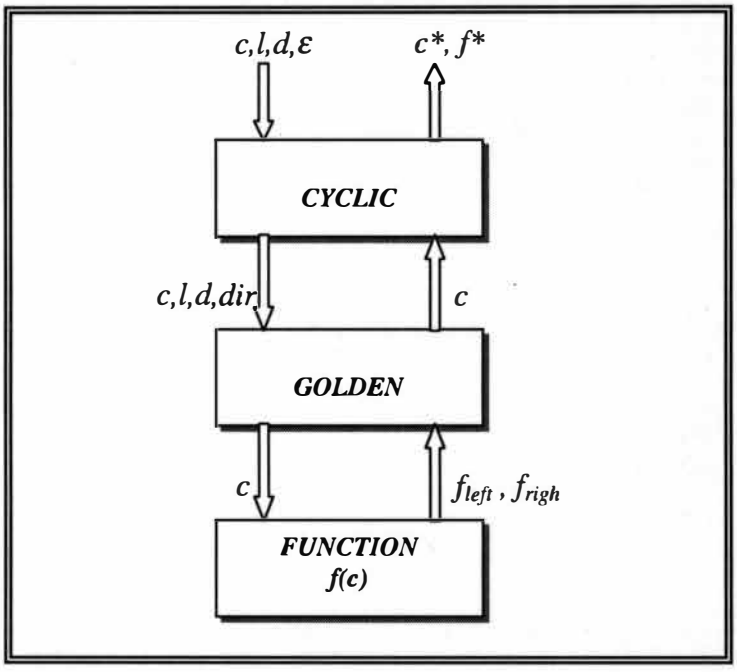

Figure 17. Inter-Module Communication for the Cyclic Coordinate Algorithm.

1.6 Some Mathematical Operations

In this section some basic operations on matrices and vectors, applied further as image processing tools, are explained.

1.6.1 Inner Product

Let U and V be vectors in R^n: $U = (u_1, u_2,\ldots,u_n)$ and $V = (v_1, v_2,\ldots,v_n)$. The inner or dot product of U and V, denoted by $U.V$ or $<U,V>$, is the scalar obtained by multiplying corresponding components and adding the resulting products.

$$U.V = <U,V> = u_1.v_1 + u_2.v_2 + \ldots + u_n.v_n \qquad (1.6.1\text{-}1)$$

U and V are said to be orthogonal or perpendicular if their dot product is zero: $U.V=0$.

1.6.2 Norms

Let U be a vector in R^n: $U = (u_1, u_2,\ldots,u_n)$ and A be a matrix in $R^m \times R^n$: $A = [a_{ij}]$ where $i=1,\ldots,m$ and $j = 1,\ldots,n$, then the norms of the vector U and the matrix A are defined as follows:

1. **Vector norm** or the length of the vector U, written $\|U\|$, is the nonnegative square root of $U.U$ as

$$\|U\| = \sqrt{U \cdot U} = \sqrt{< U, U >} = \sqrt{u_1^2 + u_2^2 + \cdots\cdots + u_n^2} \qquad (1.6.2-1)$$

The norm of vector U which is actually the distance between vector U and vector zero, is obtained by root square of inner product $<U,U>$.

2. **Matrix norm**, written $\|A\|$, is the minimum value of k such that

$$\|A \cdot X\| \le k\|X\| \qquad (1.6.2-2)$$

Geometrically, multiplication by a matrix A changes the length of a vector. Choose the vector X_0 whose length is increased the most, then $\|A\|$ is the ratio of the length of $A.X_0$ to length of X_0. Two major properties of any matrix norm are

$$\begin{cases} 1) \quad \|A \cdot X_0\| \le \|A\| \cdot \|X_0\| \\ 2) \quad \|A\| = 0 \quad \textit{iff} \quad A = 0 \end{cases} \qquad (1.6.2-3)$$

1.6.3 Distance and Angle Definitions in Inner Product Space

If U and V are two n-dimensional vectors defined in vector space R^n, then the distance between two vectors U and V is defined by Equation (1.6.3-1). Where $d(U,V)$ is the distance between vectors $U = (u_1, u_2,\ldots,u_n)$ and $V = (v_1, v_2,\ldots,v_n)$, which can be also considered as the norm of vector U-V, written $\|U\text{-}V\|$.

$$d(U,V) = \|U - V\| = \sqrt{(U_1 - V_1)^2 + (U_2 - V_2)^2 + \cdots\cdots + (U_n - V_n)^2} \qquad (1.6.3-1)$$

The angle between these two vectors U and V is defined by Equation (1.6.3-2). If U and V are orthogonal, then the inner product $<U,V>$ is zero and consequently the angle between the two vectors is 90^o degree.

$$\theta = COS^{-1}\left[\frac{<U,V>}{\|U\| \cdot \|V\|}\right] \qquad (1.6.3-2)$$

1.6.4 Statistical Operation

Let U be a vector in R^n: $U = (u_1, u_2,\ldots,u_n)$, then operators *max, min, mean, median* are defined over components of vector as follows:

1. **Operator '*max*'.** Maximum operation is defined on vector U by specifying maximum component u_i of U.

$$u_i = \max(U) \qquad where \qquad u_i \geq u_j \qquad for \quad j = 1,2,\ldots,n \qquad (1.6.4-1)$$

2. **Operator *'min'*.** Minimum operation is defined on vector U by specifying minimum component u_i of U.

$$u_i = \min(U) \qquad where \qquad u_i \le u_j \qquad for \quad j = 1,2,\ldots,n \qquad (1.6.4-2)$$

3. **Operator *'mean'*.** Mean operation is defined by averaging of components of vector U.

$$u_{avg} = mean(U) \qquad where \qquad u_{avg} = \frac{1}{n}\sum_{i=1}^{n} u_j \quad for \quad j = 1,2,\ldots,n \qquad (1.6.4-3)$$

4. **Operator *'median'*.** Median operation is defined on vector U by, (a) increasingly sorting the components, ordering components of U and (b) finding the center value. This operation is expressed as

$$u_{med} = median(U) \qquad (1.6.4\text{-}4)$$

This operation can be easily understood by Figure 18.

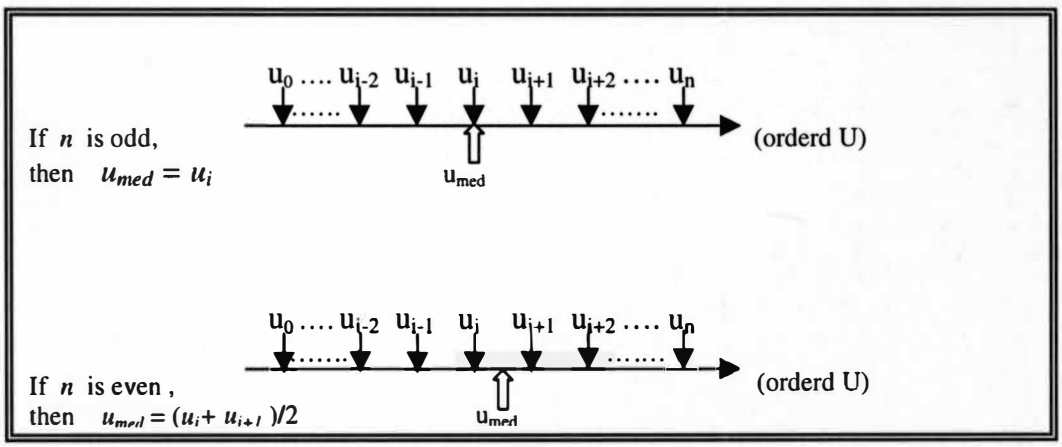

Figure 18. Illustration of Median Operation.

1.6.5 Mean and Square Errors

If e is a matrix $M \times N$, considered as a error between two matrices $A = [a_{ij}]$ and $B = [b_{ij}]$ for $i=1,\ldots,M$ and $j = 1,\ldots,N$, then e is defined as

$$e = |A - B| = [e_{ij}] \qquad such\ that \quad e_{ij} = \left|a_{ij} - b_{ij}\right| \geq 0 \qquad (1.6.5-1)$$

$E(m,n)$, mean error at pixel (m,n) can be obtained by

$$ME(m,n) = \underset{i,j}{mean}\left\{e_{ij}\right\} \qquad for \begin{cases} i = 1,\ldots,m \\ j = 1,\ldots,n \end{cases} \qquad (1.6.5-2)$$

Consequently, total mean error TME is a mean error at point (M,N) as

$$TME = ME(M,N) = \underset{i,j}{mean}\left\{e_{ij}\right\} \qquad for \begin{cases} i = 1,\ldots,M \\ j = 1,\ldots,N \end{cases} \qquad (1.6.5-3)$$

Let e be an array of $M \times N$ considered as a error matrix, then the square error can be expressed as

$$SQerror = \|e\|^2 \qquad (1.6.5\text{-}4)$$

The term $\|e\|$ is the norm of matrix e defined by Equation (1.6.5-1). In the case of e is a vector, then the above defined square error represents the length of e.

1.6.6 Two Dimensional Correlation

Consider two matrices $A = [a_{ij}]$ and $B = [b_{ij}]$ for $i=1,\ldots,M$ and $j = 1,\ldots,N$, then two dimensional correlation between A and B matrices is defined as

$$TDC = \frac{\sum_i \sum_j a_{ij} \cdot b_{ij}}{\sqrt{\sum_i \sum_j a_{ij}^2 \cdot \sum_i \sum_j b_{ij}^2}} \qquad for \begin{cases} i = 1,2,\ldots,M \\ j = 1,2,\ldots,N \end{cases} \qquad (1.6.6-1)$$

1.6.7 The *t*-norm, *t*-conorm, and Aggregation Operators

The *t*-norm T and the *t*-conorm S are two algebraic operators defined over the continuous interval [0,1] by taking the combination of algebraic *product* (.), *sum* (+), *min* ($\wedge$) and *max* ($\vee$). These operators map the 2-dimentional point $(x,y) \in [0,1] \times [0,1]$ to the point $z \in [0,1]$. Some *t*-(co)norm operators are given in Table 2.

$$\begin{cases} (x,y) \xrightarrow{T} z \\ \\ (x,y) \xrightarrow{S} z \end{cases} \qquad where \qquad x,y,z \in [0,1] \qquad (1.6.7-1)$$

The *t*-norm operator *T* must satisfy at least the properties called axiomatic skeleton for all $x,y,z \in [0,1]$. These properties are (a) boundary conditions: $T(x,1) = x$ and $T(x,0) = 0$, (b) monotonicity: if $y \le z$, then $T(x,y) \le T(x,z)$, or strict monotonicity: if $x_1 \le x_2$ and $y_1 \le y_2$, then $T(x_1,y_1) \le T(x_2,y_2)$, (c) commutativity: $T(x,y) = T(y,x)$, and (d) associativity: $T(x,T(y,z)) = T(T(x,y),z)$.

The *t*-conorm operator *S* must also satisfy at least the properties of axiomatic skeleton for all $x,y,z \in [0,1]$. These properties are (a) boundary conditions: $S(x,1) = 1$ and $S(x,0) = x$; (b) monotonicity: if $y \le z$, then $S(x,y) \le S(x,z)$, or strict monotonicity: if $x_1 \le x_2$ and $y_1 \le y_2$, then $S(x_1,y_1) \le S(x_2,y_2)$; (c) commutativity: $S(x,y)$

$= S(y,x)$; and (d) associativity: $S(x,S(y,z)) = S(S(x,y),z)$.

Table 2

Illustration of Some *t*-norms and *t*-conorm

Operators	***t*-norm $T(x,y)$**	***t*-conorm $S(x,y)$**
Standard operators	Min: $min(x, y)$, $(x \wedge y)$	Max: $Max(x, y)$, $(x \vee y)$
Algebraic operators	Product: $x.y$	Sum: $x+y-x.y$
Bounded operators	Difference: $Max(0,x+y-1)$, $(0 \vee (x+y-1))$	Sum: $Min(1,x+y)$, $(1 \wedge (x+y))$

The Quasi *t*-norm Q_t and the Quasi *t*-conorm Q_s [17] are the special kinds of *t*-norm and *t*-conorm operators which meet all above mentioned axiomatic skeleton properties except the associativity. These operators are represented as

$$\begin{cases} Q_t(x,y) = T\left(T(x,y), S(x,y)\right) & (1.6.7-2) \\ Q_{st}(x,y) = S\left(S''(x,y), T(x,y)\right) & \\ \textit{where} \quad x,y \in [0,1],\ Q_t \xleftrightarrow{dual} Q_s,\ T \xleftrightarrow{dual} S,\ T \xleftrightarrow{dual} S'',\ S \xleftrightarrow{dual} T'' & \end{cases}$$

T, T', T" are different *t*-norms and *S, S', S"* are also different *t*-conorms, If the operator *T* and *S* are Demorgan's like dual, then $S=S''$ and $T=T''$. Quasi *t*-norms and Quasi *t*-conorms do not necessarily meet associativity property, therefore they are not necessarily *t*-norms and *t*-conorms. Q_t and Q_s are Demorgan's like dual, therefore we

have $Q_s(x,y) = 1- Q_t(1-x,1-y) = 1- T'(T(1-x,1-y) , S(1-x,1-y))$. The Quasi t-norm Q_t satisfies at least boundary conditions, strict monotonicity, and commutativity properties of other *t*-norms as well as the property of inequality $Q_t(x,y) \leq T(x,y)$. Also The Quasi *t*-conorm Q_s satisfies at least boundary conditions, strict monotonicity, and commutativity properties of other t-norms as well as the property of inequality $Q_s(x,y) \geq S(x,y)$. Table 3 illustrates how to make the desired *t*-(co)norms.

Table 3

Illustration of Constructing the Quasi Operators Using Some *t*-(co)norms

$T(x,y)=a$	$S(x,y)=b$	$T'(x,y)$	**Quasi *t*-norm** $Q_t(x,y)$
$x.y$	$x+y-x.y$	$a.b$	$x.y(x+y-x.y)$
Hamacher product: $\frac{x+y}{x+y-x\cdot y}$	Hamacher sum: $\frac{x+y-2x.y}{1-x\cdot y}$	$a.b$	$\frac{(x\cdot y)\cdot(x+y-2x\cdot y)}{(x+y-x\cdot y)\cdot(1-x\cdot y)}$
$T''(x,y)=c$	$S''(x,y)=d$	$S'(x,y)$	**Quasi *t*-conorm** $Q_s(x,y)$
$x.y$	$x+y-x.y$	$c+d+c.d$	$X+y-x.y(x+y-x.y)$
Hamacher product: $\frac{x+y}{x+y-x\cdot y}$	Hamacher sum: $\frac{x+y-2x.y}{1-x\cdot y}$	$c+d+c.d$	$\frac{(x+y)^2+(x\cdot y)\cdot(1-2x-2y+x\cdot y)}{(x+y-x\cdot y)\cdot(1-x\cdot y)}$

Aggregation operator *g* is an averaging operator defined over the continuous interval [0,1] by taking the combination of algebraic *product* (.), *sum* (+), *min* ($\wedge$) and *max* ($\vee$). These operators map the *n*-dimensional point $(x_1,\ldots, x_n) \in [0,1]^n$ to the point $z \in [0,1]^n$.

$$(x_1,\ldots,x_n) \xrightarrow{g} z \qquad \textit{where} \qquad x_1,\ldots,x_n,z \in [0,1] \qquad (1.6.7-3)$$

All aggregation operations must satisfy at least the, (a) boundary conditions: $g(0,0,\ldots,0) = 0$ and $g(1,1,\ldots,1) = 1$, (b) monotonicity: if $x_n \le y_n$, then $g(x_1,\ldots,x_n) \le g(y_1,\ldots,y_n)$, and (c) continuity. Table 4 shows some two-dimensional averaging operators dented by M.

Table 4

Illustration of Some Averaging Operators

Averaging Operator	**Arithmetic Mean**	**Root Square Mean**	**Harmonic Mean**	**Quasi Linear Mean**
$M(x,y)$	$\frac{x+y}{2}$	$\sqrt{x \cdot y}$	$\frac{2x \cdot y}{x+y}$	$\sqrt[p]{\frac{1}{2} \cdot (x^p + y^p)}$ $0 \le p \le 1$

The t-norms and t-conorms are the tools to define respectively the intersection and union between two fuzzy set A and B. The aggregation operators are also used to combine the fuzzy sets such a way to produce the desired fuzzy set. In Chapter II we apply these operators to modify an intensity image to obtain the desired intensity image. Since intensity image processing is defined as an operation over the intensity interval [0,1] (with L gray level), then t-norm, t-conorm, and the aggregation operators can be used as the tools of image modification. We will also discuss about how these operators can be applied for extension of the two-valued algebraic operators (Boolean algebra) to n-valued algebraic operators.

The standard *t*-norm, *min* operator, results in the biggest value among the other t-norms. Also the standard *t*-conorm, *max* operator, generates the least value among the other *t*-conorms. If the aggregation operator g satisfies the additional property of idempotency which is $g(x_1, x_1, \ldots, x_1) = x_1$, then the values of all aggregation operations fall between two values obtained by the standard t-norm and *t*-conorm operators, *max* and *min*. Also As said, Since Quasi t-norms Q_t and Quasi *t*-conorms Q_s does not necessarily satisfy the associativity property, They are not necessarily t-norms and *t*-conorms. However, the following inequality is true between Q_t, Q_s, T, S operators and the standard operators, *min* ($\wedge$) and *max*($\vee$).

$$Q_t(x,y) \le T(x,y) \le min(x,y) \le g(x,y) \le max(x,y) \le S(x,y) \le Q_s(x,y) \qquad (1.6.7\text{-}4)$$

As seen, the Quasi t-norm Q_t and its dual obtained by combinations of t-norms and *t*-conorms. Consequently, by combinations of either t-norms T_1, T_2 or *t*-conorms S_1, S_2, we can also define different operators such as the t-norm A_t and its dual *t*-conorm A_s or the t-norm B_t and its dual *t*-conorm B_s.

$$\begin{cases} \begin{cases} A_t(x,y) = T\big(T_1(x,y), T_2(x,y)\big) & (1.6.7-5) \\ A_s(x,y) = S\big(S_1(x,y), S_2(x,y)\big) & (1.6.7-6) \end{cases} \\ \begin{cases} B_t(x,y) = S\big(T_1(x,y), T_2(x,y)\big) & (1.6.7-7) \\ B_s(x,y) = T\big(S_1(x,y), S_2(x,y)\big) & (1.6.7-8) \end{cases} \\ \text{where} \quad x,y \in [0,1],\ A_t \xleftrightarrow{dual} A_s,\ T \xleftrightarrow{dual} S,\ T_1 \xleftrightarrow{dual} S_1,\ T_2 \xleftrightarrow{dual} S_2 \end{cases}$$

The operators A_t and B_t must meet at least the boundary conditions, strict monotonicity and commutativity properties of t-norms plus the inequality property $A_t(x,y) \leq min(T_1(x,y),T_2(x,y)) \leq min(x,y)$ for operator A_t and $B_t(x,y) \geq max(T_1(x,y),T_2(x,y))$ for operator B_t. Also the operators A_s and B_s must satisfy the boundary conditions, strict monotonicity and commutativity properties of t-conorms plus the inequality property $A_s(x,y) \geq max(S_1(x,y),S_2(x,y)) \geq max(x,y)$ for operator A_s and $B_s(x,y) \leq min(T_1(x,y),T_2(x,y))$ for operator B_s. A_t, A_s, B_t, B_s are not necessarily associative.

Compensatory operator *C* was first defined by Zimmerman to model the human use of the "and" more precisely. Since the use of the operator *min* ($\wedge$) and algebraic product (.) is not very appropriate for this purpose, he defined the compensatory operators as: (a) by taking the combination of algebraic product and sum for example, $(x.y)^{1-p}$. $(x_+ y\text{-}x.y)^p$. (b) by taking the convex combination of *min* ($\wedge$) and *max* ($\vee$) operators such as, $(x \wedge y)(1\text{-}p) + (x \vee y)p$. In general, we can define the compensatory operator as

$$\begin{cases} C(x,y) = F(x,y)^{1-p} \cdot G(x,y)^{p} & (1.6.7-9) \\ C(x,y) = F(x,y) \cdot (1-p) + G(x,y) \cdot p & (1.6.7-10) \\ where \quad x,y,p \in [0,1] \quad and \quad F,G \in \{T,S,Q_t,Q_s,A_t,A_s,B_t,B_s,M,S_s\} \end{cases}$$

The operators F and G can be the above defined operators, T, S, Q_t, Q_s, A_t, A_s, B_t, B_s, the averaging operators M (aggregation operators $g(x,y)$) and symmetric sums

operators can be defined by using different combinations of above mentioned operators. The compensatory operators C and its dual $C^*=1-C(1-x,1-y)$ must satisfy at least the boundary conditions $C(0,0)=C^*(0,0)=0$ and $C(1,1)=C^*(1,1)=1$, strict monotonicity and commutativity properties. Besides, They must also meet continuity and inequality as: if $F(x,y) \le G(x,y)$ then $F(x,y) \le C(x,y) \le G(x,y)$ for operator C, and if $F^*(x,y) \le G^*(x,y)$ then $F^*(x,y) \le C^*(x,y) \le G^*(x,y)$ for operator C^*.

Generalized compensatory operator C_m is defined by averaging operation M between previously defined F and G as given in Equation (1.6.7-11). The dual of C_m denoted by C_m^* can be derived by converting M, F, G to their dual M^*, F^*, G^* respectively.

$$\begin{cases} C_m(x,y) = M(F(x,y), G(x,y)) & (1.6.7-11) \\ C_m^*(x,y) = M^*(F^*(x,y), G^*(x,y)) & (1.6.7-12) \\ \text{where} \quad C_m \xleftrightarrow{dual} C_m^*,\ M \xleftrightarrow{dual} M^*,\ F \xleftrightarrow{dual} F^*,\ G \xleftrightarrow{dual} G^* & \\ \text{for} \quad x,y,p \in [0,1] \quad \text{and} \quad F,G \in \{T, S, Q_t, Q_s, A_t, A_s, B_t, B_s, M, S_s\} & \end{cases}$$

The compensatory operator C_m and its dual C_m^* must satisfy at least the (a) boundary condition: $C(0,0)=C^*(0,0)=0$; (b) strict monotonicity; (c) commutativity; and (d) increasing, properties. Besides, They must also meet inequality such that if $F(x,y) \le G(x,y)$ then $F(x,y) \le C_m(x,y) \le G(x,y)$ for operator C, and if $F^*(x,y) \le G^*(x,y)$ then $F^*(x,y) \le C_m^*(x,y) \le G^*(x,y)$ for operator C^*. Table 5 gives the idea of how to construct compensatory operators from formerly defined operators T, S, Q_t,

Q_s, A_t, A_s, B_t, B_s, M (aggregation operators $h(x,y)$), and symmetric sums S_s which will be discussed later.

Table 5

Illustration of Some Generalized Compensatory Operators

$F(x,y)$	$G(x,y)$	$M(x,y)$	$C_m(x,y)$
$x.y$	$x \vee y$, $max(x,y)$	Arithmetic Mean: $\frac{F+G}{2}$	$\frac{x \cdot y + max(x,y)}{2}$
$\sqrt{x \cdot y}$	$\frac{x+y}{2}$	Harmonic Mean: $\frac{2F \cdot G}{F+G}$	$\frac{2 \cdot \sqrt{x \cdot y} + x + y}{4}$
Hamacher product: $\frac{x+y}{x+y-x \cdot y}$	Hamacher sum: $\frac{x+y-2x.y}{1-x \cdot y}$	Root Square Mean: $\sqrt{F \cdot G}$	$\sqrt{\frac{(x \cdot y) \cdot (x+y-2x \cdot y)}{(x+y-x \cdot y) \cdot (1-x \cdot y)}}$
$x.y$	$x + y - x \cdot y$	Quasi Averaging: $\sqrt[p]{\frac{F^p + G^p}{2}}$ $0 \le p \le 1$	$\sqrt[p]{\frac{(x \cdot y)^p + (x+y-x \cdot y)^p}{2}}$

Self-dual operator D is the special case of generalized compensatory operators in which M is defined by the operator $M(F,G)=(F+G)/2$ such that M is an arithmetic mean derived from convex combination of F and G using compensatory operator of $(F \wedge G).(1-p)+(F \vee G)p$, for $p=0.5$. The operators F and G are dual. Therefore, $G=F^*$ and finally, we can generally define the self-dual operators as given by Equation (1.6.7-13). The operator F is one of the previously defined operators, T, S, Q_t, Q_s, A_t, A_s, B_t, B_s, M, and symmetric sums S_s which will be discussed later.

The self dual operators $D(x,y)$ and its dual $D^*(x,y)$ must satisfy at least the, (a) boundary conditions $D(0,0)=D^*(0,0)=0$ and $C(1,1)=D^*(1,1)=1$; (b) commutativity; (c) continuity and increasing; (d) self-duality $D(x,y)= D(1-x,1-y)=D^*(x,y)$; and (e) $D(x,1-x)$, properties.

$$\begin{cases} D(x,y) = \dfrac{F(x,y) + F^*(x,y)}{2} \\ where \quad x,y \in [0,1] \quad and \quad F \in \left\{T, S, Q_t, Q_s, A_t, A_s, B_t, B_s, M, S_s\right\} \end{cases} \qquad (1.6.7-13)$$

Symmetric sum S_s is the special case of self dual operator which is first defined by Silvert. The general form of symmetric sums is given by Equation (1.6.7-14). The operator F is one of the previously defined operators, T, S, Q_t, Q_s, A_t, A_s, B_t, B_s, M. Some examples of symmetric sum operators $S_s(x,y)$ are given in Table 6.

$$\begin{cases} S_s(x,y) = \dfrac{F(x,y)}{F(x,y) + F(1-x,1-y)} \\ where \quad x,y \in [0,1] \quad and \quad F \in \left\{T, S, Q_t, Q_s, A_t, A_s, B_t, B_s, M, S_s\right\} \end{cases} \qquad (1.6.7-14)$$

Table 6

Illustration of Some Symmetric Operators

Type of F(x,y)	***F(x,y)***	***$S_s(x,y)$***
t-norm, T	$x.y$	$\dfrac{x \cdot y}{1 - x - y + 2 \cdot x \cdot y}$
t-conorm, S	$Max(x,y)$	$\dfrac{max(x,y)}{1 + \lvert x - y \rvert}$
Quasi t-norm, Q_t	$x.y(x+y-x.y)$	$\dfrac{x \cdot y \cdot (x + y - x \cdot y)}{1 - x - y + 2 \cdot x \cdot y \cdot (x + y - x \cdot y)}$

The symmetric operator $S_s(x,y)$ and its dual $S_s^*(x,y)$ must satisfy at least, (a) all properties defined for self-dual operators; (b) the condition, $S_s(x,1\text{-}x)=0.5$; and (c) the continuity, if $F(0,x)=0$ for $\forall x \in [0,1]$, then $S_s(0,1)$ is not defined, that is, $S_s(x,y)$ is not continuous at points (0,1) and (1,0), otherwise $S_s(x,y)= S_s(x,y)=0.5$.

CHAPTER II

QCW EDGE DETECTION

In this chapter an edge characteristic function (*ECF*) is proposed using a structure of ideal edge patterns based on quadruple child windowing (*QCW*) within a specified block of an image. Also, a correlation, using distance and angle, between *QCW* pattern (defined within processing block) and an ideal edge pattern is applied to create an edge estimator within a processing block of an intensity image.

2.1 Intensity or Gray Tone Distance

Let X_{ij} and X_{mn} be the respectively intensities (gray levels) of $(i,j)^{th}$ and $(m,n)^{th}$ pixels. The intensity distance is defined as

$$d((m,n),(i,j)) = | X_{mn} - X_{ij}| \qquad (2.1\text{-}1)$$

Thus, the difference between the intensity values is called intensity distance. This is applied in section 2.1.3 to define *ECF* with respect to four defined distances within a specified block of an image based on *QCW*.

2.1.1 Analyzing Structure (Morphological Operation)

Morphological operations provide information concerning the form or structure of an image. Morphology is mathematically introduced by Matheron and

Serra [10]. The morphological operators decompose an image to its main features and characteristics of its objects. Operations on binary images such as dilation and erosion (respectively adding and removing pixels at the boundaries of objects), perimeter determination (finding boundaries of objects), and area estimation (estimating for total area of the objects) are examples of morphological operations. The operations are applied to certain sub-groups of pixels within the running block(called filter window). We investigate sub-grouping of the pixels on/within a $W \times W$ block of an image based on an operation called quadruple child windowing (*QCW*). *QCW* divides each $W \times W$ block into four sub-groups, then applies certain operations to obtain desired features such as edges.

2.1.2 Presentation of Binary Edge Patterns

Let B be a running block 3×3 over an binary image BI at point (m,n) as illustrated in Figure 3. As known, edges are points where the intensity changes abruptly. To present edge patterns in a binary image, without loss of the generality, the edge points can be considered as white pixels surrounded by some black pixels in neighborhoods. Consider block B with a white pixel (high intensity) in the center. The possible structures of edge patterns can be classified as Figure 19.

The illustrated configurations for classes 1 and 2 denote the vertical edge patterns in a binary image. Similarly, classes 3 and 4 indicate horizontal edge patterns. Therefore, according to the above classification, if any 3×3 block within a

binary image matches with one of these 9 patterns then the middle pixel of that block is considered as an edge pixel.

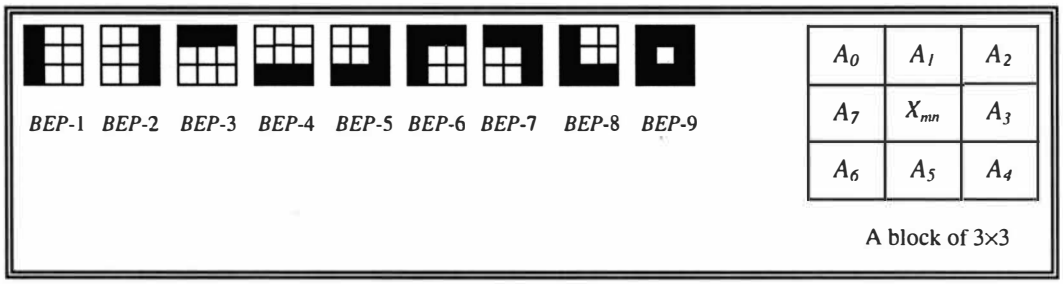

Figure 19. Presentation of Nine Binary Edge Patterns Within a Block of 3×3.

Using the intensity distance Equation (2.1-1), each of above defined edge patterns can be coded as 8-bit words (or vector), $[d_0, d_1, d_2, d_3, d_4, d_5, d_6, d_7]$, where the components of this vector denote the eight intensity distances between middle pixel (m,n) and its eight neighborhoods. Generally these distances are found by

$$d_k = d_k(m,n) = | X_{mn} - A_k | \quad for \quad k=0,1,2,\ldots,7 \qquad (2.1.2\text{-}1)$$

A_k s are the intensities of neighbors of the middle pixel (m,n). This is illustrated in Figure 20.

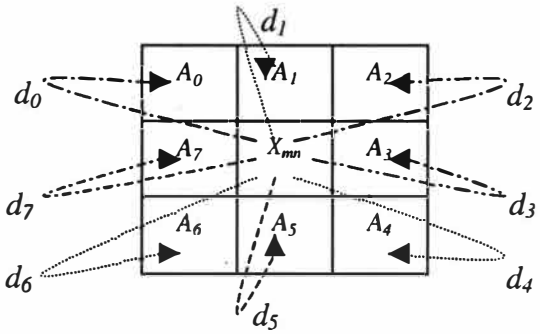

Figure 20. Presentation of Intensity Distances Within the Block of 3×3.

According to this definition we can assign 9 codes for all 9 edge patterns as given in Table 7.

Table 7

Binary Edge Pattern Codes in Block of 3×3

Classes	BEP-1	BEP-2	BEP-3	BEP-4	BEP-5	BEP-6	BEP-7	BEP-8	BEP-9
Codes	1 0 0 0 0 0 1 1	0 0 1 1 0 0 0 0	1 1 1 0 0 0 0 0	0 0 0 0 1 1 1 0	0 0 1 1 1 1 1 0	1 1 1 0 0 0 1 1	1 1 1 1 1 0 0 0	1 0 0 0 1 1 1 1	1 1 1 1 1 1 1 1

In edge extraction of a binary image, the edge characteristic function f can be derived according to the assigned edge pattern codes. This can be achieved by logic design (using Karnough-map) to define f in terms of $d_0, d_1, d_2, d_3, d_4, d_5, d_6, d_7$.

Binary image edge detector can be easily designed to find edge pixels over a binary image using f. As illustrated in Figure 21, the detector has eight binary inputs (eight distances obtained from each 3×3 processing block as inputs) and one binary output, Y. If any processing block (running block over a binary image) matches one of the 9 edge patterns, then the output of detector goes to 1 (the intensity value of middle pixel X_{mn}=1); otherwise the output is zero.

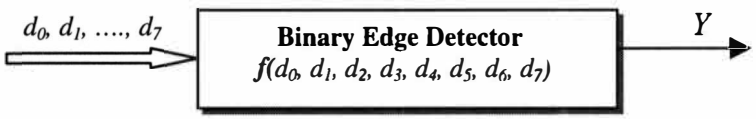

Figure 21. A Binary Edge Detector for 3×3 Block.

In the case of a noisy image this kind of detector has errors and may detect a noise pixel as edge. Therefore, noise removal algorithms must be used before using this method for edge detection. One technique by which we can remove the noise as well as decrease the number of inputs to the edge detector is to use representative pixels of sub-windows. That is, by dividing the pixels on/within the main block (window) into smaller groups (sub-windows), it is possible to find an appropriate representative pixel for each sub-group. Further we will find, to present the edge patterns in each processing block, we need at least four representatives neighboring the middle pixel (m,n). Thus, we choose four sub-widows within the block B of an image and we call these quadruple child windows, (QCW). We apply noise removal operations over each sub-window to find a proper representative intensity for each sub-window. Finally, by determining four intensity distances of d_1, d_2, d_3, d_4 between the middle pixel (m,n) and four representatives, we derive a four dimension ECF, written $f(d_1, d_2, d_3, d_4)$, to detect the edge within any desired size of main block B.

2.1.3 Quadruple Child Windowing

Let B be a running $W \times W$ block (where W is odd) over an intensity image II at point (m,n). This block B can be defined as

$$B = [X_{ij}] \qquad for \quad \begin{cases} i = m - \dfrac{W-1}{2}, \ldots, m + \dfrac{W-1}{2} \\ j = n - \dfrac{W-1}{2}, \ldots, n + \dfrac{W-1}{2} \end{cases} \qquad (2.1.3-1)$$

X_{mn} denotes the intensity value of the middle pixel of the processing block. Now consider four specified child windows B_1, B_2, B_3 , B_4 defined inside the main block B. Each child window contains pixels X_{ij} on/within the main block B-{(m,n)}. The QCW on block B at pixel (m,n) is a partition which results in four groups of pixels as B_k ={(p,q),}for k=1,2,3,4 where the elements $(p,q)\in$ B-{(m,n)}. Child windows are exhaustive and mutually exclusive. This is mathematically represented in Equation (2.1.3-2).

$$\begin{cases} 1) \quad B \xrightarrow{QCW} \left\{ \{B_k,\} \mid (m,n) \notin B_k \quad for \ k = 1,2,3,4 \right\} \\ 2) \quad \left\{ \{B_1 \cup B_2 \cup B_3 \cup B_4\} \cup \{(m,n)\} \right\} \subseteq B \\ B_1 \cap B_2 \cap B_3 \cap B_4 = \varnothing \end{cases} \qquad (2.1.3-2)$$

The structure of QCW (the configurations of these four child windows) within the running block B can be geometrically altered region by region over an image based on a specific application. For example, in an image smoothing algorithm, this structure can be fixed and for the edge detection may change region by region depending on the edge patterns within the block B.

We investigate the various structures of QCW (QCW patterns) within a main block B with different sizes of 3×3, 5×5, 7×7 as follows:

1. **Main Block of 3×3**. The possible QCW patterns within block 3×3 can be illustrated as shown in Figure 22. We consider these structures an standard QCW configurations within block 3×3.

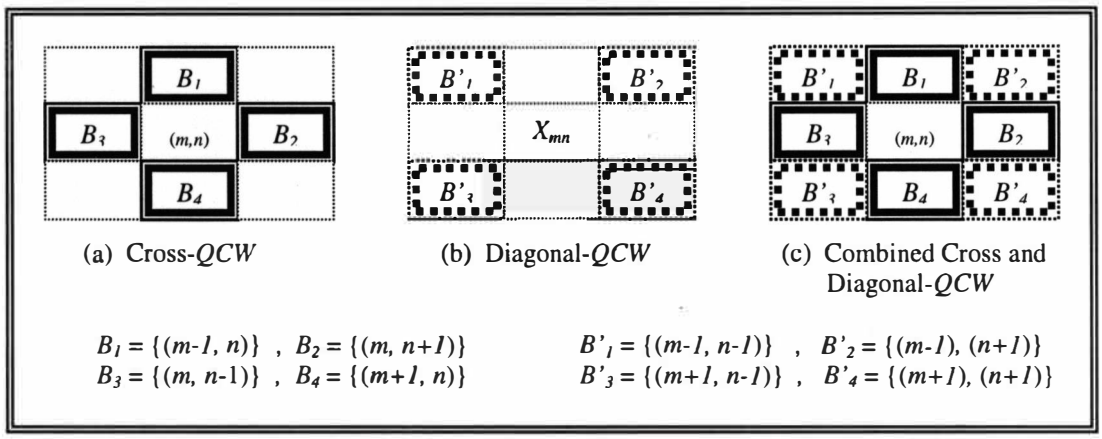

Figure 22. *QCW* Configurations Within a Block of 3×3.

As seen, some pixels on/within the block 3×3 participate in sub-grouping. parts *a* and *b* of Figure 22 illustrate respectively a cross-shaped and diagonal-shaped *QCW*. Further we will see the combination of the results obtained by pixel manipulation over cross-*QCW* and diagonal-*QCW* gives us a better result in edge detection. This combination of diagonal and cross *QCW* patterns is illustrated in part *c* of Figure 22. The type of structure of *QCW* affects the outcome of the operations over main block *B*. The cross-*QCW* results differ from the diagonal-*QCW* and also from the combination of cross and diagonal types. The result quality of each type depends on the edge pattern and the transition of gray scale within the main block *B*.

2. **Main Block of 5×5**. The possible structures for *QCW* patterns over block 5×5 are illustrated as Figure 23. We consider these structures an standard QCW configurations within block 5×5.

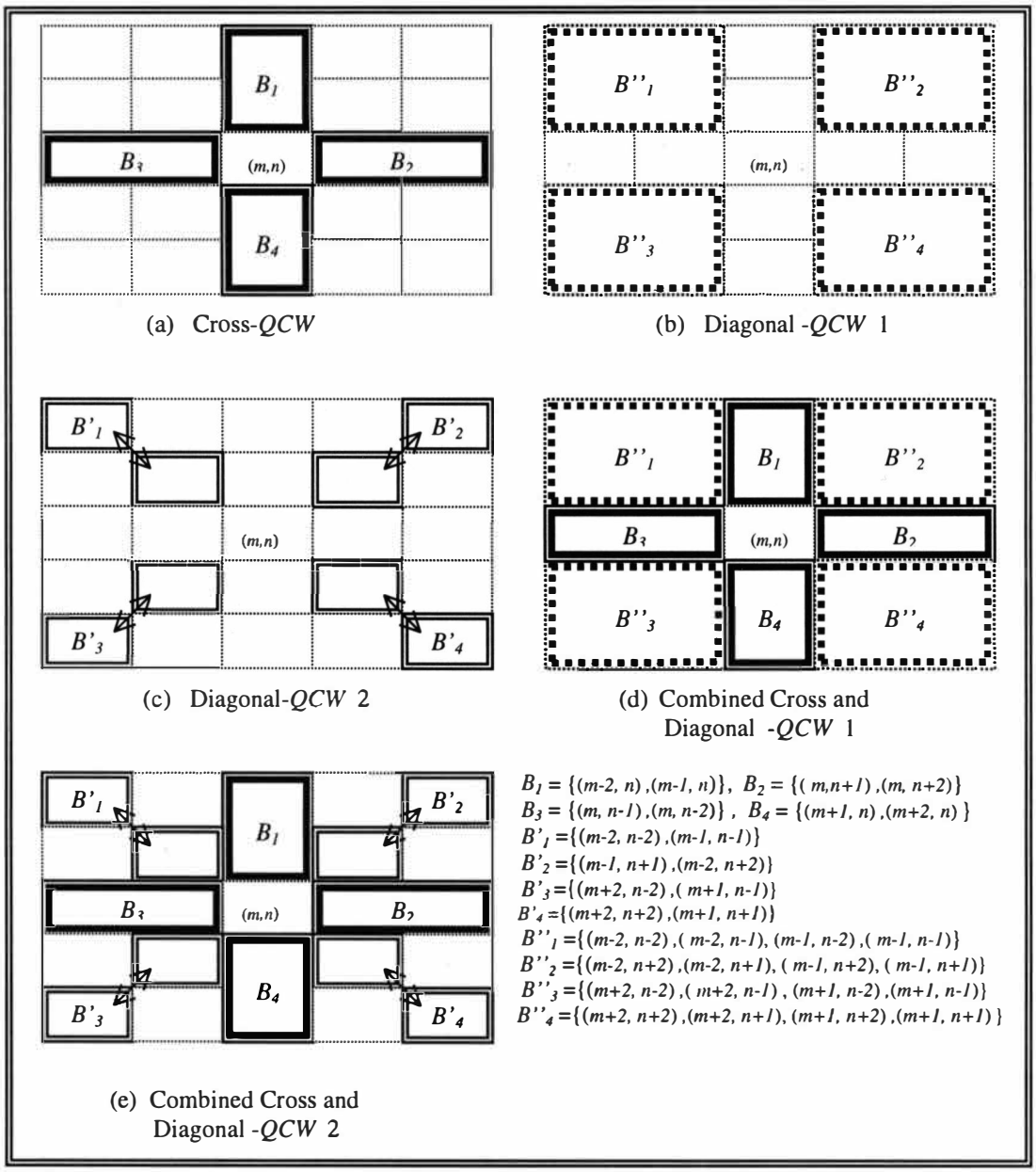

Figure 23. *QCW* Configurations Within a Block of 5×5.

The above *QCW* configurations are based on sub-grouping of the pixels which are diagonally or crossly located neighboring the middle pixel. Depending on specific applications, we may take all pixels into consideration in *QCW*. The possible morphological structures for 5×5 windows are illustrated in [10]. For example, one

possible configuration, which is applied for detecting the edge within a 5×5 block in Chapter IV, is illustrated in Figure 24.

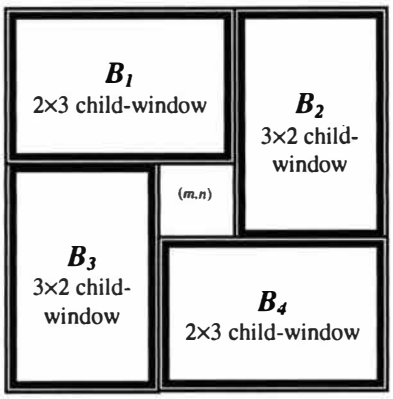

Figure 24. A Possible *QCW* Configuration (Non-Standard) Within a Block of 5×5.

3. **Main Block of 7×7**. The possible structures for *QCW* patterns over a 7×7 block can be easily figured. Each sub-window in a cross-*QCW* structure within a block of 7×7 consists of three pixels. Consequently, it may contain three or nine pixels in the two possible diagonal-*QCW* structures. The other configurations in which all pixels are involved in structure of *QCW* pattern are given in [10]. As the size of the block *B* increases, the number of pixels participating in *QCW* increases. This obviously helps to improve the noise removal, but it also diminishes the quality of the output in edge enhancement. We have applied 5×5 and 3×3 block processing for edge detection algorithms. In the case of processing a noisy image, a 5×5 block is adopted to remove the noise by child window filtering.

2.1.4 Child Window Processing

Let B_1, B_2, B_3, B_4 be an appropriate *QCW* over a $W \times W$ block B. Each B_k can be considered as a child-filter specified by an operation (modification) g on pixels belonging in each the child window. This operation may apply for removing the noise, increasing the contrast or for other purposes. The result of this operation is a scalar function of each child window (output of each child filter) is considered as the representative intensity value for that child window. Commonly used tools for the operation g include *max, min, median, mean* operators or any aggregation operator defined in section 1.6.7. In section 1.2.7, we defined a median filter as a noise removal tool, now we can apply median operation on pixels belonging to each child window to remove noise before edge detecting process. Applying median filtering over four child windows results in four scalar outputs Y_1, Y_2, Y_3, Y_4 representing four intensity representatives respectively relating to four child windows B_1, B_2, B_3, B_4. These representatives can be generally expressed by

$$Y_k = g\{ X_{ij} \mid (i,j) \in B_k \} \quad for \quad k = 1,2,3,4. \qquad (2.1.4\text{-}1)$$

By choosing an appropriate *QCW* pattern discussed in section 2.1.3, we apply median filtering over the four child windows to obtain Y_1, Y_2, Y_3, Y_4 as representatives of *QCW*. Consequently, *QCW* patterns which are equivalent to those *QCW* patterns introduced in section 2.1.3, can be reconstructed by means of representative pixel intensities Y_1, Y_2, Y_3, Y_4 in neighboring the middle pixel intensity X_{mn}. The possible *QCW* configurations are represented in Figure 25.

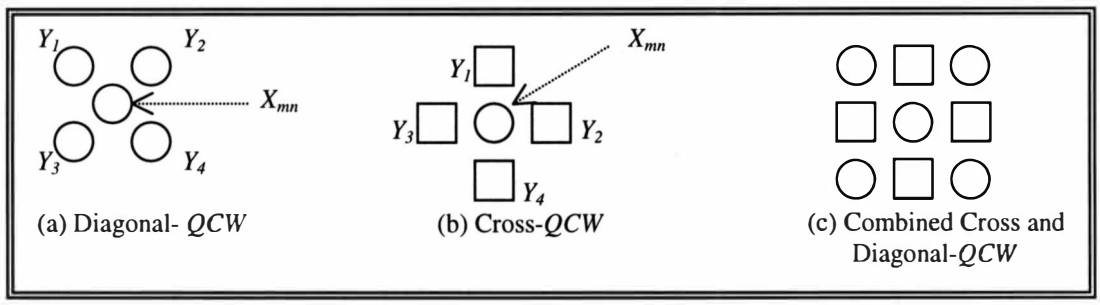

Figure 25. Illustration of QCW Configurations.

In case of processing of a noisy image, X_{mn} must be replaced with the representative intensity X'_{mn} obtained by the following operation g over the $B-(m,n)$. Operation g can be either defined by Equation 1.6.7-3 or chosen from Table 4.

$$X'_{mn} = g\{ X_{ij} \mid (i,j) \in \{B-(m,n)\} \} \qquad (2.1.4\text{-}2)$$

or

$$X'_{mn} = g\{Y_1, Y_2, Y_3, Y_4\} \qquad (2.1.4\text{-}3)$$

2.1.5 Presentation of Binary QCW-Edge Patterns

Assume B_1, B_2, B_3, B_4 denote an appropriate QCW within a $W \times W$ block B of a binary image. Also let Y_1, Y_2, Y_3, Y_4 be four intensity representatives of four child windows. Now we can represent possible binary QCW-edge patterns considering intensity values of middle pixel X_{mn} and the representatives Y_1, Y_2, Y_3, Y_4. Consider the diagonal configuration for QCW pattern illustrated in Figure 25. The physical binary edge patterns can be illustrated as Figure 26. Classes 1 and 2 (BEP_1 *and* BEP_2) represent vertical edge patterns while class 3 and 4 indicate horizontal edge patterns. In all nine defined configurations, edge points posses high intensity (white).

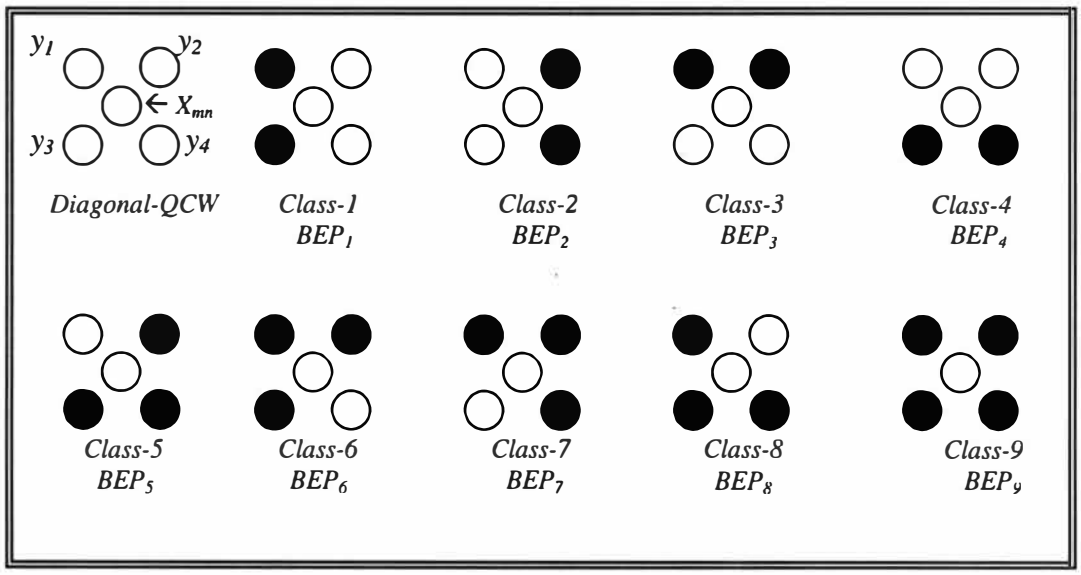

Figure 26. Presentation of Binary Diagonal *QCW*-Edge Pattern Configurations.

The cross configuration of *QCW* can be considered as a 45° degree rotation of the diagonal shape; that is, if we rotate an image 45° degree then the vertical and horizontal edges turn to diagonal edges. Now consider cross-shaped *QCW* as illustrated in Figure 2.4.1-1, then *QCW*-edge patterns based on the representative pixels Y_1, Y_2, Y_3, Y_4 and the middle pixel X_{mn} can be presented as Figure 27.

As seen in Figure 27 for binary cross *QCW*-edge pattern configurations, the patterns are characterized by a 45° degree clock-wise rotation of the respective diagonal *QCW* configurations from Figure 26. Classes 1 and 2 are results of rotation of the vertical edges and now they represent the edges in a northeast to southwest direction. Classes 3 and 4 are results of rotation of the horizontal edges and now they represent the edges in a northwest to southeast direction.

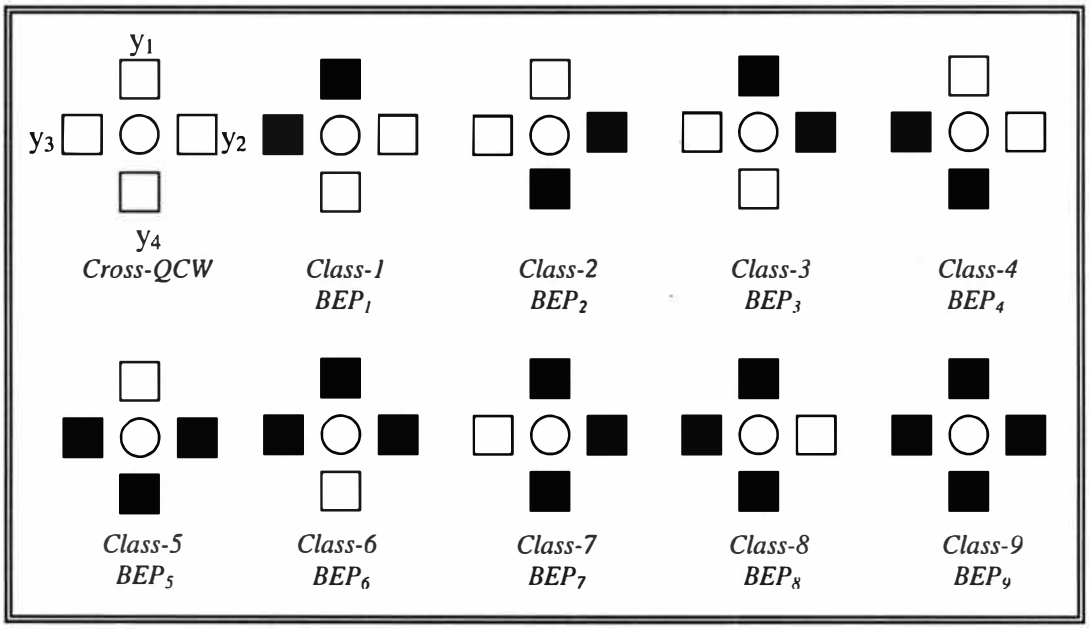

Figure 27. Presentation of Binary Cross *QCW*-Edge Pattern Configurations.

If any *QCW* pattern within a block *B* running over an binary image matches with one of the above ideal edge pattern classes, then the middle pixel X_{mn} is considered an edge point. This can be implemented by comparing the processing *QCW* pattern within block *B* with all nine ideal *QCW*-edge patterns. To achieve this purpose, we can assign a 4-bit code word addressing each of the above defined *QCW*-edge patterns, BEP_p for p=1,2,...,9. These code words can be meaningfully constructed by means of four intensity distances between the binary middle pixel intensity X_{mn} and the four binary representatives Y_1, Y_2, Y_3, Y_4. These distances are generally obtained by following Equation.

$$d_k = d_k(m,n) = | X_{mn} - Y_k | \quad for \quad k = 1,2,3,4. \qquad (2.1.5\text{-}1)$$

Y_k represents the result of operation g over the pixels belonging to child window B_k, (out put of child filter k-th). Here, the operation g is a median filtering as noise removal tool. These intensity distances d_1, d_2, d_3, d_4 are illustrated in Figure 28.

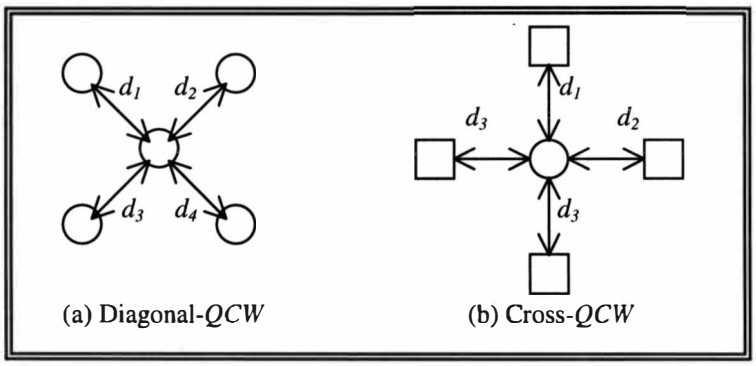

Figure 28. Intensity Distances in QCW- Patterns.

By convention, we consider that a black pixel possesses 0 intensity value and a white pixel has intensity 1. We can now assign a code word for each of the binary QCW-edge patterns given in Figure 26 and 27 using Equation (2.1.5-1). These words are tabulated in Table 8.

Table 8

Binary QCW -Edge Pattern Codes

Classes	BEP_1	BEP_2	BEP_3	BEP_4	BEP_5	BEP_6	BEP_7	BEP_8	BEP_9
Codes	1010	0101	1100	0011	0111	1110	1101	1011	1111

As seen in Table 8, the nine classes of edge patterns are specified by 9 code words BEP_p for p=1,2,..,9. These code words can be generally defined as

$$BEP_p = [d_k,]_p \qquad for\ p=1,2,\ldots,9 \ \text{ and } \ k=1,2,3,4 \qquad (2.1.5\text{-}2)$$

The element d_k is defined by Equation (2.1.5-1). As a comparison, the code word assigned for *QCW*-edge patterns in Table 8 possess fewer components than those code words given in Table 7. Since the number of intensity distances within the block B is decreased from at least 9 to 4 using *QCW* technique, the determination of binary *ECF* based on intensity distances d_1, d_2, d_3, d_4 is more efficient. This Binary edge characteristic function is determined in next section.

2.1.6 QCW-Edge Characteristic Function for Binary Images

In preceding sections, we have explained *QCW* over a $W\times W$ block B of a binary image, introduced the possible configurations of binary edge patterns based on *QCW*, and finally, assigned a 4-bit code word for each edge pattern as an identification based on defined intensity distances within *QCW* as d_1, d_2, d_3, d_4.

Now our special attention is given to derive a logical function in terms of d_1, d_2, d_3, d_4 by using the tools of switching theory. These tools include switching algebra, truth tables, and the minimization procedures. By employing these tools, we derive the logical function considered as the binary *QCW* edge characteristic function, *QCW-ECF*. This system function, $E_{qcw}(d_1, d_2, d_3, d_4)$, is illustrated in Figure 29.

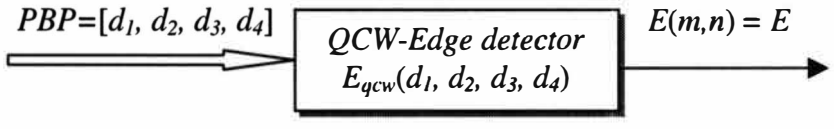

Figure 29. Edge detector Functioning Based on *QCW-ECF*.

The binary *QCW*-edge detector can be designed based on logical function E_{qcw}. The vector *PBP* represents the QCW pattern within the processing block *B*. Now, we explain how to derive the binary *QCW-ECF* step by step by means of logic design as follows:

1. **Truth table**. In the first step of our design, we construct the truth table. Let d_1, d_2, d_3, d_4 (vector *PBP)* be the inputs and *E* be a single output, then the truth table can be constructed based on the idea that the output *E* is active high (=1), if and only if d_1, d_2, d_3, d_4 match with one of the code words assigned for edge patterns (*PBP* = BEP_p). Since there are four input variables, then there are 2^4=16 possible 4-bit word *PBP* while nine words out of 16 words are just the edge patterns BEP_p for p=1,2,…,9. Table 9 illustrates the truth table for this binary edge detector.

Table 9

Truth Table for the Binary *QCW* Edge Detector

PBP			*E*
Input	Minterms	Pattern	Output
0000	0	NE	0
0001	1	NE	0
0010	2	NE	0
0011	3	E	1
0100	4	NE	0
0101	5	E	1
0110	6	NE	0
0111	7	E	1
1000	8	NE	0
1001	9	NE	0
1010	10	E	1
1011	11	E	1
1100	12	E	1
1101	13	E	1
1110	14	E	1
1111	15	E	1
Note: NE: Input is Not an Edge pattern. E: Input is an Edge pattern.			

Edge characteristic function according to this table is the sum of min-terms 3,5,7,10,11,12,13,14,15 which is given in Equation (2.1.6-1).

$$E = E_{qcw}(d_1, d_2, d_3, d_4) = \Sigma(3,5,7,10,11,12,13,14,15) \qquad (2.1.6-1)$$

2. **Minimization of E_{qcw}.** In the second step, with the aid of the Karnough map, the algebraic expression corresponding to E_{qcw} can be minimized. Figure 30 shows the map of edge classes along with their respective inputs, and the minimization procedure for *ECF* given in Equation (2.1.6-1) is also illustrated where (+) and (.) are respectively the Boolean logic operators OR and AND. To minimize E_{qcw}, we classify the above mentioned min-terms 3, 5, 7, 10, 11, 12, 13, 14, 15 as

		d'1 . d'2	d'1 . d2	d1 . d2	d1 . d'2
		00	01	11	10
d'3 . d'4	00			1	
d'3 . d4	01		1	1	
d3 . d4	11	1	1	1	1
d3 . d'4	10			1	1

Figure 30. Karnough Map.

$$E = \underbrace{\Sigma(12,13,14,15)}_{E_{h1}} + \underbrace{\Sigma(3,7,11,15)}_{E_{h2}} + \overbrace{\Sigma(5,7,13,15)}^{E_{v1}} + \overbrace{\Sigma(10,11,14,15)}^{E_{v2}} \qquad (2.1.6-2)$$

$$\begin{cases} E_{h1} = \Sigma(12,13,14,15) = d_1 \cdot d_2 & (2.1.6-3) \\ E_{h2} = \Sigma(3,7,11,15) = d_3 \cdot d_4 & (2.1.6-4) \\ E_{v1} = \Sigma(5,7,13,15) = d_2 \cdot d_4 & (2.1.6-5) \\ E_{v2} = \Sigma(10,11,14,15) = d_1 \cdot d_3 & (2.1.6-6) \end{cases}$$

Considering diagonal configuration of *QCW*, the expressions E_{h1} and E_{h2} denote the horizontal edges and the expressions E_{v1} and E_{v2} indicate vertical edges. The algebraic expression defining the horizontal edges can be obtained as

$$E_h = E_{h1} + E_{h2} = d_1 \,.\, d_2 + d_3 \,.\, d_4 \qquad (2.1.6\text{-}7)$$

Consequently, the algebraic expression for the vertical edges is obtained as

$$E_v = E_{v1} + E_{v2} = d_2 \,.\, d_4 + d_1 \,.\, d_3 \qquad (2.1.6\text{-}8)$$

As said, vertical and horizontal edges E_v, E_h is just defined for diagonal-*QCW* configurations. They are called diagonal edges for cross-*QCW* configurations. Obviously, when the *QCW* configuration is based on some interest pixels such as *QCW* configuration represented in Figure 24, then E_v and E_h do not precisely indicate the vertical and horizontal edges. Anyway, the minimal expression E, can be finally written in terms of algebraic expressions E_h and E_v as the Equation (2.1.6-9). This minimal expression corresponding to E_{qcw} expressed by the sum of products of input variables is considered as *QCW*-Edge Characteristic Function, *QCW-ECF*, for binary images.

$$E = E_{qcw}(d_1, d_2, d_3, d_4) = E_h + E_v = d_1 \,.\, d_2 + d_3 \,.\, d_4 + d_2 \,.\, d_4 + d_1 \,.\, d_3 \qquad (2.1.6\text{-}9)$$

The Equation (2.1.6-8) can be expressed in terms of product of sums and is valid for both the diagonal and the cross configurations of *QCW*. Inputs d_1, d_2, d_3, d_4 can be obtained by Equation (2.1.5-1).

$$E = E_{qcw}(d_1, d_2, d_3, d_4) = (d_1 + d_4) \,.\, (d_2 + d_3) \qquad (2.1.6\text{-}10)$$

Each processing block B may generally contain a diagonal, vertical or horizontal edges. Obviously, the diagonal-QCW works the best for diagonal edge detection and consequently the cross-QCW is good for vertical and horizontal edges. The combination of the detected edges by cross-QCW configuration, denoted by E_{cross}, and by diagonal-QCW, denoted by $E_{diagonal}$, within each processing block B improves the result. Since one of the configuration diagonal-QCW or cross-QCW may function well within each processing block, then we can combine the results of both configuration as

$$E_{combined} = (E_{cross} + E_{diagonal}) \qquad (2.1.6\text{-}11)$$

E_{cross} can be obtained by Equation (2.1.6-11) based on d_1, d_2 , d_3 ,d_4 given in configuration (a) of Figure 28. $E_{diagonal}$ can be also obtained by Equation (2.1.6-11) based on d_1 , d_2 , d_3 ,d_4 given in configuration (b) of Figure 28.

2.1.7 *QCW*-Edge Characteristic Function for Intensity Images

The two-valued (binary) logical function, binary *QCW-ECF* in Equation (2.1.6-10), possesses the value 1 if the variables d_1, d_2, d_3, d_4 are the binary values matching one of the edge pattern code words, otherwise it possesses the value 0. In an intensity image, the input variables d_1, d_2, d_3, d_4 possess a continuum of intensity values on [0,1] (a discrete gray level l between 0-255). Therefore, we should derive a multi-valued logical function E_{qcw} to define edge based on multi-valued input

variables d_1, d_2, d_3, d_4. This can be achieved by applying the multi-valued logic operators instead of Boolean logic operators in Equation (2.1.6-10). Using operator conversions given in Table 1, the Equation (2.1.6-10) can be extended to Equation (2.1.7-2) as the generalized *QCW-ECF* for both binary and intensity images. It is possible to derive directly the *ECF* for intensity image from binary *ECF*, Equation (2.1.6-10), without the conversion of operators. One may consider the Boolean operators (+) and (.) as the ordinary arithmetic operation. Since an intensity values for d_1, d_2, d_3, d_4 are ranged over interval [0,1], the maximum possible intensity value resulted by Equation (2.1.6-10) for E_{qcw} is 4. Then, by dividing this equation by 4, we can define a function representing a normalized intensity *ECF*. This function can be simply expressed as Equation (2.1.7-2), but it results in a low intensity value.

$$E_{qcw}(d_1, d_2, d_3, d_4) = 0.25\,(d_1 + d_4)\,.\,(d_2 + d_3) \qquad (2.1.7\text{-}1)$$

Generalized *QCW-ECF* for intensity images based on t-norm and *t*-conorm can be defined by extension of Equation (2.1.6-10) to (2.1.7-2). For further reference, we call it the general *JK*-type edge characteristic function based on quadruple child windowing.

$$\begin{cases} E = E_{qcw}(d_1, d_2, d_3, d_4) = T_{qcw}\left(S_{qcw}(d_1, d_4), S_{qcw}(d_2, d_3)\right) \\ \text{for} \quad d_1, d_2, d_3, d_4 \in [0,1] \quad , \quad T_{qcw} \xleftrightarrow{\text{dual}} S_{qcw} \\ \text{where} \quad T_{qcw} \in \{T, Q_t, A_t, B_t,\} \quad , \quad S_{qcw} \in \{S, Q_s, A_s, B_s\} \end{cases} \qquad (2.1.7-2)$$

E is the degree of edginess of PBP at middle pixel (m,n). T_{qcw} and S_{qcw} are t-norm and t-conorm operators which can be desirably derived based on the given definitions in section 1.6.7 and Equations (1.6.7-1) and (1.6.7-2). As discussed in section 1.6.7, we can derive a lot of t-norms and t-conorms. Therefore, the generalized *QCW-ECF* given in Equation (2.1.7-2) is a base to generate a lot of edge characteristic functions.

Consequently, we can extend the Boolean logical expressions concerning the horizontal and vertical edges, E_h and E_v for diagonal-*QCW* configuration, given by Equations (2.1.6-7) and (2.1.6-7), to multi-valued logical functions as

$$E_h(d_1, d_2, d_3, d_4) = S_{qcw}(T_{qcw}(d_1 , d_2) , T_{qcw}(d_3 , d_4)) \qquad (2.1.7\text{-}3)$$

$$E_v(d_1, d_2, d_3, d_4) = S_{qcw}(T_{qcw}(d_2 , d_4) , T_{qcw}(d_1 , d_3)) \qquad (2.1.7\text{-}4)$$

Also by extension of Equation (2.1.6-9), another expression is obtained for the intensity *QCW-ECF* as

$$E_{qcw}(d_1, d_2, d_3, d_4) = S_{qcw}(E_h , E_v) \qquad (2.1.7\text{-}5)$$

E_h and E_v are defined in Equations (2.1.7-3) and (2.1.7-4). It is reassuring to note that the Equations (2.1.7-2) and (2.1.7-5) do not always result in the same value, since t-norms and t-conorms do not satisfy the property of associativity. This is simulated in Chapter IV and, based on choosing the appropriate *QCW* configuration, the result is competitive with the best traditional algorithms in edge detection.

As said, since either the diagonal-*QCW* or cross-*QCW* configuration may work properly within each processing block, then we can combine the results of both configuration as

$$E_{combined} = S_{com}(E_{cross},\ E_{diagonal}) \qquad (2.1.7\text{-}6)$$

This equation is the extension of Equation (2.1.6-11). The operator S_{com} is a t-conorm operator previously defined in section 1.6.7 such that $S_{com} \in \{ S, Q_s, A_s, B_s\}$. Both E_{cross} and $E_{diagonal}$ can be individually obtained by Equation (2.1.7-2) or (2.1.7-5) based on d_1 , d_2 , d_3 ,d_4 illustrated respectively in parts (a) and (b) of Figure 28.

As discussed in section 1.6.7, we have $Q_t(x,y) \le T(x,y) \le min(x,y) \le g(x,y) \le max(x,y) \le S(x,y) \le Q_s(x,y)$ given by Equation (1.6.7-4). We just consider Quasi t-(co)norms and standard t-(co)norms to generate the least and the biggest values among the other t-(co)norms. Referring to the general operator given by Equation (1.6.7-8), Equation $E_{qcw}(d_1, d_2, d_3, d_4)$ defined by t-norm combination of two *t*-conorms must be a *t*-conorm operation over d_1, d_2, d_3, d_4. Based on the Table 10 containing some desired *t*-(co)norms, we derive five special cases of *QCW-ECF* from general Equation (2.1.7-2). The quasi-type *t*-(co)norms mentioned in rows 3,4,5 of this table, are derived using the Equation (1.6.7-2) and the standard and algebraic *t*-(co)norm operators represented in first and second rows. These five special cases of *QCW-ECF* are constructed based on the operators mentioned in rows 1,2,3,4,5 of Table 10. We call these edge characteristic functions *JK*-type1, 2, 3, 4, 5 and can be obtained as follows:

Table 10

Illustration of Some *t*-(co)norm Operators Applied for *QCW-ECF*

No.	Operators	*t*-norms, T_{qcw}	*t*-conorms, S_{qcw}
1	Standard operators	Min: $Min(x, y)$	Max: $max(x, y)$
2	Algebraic operators	Product: $x.y$	Sum: $x+y-x.y$
3	Quasi operator	$Q_t=T'(T,S)$: $[min(x.y)].(x+y-x.y)$	$Q_s=S'(S'',T'')$: $x.y+(1-x.y).[max(x, y)]$
4	Quasi operator	$Q_t=T'(T,S)$: $(x.y).[\ max(x, y)]$	$Q_s=S'(T'',S'')$: $x+y-x.y+(1-x-y+x.y).[min(x, y)]$
5	Quasi operator	$Q_t=T'(T,S)$: $(x.y).(\ x+y-x.y)$	$Q_s=S'(T'',S'')$: $X+y\ -(x.y).(x+y-x.y)$

1. ***JK*-type 1** of generalized *QCW-ECF* can be obtained from Equation (2.1.7-2) by simply using the standard operators *min* and *max* which are respectively *t*-norm T_{qcw} and *t*-conorms S_{qcw}. Therefore, the *JK*-type1 of *QCW-ECF* can be defined as

$$E = E_{qcw}(d_1, d_2, d_3, d_4) = min[\ max(d_1\ ,\ d_4)\ ,\ max(d_2\ ,\ d_3)\ ] \qquad (2.1.7\text{-}7)$$

Consequently we can apply these operators to find *JK*-type1 of vertical and horizontal edges, E_v and E_h, as follows

$$E_h = E_h(d_1, d_2, d_3, d_4) = max(\ min(d_1\ ,\ d_2)\ ,\ min(d_3\ ,\ d_4)\ ) \qquad (2.1.7\text{-}8)$$

$$E_v = E_v(d_1, d_2, d_3, d_4) = max(\ min(d_2\ ,\ d_4)\ ,\ min(d_1\ ,\ d_3)\ ) \qquad (2.1.7\text{-}9)$$

$$E=E_{qcw}(d_1, d_2, d_3, d_4) = max(E_h\ ,\ E_v) \qquad (2.1.7\text{-}10)$$

In case of considering both diagonal and cross *QCW-ECF*, to combine these two configuration we can use Equation (2.1.7-11) as the special case of Equation (2.1.7-6) where the *t*-conorm S_{com} is considered the standard operator, *max*.

$$E_{combined} = max(E_{cross},\ E_{diagonal}) \qquad (2.1.7\text{-}11)$$

2. ***JK*-type 2** of generalized *QCW-ECF* can be derived from Equation (2.1.7-2) by simply using the algebraic operators, product ($x.y$) and sum ($x+y-x.y$), (refer to the second row of table (2.1.7-1)) considered respectively *t*-norm T_{qcw} and *t*-conorms S_{qcw}. Therefore, the *JK*-type2 of *QCW-ECF* can be defined by Equation (2.1.7-14).

$$S_{14} = S_{qcw}(d_1, d_4) = d_1 + d_4 - d_1.d_4 \qquad (2.1.7\text{-}12)$$

$$S_{23} = S_{qcw}(d_2, d_3) = d_2 + d_3 - d_2.d_3 \qquad (2.1.7\text{-}13)$$

$$\boldsymbol{E = E_{qcw}(d_1, d_2, d_3, d_4)} = T_{qcw}(S_{14}, S_{23}) = S_{14}.S_{14}$$

$$\boldsymbol{= (d_1 + d_4 - d_1.d_4).(d_2 + d_3 - d_2.d_3)} \qquad (2.1.7\text{-}14)$$

Consequently, we can apply this operators to find *JK-type*2 of vertical and horizontal edges, E_v and E_h. Therefore, using Equations (2.1.7-3), (2.1.7-4) and (2.1.7-5), we have $T_{12} = T_{qcw}(d_1, d_2) = d_1.d_2$, $T_{34} = T_{qcw}(d_3, d_4) = d_3.d_4$, $T_{13} = T_{qcw}(d_1, d_3) = d_1.d_3$, $T_{24} = T_{qcw}(d_2, d_4) = d_2.d_4$. Finally we can write

$$\boldsymbol{E_h = E_h(d_1, d_2, d_3, d_4)} = S_{qcw}(T_{12}, T_{34}) = T_{12} + T_{34} - T_{12}.T_{34}$$

$$\boldsymbol{= d_1.d_2 + d_3.d_4 - d_1.d_2.d_3.d_4} \qquad (2.1.7\text{-}15)$$

$$\boldsymbol{E_v = E_v(d_1, d_2, d_3, d_4)} = S_{qcw}(T_{24}, T_{13}) = T_{24} + T_{13} - T_{24}.T_{13}$$

$$\boldsymbol{= d_2.d_4 + d_1.d_3 - d_2.d_4.d_1.d_3} \qquad (2.1.7\text{-}16)$$

$$\boldsymbol{E=E_{qcw}(d_1, d_2, d_3, d_4) = S_{qcw}(E_h , E_v) = E_h + E_v - E_h . E_v} \qquad (2.1.7\text{-}17)$$

To combine the values resulting from two diagonal and cross-*QCW* configurations, we can apply the algebraic operator sum in Equation (2.1.7-6) as *t*-conorm $S_{com}(x,y)=(x+y+x.y)$ to derive the Equation (2.1.7-18).

$$E_{combined} = S_{com}(E_{cross}, E_{diagonal}) = E_{cross} + E_{diagonal} - E_{cross} . E_{diagonal} \qquad (2.1.7\text{-}18)$$

3. ***JK*-type 3** of generalized *QCW-ECF* can be derived from Equation (2.1.7-2) by simply using the combination of algebraic and standard operators. For this combination, we apply Quasi *t*-(co)norms as derived and mentioned in third row of Table 10. The Quasi operators Q_t and Q_s are considered respectively *t*-norm T_{qcw} and *t*-conorms S_{qcw}. Therefore, the *JK*-type3 of *QCW-ECF* can be defined by Equation (2.1.7-21).

$$S_{14} = S_{qcw}(d_1, d_4) = d_1.d_4 + (1 - d_1.d_4).[max(d_1, d_4)] \qquad (2.1.7\text{-}19)$$

$$S_{23} = S_{qcw}(d_2, d_3) = d_2.d_3 + (1 - d_2.d_3).[max(d_2, d_3)] \qquad (2.1.7\text{-}20)$$

$$\boldsymbol{E = E_{qcw}(d_1, d_2, d_3, d_4) = T_{qcw}(S_{14} , S_{23})}$$

$$\boldsymbol{= [min(S_{14}, S_{23})].(S_{14}+S_{23} - S_{14}.S_{23})} \qquad (2.1.7\text{-}21)$$

Consequently, we can apply theses operators to find *JK*-type2 of vertical and horizontal edges, E_v and E_h. Therefore, using Equations (2.1.7-3), (2.1.7-4) and (2.1.7-5), we can write

$$T_{12} = T_{qcw}(d_1, d_2) = [min(d_1, d_2)] .(d_1 + d_2 - d_1.d_2) \qquad (2.1.7\text{-}22)$$

$$T_{34} = T_{qcw}(d_3, d_4) = [min(d_3, d_4)] .(d_3 + d_4 - d_3.d_4) \quad (2.1.7\text{-}23)$$

$$\boldsymbol{E_h = E_h(d_1, d_2, d_3, d_4) = S_{qcw}(T_{12}, T_{34})}$$

$$\boldsymbol{= T_{12}.T_{34} + (1 - T_{12}.T_{34}).[max(T_{12}, T_{34})]} \quad (2.1.7\text{-}24)$$

$$T_{24} = T_{qcw}(d_2, d_4) = [min(d_2, d_4)] .(d_2 + d_4 - d_2.d_4) \quad (2.1.7\text{-}25)$$

$$T_{34} = T_{qcw}(d_1, d_3) = [min(d_1, d_3)] .(d_1 + d_3 - d_1.d_3) \quad (2.1.7\text{-}26)$$

$$\boldsymbol{E_v = E_v(d_1, d_2, d_3, d_4) = S_{qcw}(T_{24}, T_{13})}$$

$$\boldsymbol{= T_{24}.T_{13} + (1 - T_{24}.T_{13}).[max(T_{24}, T_{13})]} \quad (2.1.7\text{-}27)$$

$$\boldsymbol{E = E_{qcw}(d_1, d_2, d_3, d_4) = S_{qcw}(E_h, E_v)}$$

$$\boldsymbol{= E_h.E_v + (1 - E_h.E_v).[max(E_h.E_v)]} \quad (2.1.7\text{-}28)$$

In case of considering the combination of the diagonal and cross-*QCW* configuration to edge detection, we can apply the Quasi operator Q_t (mentioned in the third row of the Table 2.1.7.1 for Equation (2.1.7-6) as *t*-conorm $S_{com} \equiv Q_s$, to derive the Equation (2.1.7-29).

$$E_{combined} = S_{com}(E_{cross}, E_{diagonal})$$

$$= E_{cross}.E_{diagonal} + (1 - E_{cross}.E_{diagonal}).[max(E_{cross}.E_{diagona})] \quad (2.1.7\text{-}29)$$

4. ***JK*-type 4** of generalized *QCW-ECF* can be derived from Equation (2.1.7-2) by simply using the Quasi combination of algebraic and standard operators as mentioned in fourth row of Table 10. Therefore, by considering $T_{qcw} \equiv Q_t$ and $S_{qcw} \equiv Q_s$, then the *JK*-type4 of *QCW-ECF* can be defined by Equation (2.1.7-32).

$$S_{14} = S_{qcw}(d_1, d_4) = d_1 + d_4 - d_1.d_4 + (1 - d_1 - d_4 + d_1.d_4).[min(d_1, d_4)] \quad (2.1.7\text{-}30)$$

$$S_{23}= S_{qcw}(d_2, d_3)= d_2+d_3 - d_2.d_3 +(1- d_2 - d_3 + d_2.d_3).[min(d_2, d_3)] \quad (2.1.7\text{-}31)$$

$$\boldsymbol{E = E_{qcw}(d_1, d_2, d_3, d_4) = T_{qcw}(S_{14} , S_{23})}$$

$$\boldsymbol{= (S_{14} . S_{23}).[max(S_{14}, S_{23})]} \quad (2.1.7\text{-}32)$$

Consequently, we can apply these operators to find *JK*-type4 of vertical and horizontal edges, E_v and E_h. Therefore, using Equations (2.1.7-3), (2.1.7-4) and (2.1.7-5), we can write

$$T_{12} = T_{qcw}(d_1, d_2) = (d_1.d_2).[max(d_1, d_2)] \quad (2.1.7\text{-}33)$$

$$T_{34} = T_{qcw}(d_3, d_4) = (d_3.d_4).[max(d_3, d_4)] \quad (2.1.7\text{-}34)$$

$$\boldsymbol{E_h = E_h(d_1, d_2, d_3, d_4) = S_{qcw}(T_{12}, T_{34})}$$

$$\boldsymbol{= T_{12}+T_{34} -T_{12}.T_{34} + (1- T_{12} -T_{34}+T_{12}.T_{34}).[min(T_{12},T_{34})]} \quad (2.1.7\text{-}35)$$

$$T_{24} = T_{qcw}(d_2, d_4) = (d_2.d_4).[max(d_2, d_4)] \quad (2.1.7\text{-}36)$$

$$T_{13} = T_{qcw}(d_1, d_3) = (d_1.d_3).[max(d_1, d_3)] \quad (2.1.7\text{-}37)$$

$$\boldsymbol{E_v = E_h(d_1, d_2, d_3, d_4) = S_{qcw}(T_{24}, T_{13})}$$

$$\boldsymbol{= T_{24} +T_{13} -T_{24}.T_{13} + (1-T_{24} -T_{13}+T_{24}.T_{13}).[min(T_{24},T_{13})]} \quad (2.1.7\text{-}38)$$

$$\boldsymbol{E = E_{qcw}(d_1, d_2, d_3, d_4) = S_{qcw}(E_h , E_v)}$$

$$\boldsymbol{= E_h +E_v - E_h.E_v + (1-E_h -E_v + E_h .E_v).[min(E_h .E_v)]} \quad (2.1.7\text{-}39)$$

In case of processing both cross and diagonal *QCW* configurations, we can apply the Quasi operator Q_t (mentioned in forth row of Table 10) for Equation (2.1.7-6) as *t*-conorm $S_{com} \equiv Q_s$ to derive the following equation.

$$E_{combined} = S_{com}(E_{cross}, E_{diagonal})$$

$$= E_{cross} + E_{diagona} - E_{cross}.E_{diagonal}$$

$$+(1- E_{cross} - E_{diagona} + E_{cross}.E_{diagonal}).[min(E_{cross}.E_{diagona})] \quad (2.1.7\text{-}40)$$

5. ***JK*-type 5** of generalized *QCW-ECF* can be derived from Equation (2.1.7-2) by simply using the Quasi combination of algebraic operators as mentioned in fifth row of the Table 10. Therefore, by considering $T_{qcw} \equiv Q_t$ and $S_{qcw} \equiv Q_s$, then the *JK*-type5 of *QCW-ECF* can be defined by Equation (2.1.7-43).

$$S_{14} = S_{qcw}(d_1, d_4) = d_1 + d_4 - (d_1.d_4).(d_1 + d_4 - d_1.d_4) \quad (2.1.7\text{-}41)$$

$$S_{23} = S_{qcw}(d_2, d_3) = d_2 + d_3 - (d_2.d_3).(d_2 + d_3 - d_2.d_3) \quad (2.1.7\text{-}42)$$

$$\boldsymbol{E = E_{qcw}(d_1, d_2, d_3, d_4) = T_{qcw}(S_{14}, S_{23})}$$

$$\boldsymbol{= (S_{14}.S_{23}).(S_{14} + S_{23} - S_{14}.S_{23})} \quad (2.1.7\text{-}43)$$

Consequently, using Equations (2.1.7-3), (2.1.7-4) and (2.1.7-5), we can apply theses operators to find *JK*-type5 of vertical and horizontal edges, E_v and E_h as follows.

$$T_{12} = T_{qcw}(d_1, d_2) = (d_1.d_2).(d_1 + d_2 - d_1.d_2) \quad (2.1.7\text{-}44)$$

$$T_{34} = T_{qcw}(d_3, d_4) = (d_3.d_4).(d_3 + d_4 - d_3.d_4) \quad (2.1.7\text{-}45)$$

$$\boldsymbol{E_h = E_h(d_1, d_2, d_3, d_4) = S_{qcw}(T_{12}, T_{34})}$$

$$\boldsymbol{= T_{12} + T_{34} - (T_{12}.T_{34}).(T_{12} + T_{34} - T_{12}.T_{34})} \quad (2.1.7\text{-}46)$$

$$T_{24} = T_{qcw}(d_2, d_4) = (d_2.d_4).(d_2 + d_4 - d_2.d_4) \quad (2.1.7\text{-}47)$$

$$T_{13} = T_{qcw}(d_1, d_3) = (d_1.d_3).(d_1 + d_3 - d_1.d_3) \quad (2.1.7\text{-}48)$$

$$\boldsymbol{E_v = E_h(d_1, d_2, d_3, d_4) = S_{qcw}(T_{24}, T_{13})}$$

$$= T_{24} + T_{13} - (T_{24} . T_{13}).(T_{24} + T_{13} - T_{24} . T_{13}). \qquad (2.1.7\text{-}49)$$

$$E = E_{qcw}(d_1, d_2, d_3, d_4) = S_{qcw}(E_h, E_v)$$

$$= E_h + E_v - (E_h . E_v).(E_h + E_v - E_h . E_v). \qquad (2.1.7\text{-}50)$$

Also, we can apply the Quasi operator Q_t (mentioned in forth row of Table 10) for Equation (2.1.7-6) as t-conorm $S_{com} \equiv Q_s$, to derive the following Equation.

$$E_{combined} = S_{com}(E_{cross}, E_{diagonal})$$

$$= E_{cross} + E_{diagona} - (E_{cross} . E_{diagonal}).(E_{cross} + E_{diagona} - E_{cross} . E_{diagonal}). \qquad (2.1.7\text{-}51)$$

The edge detectors functionally find the edge (an intensity value for edge point) based on the above mentioned equations. Assume, B to be a processing block $W \times W$ at point (m,n) of an intensity image. Let B_1, B_2, B_3, B_4 be QCW within the block B, and also Y_1, Y_2, Y_3, Y_4 be representative intensity values for QCW obtained by Equation (2.1.5-2), then processing block pattern PBP is a vector defined by

$$PBP = [d_k]_p \quad for \quad k = 1,2,3,4. \qquad (2.1.7\text{-}52)$$

The terms d_1, d_2, d_3, d_4 are four intensity distances obtained by Equation (2.1.5-1) based on QCW within the block B. PBP is also considered as the characteristic vector of the intensity of QCW-pattern within the processing block B. The processing block B with a certain pattern PBP can be evaluated by the edge detector which is operating functionally based on QCW-ECF given by the Equations (2.1.7-2) or (2.1.7-4) or (2.1.7-6). This has been illustrated in Figure 29. The function

E_{qcw} generates E as the evaluation value for the intensity pattern of processing block B. This evaluation value indicates the maximum degree of correspondence of processing block pattern PBP to the binary edge patterns BEP_p (for p=1,2,..9) defined in section 2.1.5. The evaluation value E is obtained as

$$E = E_{qcw}(d_1, d_2, d_3, d_4) = E_{qcw}(PBP). \qquad (2.1.7\text{-}53)$$

E possesses a value within [0,1]. The value E=1 indicates a perfect correspondence between PBP and one of the binary edge patterns. Similarly, E=0 shows no correspondence. It follows that a value between 0 and 1 for E refers to the degree of correspondence of PBP to the defined binary edge patterns. On the other hand, this degree of correspondence E indicates the degree of edginess of processing block pattern PBP. Since here we are dealing with normalized value of gray level (intensity value within [0,1]) and the degree of edginess is also between [0,1], we can directly consider the value E as the actual intensity value of the edge pixel. In the block processing technique for edge detection this value of E is replaced instead of middle pixel intensity X_{mn} of a running block B over an intensity image.

2.2 Correlation Between *QCW*- Pattern and Binary Edge Patterns

Finding correlation coefficient is a an appropriate measurement for the degree of correspondence of the QCW pattern with the binary edge patterns. That is determination of maximum correlation between PBP vector and the space vector $BEP=\{BEP_p \mid p=1,2,\ldots,9\}$. Correlation between PBP and BEP is shown in Figure 31.

The correlation method results in a maximum evaluation value in interval [0,1] as the maximum degree of correspondence between processing block pattern *PBP* to one of the 9 binary edge patterns BEP_p . This value represents the degree of edginess of pattern *PBP*. In the case of the normalized gray scale (intensity image), this degree of edginess can be considered as the actual intensity value of the edge pixel. The closer the *PBP* vector to the space vector *BEP*, the brighter the edge pixel. In processing a binary image this correlation result in a value 0 or 1, while in an intensity image it results in a value within interval [0,1].

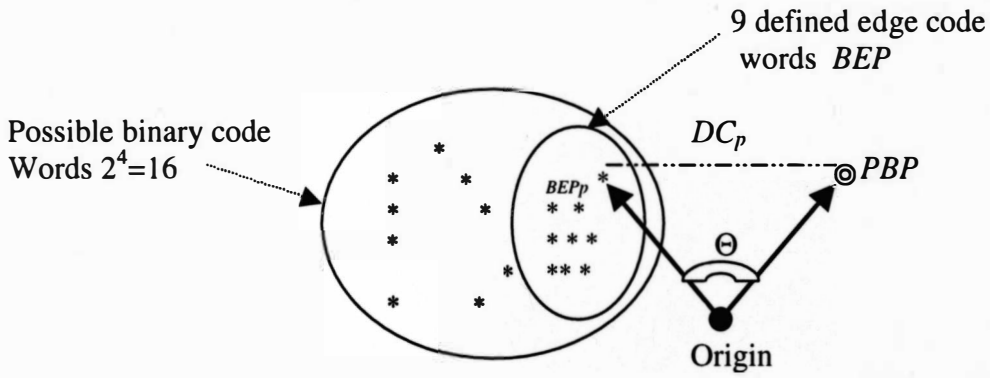

Figure 31. Illustration of Correlation Between Vectors *PBP* and BEP_p.

2.2.1 Distance Correlation

Consider a *QCW* within a processing block *B* of an image (binary or intensity) and let *PBP* be the relevant characteristic vector specifying this *QCW* pattern. Then the distances between the *PBP* vector and the BEP_p vectors are generally defined as DC_p by Equation (2.2.1-1). This equation represents the correlation between the processing block pattern and the binary edge patterns.

$$DC_p = \| PBP - BEP_p \| \qquad for \quad p=1,2,3,\ldots 9 \qquad (2.2.1\text{-}1)$$

Distance correlation results in a value denoting the degree of closeness of PBP vector to BEP_p vector. The space of the edge pattern vectors consists of nine vectors. Therefore, there are nine values indicating the degree of correspondence of PBP to the edge pattern vector space. Since we are looking for closest BEP_p vector to PBP, then the minimum value of DC_p meets our need. As DC_p decreases toward zero the degree of edginess of PBP approaches the highest value 1. We can define the degree of edginess of PBP as

$$E_{dc} = 1 - \frac{\min_p \left\{ \left\| PBP - BEP_p \right\| \right\}}{\max_p \left\{ \left\| PBP - BEP_p \right\| \right\}} \quad for \quad p = 1,2,,3,\ldots,9 \qquad (2.2.1-2)$$

According to this definition, the closer the vector PBP is to the binary code word space BEP, the function E_{dc} results in the greater value as the degree of edginess for the processing block pattern. Considering this value directly as the actual edge intensity value, then the bigger value of E_{dc} results in a brighter edge point.

2.2.2 Angular Correlation

Consider a QCW within a processing block B of an image (binary or intensity) and let PBP be a vector containing the intensity distances defined within this QCW pattern. The degree of correspondence of PBP to binary edge patterns BEP_p is to find the minimum angle Θ_p (or maximum $\text{Cos}(\Theta_p)$) between PBP vector and BEP_p

vectors. The angular correlation between the processing block pattern and binary edge patterns is generally obtained by

$$Cos\left(\Theta_p\right)=\left[\frac{< PBP \cdot BEP_p >}{\left\|PBP\right\| \cdot \left\|BEP_p\right\|}\right] \qquad for \quad p=1,2,\ldots\ldots,9 \qquad (2.2.2-1)$$

This equation results in a value within interval [0,1]. Therefore for p=1,...9, there are 9 different values representing the degree of correspondence of PBP vector to BEP_p vectors. When the *PBP* vector exactly matches with one of BEP_p vectors, then this equation possesses the value 1 (since angle between two vectors is zero) denoting the maximum degree of correspondence as well as maximum degree of edginess of *PBP*.

By increasing the Θ_p=0, the Cos(Θ_p) is approaching 0 indicating no correlation while Cos(Θ_p)=1 is denoting the maximum correlation. The degree of edginess based on the defined angular correlation in Equation (2.2.2-1) is defined as

$$E_{ac}=\max_p\left\{Cos\left(\Theta_p\right),\right\} \qquad for \quad p=1,2,\ldots\ldots,9 \qquad (2.2.2-2)$$

2.3 Edge Detectors Based on *QCW-ECF*

In preceding sections, we have introduced edge characteristic functions (*ECF*) based on *QCW* within a processing block *B* of an image (binary or intensity). We showed that all these equations result in values denoting the degree of correspondence

of *QCW* pattern *PBP* to binary edge pattern space *PEP*. On the other hand, indicating the degree of edginess of middle pixel (m,n) centered on the processing block B. In the edge detection algorithm using block processing, the above equations can be directly applied to find the edge pixels. The result of the equation E_{qcw} is considered as intensity value of edge point and replaced by middle intensity pixel X_{mn}. Finally the output image represents an edge map considering degree of edginess for each pixel of main image.

Edge detectors usually generate a binary edge map. The edge characteristic functions are applied to find the degree of edginess as an evaluation value for middle pixel X_{mn}. If this evaluation value is greater than some threshold (T_H), then the edge detector send one to output (X_{mn} is replaced by 1) indicating X_{mn} is an edge point. Consequently, if this degree is less than some threshold (T_L), then the edge detector sends 0 to output (X_{mn} is replaced by 0) denoting X_{mn} is not an edge point. The block diagram in Figure 32 depicts the edge detector functioning based on *QCW-ECF* and thresholding.

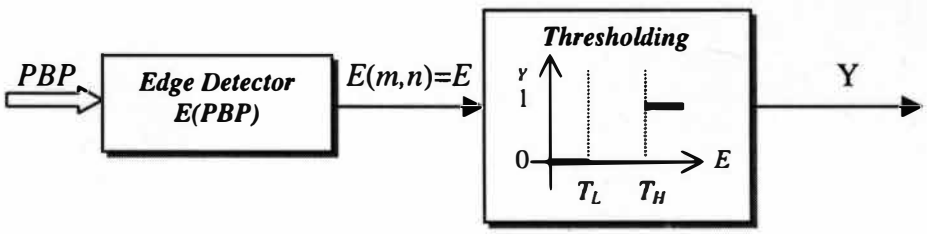

Figure 32. Edge Detection Using Thresholds.

Edge Detection algorithm based on *QCW-ECF* can be briefly written as follows:

1. Choose a proper size of block B, $W\times W$, with the middle intensity X_{mn}.

2. Do the QCW within block B using the diagonal, cross, or/and other desired configurations (based on desired pixels neighboring the middle pixel), to find four child windows B_1, B_2, B_3, B_4.

3. Choose an appropriate aggregation operator g (such as averaging, median, ...)and apply it over each child window to find four representative intensities $Y_k = g\{ X_{ij} \mid (i,j) \in B_k\}$ for k=1,2,3,4. Also, in case of processing a noisy image, replace the middle intensity pixel X_{mn} with the intensity representative X'_{mn} where $X'_{mn} = g\{ X_{ij} \mid (i,j) \in \{B -(m,n)\}\}$.

4. Find the processing block pattern vector $PBP=[d_1, d_2, d_3, d_4]$ by finding the four difference intensities (distances) $d_k = |X_{mn} - Y_k|$, for k=1,2,3,4.

5. Choose or construct a desired t-norm T_{qcw} and t-conorm S_{qcw} using Tables 2 and 10.

6. Apply the *JK*-type generalized *QCW-ECF*, distance correlation, or angular correlation given respectively by Equations 2.1.7-2, 2.2.1-2, and 2.2.2-2 for each individual *QCW* configuration (diagonally, crossly or any desired morphological structure), to find $E=E_{qcw}(PBP)= E_{qcw}(d_1, d_2, d_3, d_4)$ the degree of correspondence of vector *PBP* to the binary edge pattern space *BEP* given by Table 8 (or degree of edginess of *PBP* at middle pixel (m,n)). Since we applied the normalized gray scale indicating intensity is within continuous interval [0,1], then this degree of

correspondence directly represents the intensity of edge pixel (if thresholding is not applied) and is replaced instead of middle pixel intensity X_{mn}.

7. If there are more than one configuration, combine the result of each pair of configurations obtained from step 6 using a proper t-conorm, S_{com}, to find the $E_{combined}$.

8. In case of using thresholds for generating the binary edge, the edge detector sends the binary digit 1 to output if E (or $E_{combined}$ in case of combination) $\geq T_H$. Also, it sends binary digit 0 if E (or $E_{combined}$) $\leq T_L$.

CHAPTER III

FUZZY *QCW* EDGE DETECTION

In this chapter, fuzzy tools are applied to define *QCW-ECF* based on fuzzy logic. One significant problem in edge detection occurs when an monochrome image has a background of varying intensity or gray level. Finding an edge of the object at those points that have a similar intensity with background is difficult. Also, another problem is that in many cases, edge detection techniques are dependent on the appropriate choice of thresholds. The edge detection algorithm based on fuzzy logic with flexible rules as well as tunable membership functions would be an effective approach to remove the above mentioned problems.

3.1 Fuzzy Intensity Distances

Let X_{ij} and X_{mn} be fuzzy intensity singletons of $(i,j)^{th}$ and $(m,n)^{th}$ pixels within a fuzzy intensity image defined by Equation (1.4.1-1). Fuzzy intensity distance is a fuzzy singleton with a fuzzy value $d((m,n),(i,j))$, obtained by Equation (2.1-1), and its corresponding membership degree μ_d obtaining on a certain fuzzy plane (such as fuzzy plane illustrated in Figure 7. This is defined as

$$Fd = \mu_d \Big/ d\left(X_{mn}, X_{ij}\right) \qquad where \quad \begin{cases} d((m,n),(i,j)) = \left|X_{mn} - X_{ij}\right| \\ \mu_d = \mathrm{P}\left(d((m,n),(i,j))\right) \end{cases} \qquad (3.1-1)$$

The term *Fd* is considered a fuzzy singleton indicating the fuzzy intensity distance between two fuzzy singletons FX_{mn} and FX_{ij} representing two fuzzy intensity values of points (m,n) and (j,j) of image. Also, *P* is a membership function(s) in fuzzy plane.

3.1.1 Fuzzy Quadruple Child Windowing, *FQCW*

Consider the fuzzy intensity image *FII* represented by Equation (1.4.1-1). The *QCW* process defined in section 2.1.3 can be applied within a *W*×*W* block over the fuzzy intensity image, *FII*. Let *FB* be a block (fuzzy intensity block) with size *W*×*W* over an fuzzy intensity image *FII*. This block can be represented as

$$FB = [FX_{ij}] = \left[\mu_{ij} / X_{ij} \right] \quad for \quad \begin{cases} i = m - \dfrac{W-1}{2}, \ldots, m + \dfrac{W-1}{2} \\ j = n - \dfrac{W-1}{2}, \ldots, n + \dfrac{W-1}{2} \end{cases} \qquad (3.1.1-1)$$

Point $(i,j) = (m,n)$ denotes the middle pixel of *FB* and FX_{mn} is a fuzzy singleton which possesses intensity value of X_{mn} with membership degree of μ_{mn}. Also, FX_{ij} denotes the fuzzy singletons neighboring the middle pixel. *FB* can be considered as the result of fuzzification of block *B* defined by Equation (2.1.3-1) over an intensity image. Fuzzification of the intensity image *II* can be implemented by generating fuzzy blocks *FB* when the block *B* running over an intensity image. Now we apply again the *QCW* process to break down the block *FB* into four child windows as FB_1, FB_2 ,FB_3 ,FB_4. We call this process as Fuzzy quadruple Child Windowing (*FQCW*), which is mathematically represented by Equation (3.1.1-2).

$$\begin{cases} 1) \quad FB \xrightarrow{FQCW} \{FB_k, \forall (m,n) \notin FB_k \quad for\ k = 1,2,3,4\} \\ 2) \quad \{ FB_1 \cup FB_2 \cup FB_3 \cup FB_4 \cup \{X_{mn}\} \} \subseteq FB \\ FB_1 \cap FB_2 \cap FB_3 \cap FB_4 = \varnothing \end{cases} \qquad (3.1.1-2)$$

This is exactly the fuzzy approach for *QCW* defined by Equation (2.1.3-1). The structure of *FQCW* within the running fuzzy intensity block *FB* can be geometrically altered based on application during the processing of fuzzy image. The structures of *FQCW* can be chosen as explained and illustrated for structures of *QCW* within the block of (3×3), (5×5), (7×7) in section 2.1.3.

Considering the running block *FB* over an image *FII*, one can apply either a fixed structure of *QCW* or different structure of *QCW* within block *FB*. In the case of the latter, all configurations of *QCW* are simultaneously considered to choose the best structure for *QCW* based on the results at each processing pixel X_{mn}. To process an image by applying various structures of *QCW* yields the best result but it takes more time than applying the fixed structure, because in each block all structures should be examined in order to find the best structure.

3.1.2 Fuzzy Child Window Processing

Let $\{FB_1, FB_2, FB_3, FB_4\}$ be an appropriate *QCW* over a *W*×*W* block *FB*. The fuzzy child-filter can be defined by an operation (modification) *g* on pixels on/within each child window FB_k. For our purposes, the filtering operation (we use median filtering) over four child windows results in four fuzzy singletons FY_1, FY_2, FY_3, FY_4 which are respectively considered as four fuzzy intensity representative values for

child windows FB_1, FB_2, FB_3, FB_4. Finally the fuzzy singleton resulting from a fuzzy child window processing can be presented as

$$FY_k = \mu_k / Y_k \qquad for \quad k = 1,2,3,4 \qquad (3.1.2-1)$$

According to Equation 2.1.4-1, we have $Y_k = g(B_k)$ *for* k=1,2,3,4. The membership degree μ_1, μ_2, μ_3, μ_4 corresponding to these four fuzzy values Y_1, Y_2, Y_3, Y_4 are obtained using a certain fuzzy plain (fuzzification of these values). If P denotes the continuous membership function(s) defined in a fuzzy plane, then these membership degrees are generally defined as

$$\mu_k = P(Y_k) \quad where \ \mu_k \in [0,1] \quad for \quad k = 1,2,3,4 \qquad (3.1.2-2)$$

Fuzzy child window processing is sequentially depicted in Figure 33.

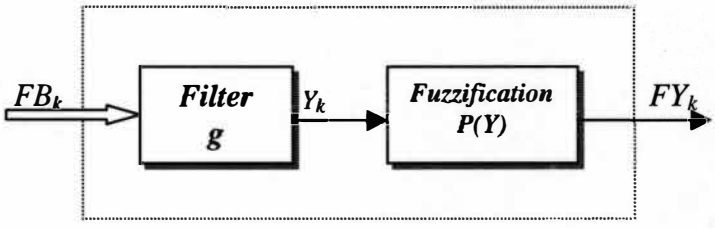

Figure 33. Fuzzy Child Window Processing.

Fuzzy child window processing results in four fuzzy singletons FY_1, FY_2, FY_3 ,FY_4 within a fuzzy block FB. Consequently, $FQCW$ patterns can be illustrated by Figure 34 using these four fuzzy singletons as representatives of child windows and the FX_{mn} as the fuzzy singleton representing the middle pixel.

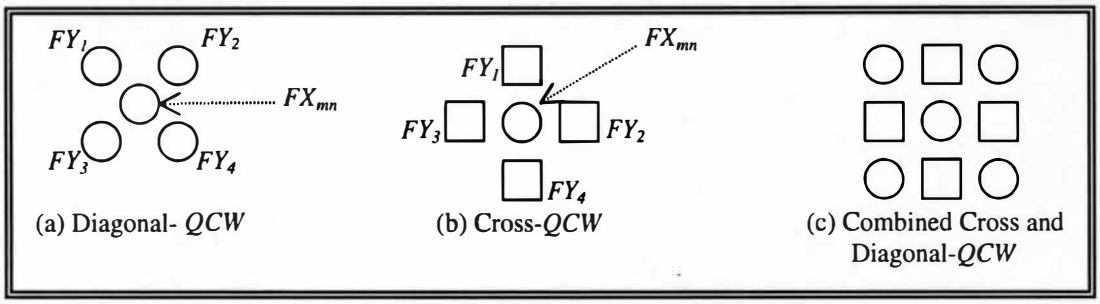

Figure 34. Illustration of $FQCW$ Configurations.

Figure 34 represents the geometrical configuration of fuzzy quadruple child windowing ($FQCW$), which is exactly like QCW but the pixels are fuzzy singletons. In case of processing of a noisy image, X_{mn} must be replaced with the representative intensity pixel X'_{mn} obtained by the following operation g over the $B-(m,n)$. Operation g can be defined by Equation 1.6.7-3 or chosen from Table 4.

$$X'_{mn} = g\{ X_{ij} \mid (i,j) \in \{B-(m,n)\} \} \qquad (2.1.2\text{-}3)$$

or

$$X'_{mn} = g\{Y_1, Y_2, Y_3, Y_4\} \qquad (2.1.2\text{-}4)$$

Consequently, the fuzzy singleton FX'_{mn} can be defined by

$$FX'_{mn} = \mu'_{mn} / X'_{mn} \quad for \quad \begin{cases} m = 1,2,\ldots,M \\ n = 1,2,\ldots,N \end{cases} \qquad (3.1.2-4)$$

$$\mu'_{mn} = P\left(X'_{mn}\right) \quad where\ \mu'_{mn} \in [0,1] \quad for \quad \begin{cases} m = 1,2,\ldots,M \\ n = 1,2,\ldots,N \end{cases} \qquad (3.1.2-5)$$

3.1.3 *FQCW* Intensity Pattern

Consider *FQCW* (diagonal or cross structure) given in Figure 34 within a block *FB*. Let FY_1, FY_2, FY_3, FY_4 be 4 fuzzy singletons as the intensity representatives of four child windows and FX_{mn} be the fuzzy singleton denoting middle pixel intensity. We can define 4 fuzzy singletons indicating the fuzzy intensity distances Fd_1, Fd_2, Fd_3, Fd_4 as

$$Fd_k = \mu d_k / d_k \qquad for \quad k = 1,2,3,4 \qquad (3.1.3-1)$$

The intensity distances d_1, d_2, d_3, d_4 and their associated membership degrees can be obtained by

$$d_k = d(X_{mn}, Y_k) = | X_{mn} - Y_k | \qquad (3.1.3\text{-}2)$$

$$\mu d_k = P(d_k) \qquad (3.1.3\text{-}3)$$

P is a membership function(s) defined over continuous intensity scale [0,1] (or discrete gray level 0 to L-1). One may choose the fuzzification of d_k using the fuzzy plane illustrated in Figure 7. The given fuzzy intensity block *FB* possesses an intensity pattern based on *FQCW*. This pattern can be specified by fuzzy vector *FPBP* containing intensity distances Fd_1, Fd_2, Fd_3, Fd_4 as

$$FPBP = [Fd_k] \qquad for \ k=1,2,3,4. \qquad (3.1.3\text{-}2)$$

Therefore, each fuzzy intensity block *FB* which is under processing can be

specified by its pattern characteristic vector *FPBP* based on *FQCW*. This fuzzy vector *FPBP* can be considered as the fuzzified vector *PBP* which has been defined as a pattern characteristic vector for intensity block *B* based on *QCW*. This vector is applied to define *FQCW*-edge Characteristic function (*FQCW-ECF*) in next section.

3.1.4 *FQCW*-Edge Characteristic Function

Consider *FQCW* within a fuzzy intensity block *FB* with its relevant code vector *FPBP* presenting the intensity pattern. If this *FQCW* intensity pattern corresponds with one of the nine binary edge patterns illustrated in Figure 26, or 27. In other words, if the fuzzy vector *FPBP* matches one of the binary code words defined in Table 8, then *FQCW* intensity pattern is considered an ideal edge pattern. This is true when the fuzzy singletons Fd_1, Fd_2, Fd_3, Fd_4 possess the ideal values like 1/1, 1/0. Normally, the fuzzy intensity block which is under processing, for each fuzzy singleton Fd_k in vector *FPBP*, the distance $d_k \in [0,1]$ (or gray level $l \in \{0,1,..,L-1\}$) and its associated membership degree $\mu d_k \in [0,1]$. We are looking to find an appropriate function represented by Equation (3.1.4-1) to evaluate the *FQCW* intensity pattern (*FPBP* vector) by comparison with nine possible ideal (binary) edge patterns given in Figures 26 or 27. The binary *QCW*-edge patterns illustrated in these figures can be considered as a special case of *FQCW*-edge patterns when the *FPBF* vector contains fuzzy singletons 1/1, 1/0 which referring respectively to 1 and 0 in a crisp set.

$$E = E_{fqcw}\left(FPBP\right) = E_{fqcw}\left(Fd_1, Fd_2, Fd_3, Fd_4\right)$$
$$= E_{fqcw}\left(\mu d_1 / d_1, \mu d_2 / d_2, \mu d_3 / d_3, \mu d_4 / d_4\right) \qquad (3.1.4-1)$$

E_{fqcw} is the edge characteristic function based on *FQCW*. The result E is a non-fuzzy (crisp) number which represents the degree of closeness to maximum intensity of an edge point 1 or maximum gray level L-1. In other words, that is maximum degree of correspondence of the *FQCW* intensity pattern to the defined binary edge pattern space or degree of edginess of the middle pixel of the fuzzy block *FB*.

As the general Equation (2.1.7-2) was developed to define *QCW-ECF* (in both diagonal and cross configurations) for evaluating the *QCW* intensity pattern (or pattern characteristic vector *PBP*) based on degree of correspondence to the nine binary edge patterns, it is time to define the Equation (3.1.4-2). This equation represents the degree of correspondence of the *FQCW* intensity pattern to binary edge patterns. On the other hand, this equation defines the maximum degree of correspondence of the vector *FPBP* to the nine binary edge code word space, *BEP* = $\{BEP_p, \}$ for p=1,2,..,9.

$$\begin{cases} E = E_{fqcw}\left(\mu d_1 / d_1, \mu d_2 / d_2, \mu d_3 / d_3, \mu d_4 / d_4\right) = \\ \quad = T_{qcw}\left[S_{qcw}\left(\mu d_1 \cdot d_1, \mu d_4 \cdot d_4\right), S_{qcw}\left(\mu d_2 \cdot d_2, \mu d_3 \cdot d_3\right)\right] \qquad (3.1.4-2) \\ \\ where \quad \begin{cases} E, d_1, d_2, d_3, d_4, \mu_{d1}, \mu_{d2}, \mu_{d3}, \mu_{d4} \in [0,1] \\ T_{qcw} \in \{T, Q_t, A_t, B_t\} \quad , \quad S_{qcw} \in \{T, Q_s, A_s, B_s\} \end{cases} \end{cases}$$

The operators T_{qcw} and S_{qcw} are respectively any t-norm and t-conorm defined in section 1.6.7. The function E_{fqcw} is denoted here as *FQCW-ECF*. That is fuzzy *QCW*-edge characteristic function. Applying this function for edge detection has two important advantages, (1) thresholding is not needed. In this equation, since the four membership degrees $\mu d_1, \mu d_2, \mu d_3, \mu d_4$ associated with the distances d_1, d_2, d_3, d_4 play the roles of weights. Also, since these membership degrees are adjustable by properly tuning each membership function, then this makes the *FQCW-ECF* more flexible and powerful in edge extraction without using thresholds, and (2) Since the function E_{fqcw} is a special operation over fuzzy variables d_1, d_2, d_3, d_4 and the result is a crisp value E, then it can be considered as a special defuzzification method by which simultaneously fuzzy singletons are mapped to a crisp value representing the degree of edginess. These two important advantages make this function powerful in edge detection and the resulted edge points by means of this equation are extraordinary as we will observe in Chapter IV.

Consequently, by considering the diagonal *QCW* configuration and the Equations (2.1.7-3), (2.1.7-4) and (2.1.7-5), we can also express E_{fqcw} for *FQCW-ECF* by the terms of vertical (E_v)and horizontal (E_h) edges as follows.

$$E_h = S_{qcw}\left[T_{qcw}\left(\mu d_1 \cdot d_1, \mu d_2 \cdot d_2\right), T_{qcw}\left(\mu d_3 \cdot d_3, \mu d_4 \cdot d_4\right)\right] \qquad (3.1.4-3)$$

$$E_v = S_{qcw}\left[T_{qcw}\left(\mu d_2 \cdot d_2, \mu d_4 \cdot d_4\right), T_{qcw}\left(\mu d_1 \cdot d_1, \mu d_3 \cdot d_3\right)\right] \qquad (3.1.4-4)$$

$$E = E_{fqcw}\left(\vec{FPBP}\right) E_{fqcw}\left(Fd_1, Fd_2, Fd_3, Fd_4\right) = S_{qcw}\left(E_h, E_v\right) \qquad (3.1.4-5)$$

Also, Equation (2.1.7-1) can be extended to E_{fqcw} as

$$E = E_{fqcw}(Fd_1, Fd_2, Fd_3, Fd_4) = \frac{(\mu d_1 \cdot d_1, + \mu d_4 \cdot d_4) \cdot (\mu d_2 \cdot d_2, + \mu d_3 \cdot d_3)}{4} \qquad (3.1.4-6)$$

Since either the diagonal-*FQCW* or cross-*FQCW* configuration functions well within each processing block, then for better result, we can combine the results of both configuration as

$$E_{fombined} = S_{qcw}(E_{fcross}\ ,\ E_{fdiagonal}) \qquad (3.1.4\text{-}7)$$

E_{fcross} and $E_{fdiagonal}$ can be obtained by Equation (3.1.4-2) based on d_1, d_2, d_3, d_4 given respectively in configurations (a) and (b) of Figure 34.

To develop the particular *QCW-ECF* (*JK*-type1,2,3,4,5 discussed in section 2.1.7) for the fuzzy model *FQCW-ECF*, we can simply replace the variables d_1, d_2, d_3, d_4 respectively with $(\mu d_1 \,.\, d_1)$, $(\mu d_2 \,.\, d_2)$, $(\mu d_3 \,.\, d_3)$, $(\mu d_4 \,.\, d_4)$. For simplicity, let define the parameter D_k as

$$D_k = \mu d_k \,.\, d_k \qquad \text{for } k=0,1,2,3,4 \qquad (3.1.4\text{-}8)$$

The special cases of the generalized *FQCW-ECF* given by Equation (3.1.4-2) can be derived as follows:

1. ***JK*-type 1** of generalized *FQCW-ECF* can be obtained by using the Table 10 and Equation (3.1.4-2) as follows.

$$E = E_{fqcw}(FPBP) = min[\ max(D_1\ ,\ D_4)\ ,\ max(D_2\ ,\ D_3)\ ] \qquad (3.1.4\text{-}9)$$

$$E_h = E_h(FPBP) = max(\, min(D_1 , D_2) , min(D_3 , D_4) \,) \qquad (3.1.4\text{-}10)$$

$$E_v = E_v(FPBP) = max(\, min(D_2 , D_4) , min(D_1 , D_3) \,) \qquad (3.1.4\text{-}11)$$

$$E = E_{fqcw}(FPBP) = max(E_h , E_v) \qquad (3.1.4\text{-}12)$$

$$E_{fcombined} = max(E_{fcross}, E_{fdiagonal}) \qquad (3.1.4\text{-}13)$$

2. ***JK*-type 2** of generalized *FQCW-ECF* can be obtained by using the Table 10 and Equation (3.1.4-2) as follows.

$$S_{14} = S_{qcw}(D_1, D_4) = D_1 + D_4 - D_1.D_4 \qquad (3.1.4\text{-}14)$$

$$S_{23} = S_{qcw}(D_2, D_3) = D_2 + D_3 - D_2.D_3 \qquad (3.1.4\text{-}15)$$

$$\boldsymbol{E = E_{fqcw}(FPBP) = T_{qcw}(\, S_{14} , S_{23} \,) = S_{14} \,.\, S_{14}}$$

$$\boldsymbol{= (D_1 + D_4 - D_1.D_4).(D_2 + D_3 - D_2.D_3)} \qquad (3.1.4\text{-}16)$$

We have $T_{12} = T_{qcw}(D_1, D_2) = D_1.D_2$, $T_{34} = T_{qcw}(D_3, D_4) = D_3.D_4$, $T_{13} = T_{qcw}(D_1, D_3) = D_1.D_3$, $T_{24} = T_{qcw}(D_2, D_4) = D_2.D_4$. Then,

$$\boldsymbol{E_h = E_h(FPBP) = S_{qcw}(T_{12} , T_{34}) = T_{12} + T_{34} - T_{12} \,.\, T_{34}}$$

$$\boldsymbol{= D_1.D_2 + D_3.D_4 - D_1.D_2.D_3.D_4} \qquad (3.1.4\text{-}17)$$

$$\boldsymbol{E_v = E_v(FPBP) = S_{qcw}(T_{24} , T_{13}) = T_{24} + T_{13} - T_{24} \,.\, T_{13}}$$

$$\boldsymbol{= D_2.D_4 + D_1.D_3 - D_2.D_4.D_1.D_3} \qquad (3.1.4\text{-}18)$$

$$\boldsymbol{E = E_{fqcw}(FPBP) = S_{qcw}(E_h , E_v) = E_h + E_v - E_h \,.\, E_v} \qquad (3.1.4\text{-}19)$$

$$E_{fcombined} = S_{com}(E_{fcross}, E_{fdiagonal}) = E_{fcross} + E_{fdiagonal} - E_{fcross} \,.\, E_{fdiagonal} \qquad (3.1.4\text{-}20)$$

3. ***JK*-type 3** of generalized *FQCW-ECF* can be obtained by using the Table 10 and Equation (3.1.4-2) as follows.

$$S_{14}= S_{qcw}(D_1, D_4)= D_1.D_4 + (1- D_1.D_4).[max(D_1, D_4)] \quad (3.1.4\text{-}21)$$

$$S_{23}= S_{qcw}(D_2, D_3)= D_2.D_3 + (1- D_2.D_3).[max(D_2, D_3)] \quad (3.1.4\text{-}22)$$

$$\boldsymbol{E = E_{fqcw}(FPBP)} = T_{qcw}(S_{14} , S_{23})$$

$$= [\boldsymbol{min}(S_{14}, S_{23})].(S_{14}+S_{23} -S_{14}.S_{23}) \quad (3.1.4\text{-}23)$$

$$T_{12} = T_{qcw}(D_1, D_2) = [min(D_1, D_2)] .(D_1+ D_2 - D_1.D_2) \quad (3.1.4\text{-}24)$$

$$T_{34} = T_{qcw}(D_3, D_4) = [min(D_3, D_4)] .(D_3+ D_4 - D_3.D_4) \quad (3.1.4\text{-}25)$$

$$\boldsymbol{E_h = E_h(FPBP)} = S_{qcw}(T_{12}, T_{34})$$

$$= \boldsymbol{T_{12}.T_{34} + (1- T_{12}.T_{34}).[max(T_{12},T_{34})]} \quad (3.1.4\text{-}26)$$

$$T_{24}= T_{qcw}(D_2, D_4)= [min(D_2, D_4)] .(D_2+ D_4 - D_2.D_4) \quad (3.1.4\text{-}27)$$

$$T_{34}= T_{qcw}(D_1, D_3)= [min(D_1, D_3)] .(D_1+ D_3 - D_1.D_3) \quad (3.1.4\text{-}28)$$

$$\boldsymbol{E_v = E_v(FPBP)} = S_{qcw}(T_{24}, T_{13})$$

$$= \boldsymbol{T_{24}.T_{13} + (1- T_{24}.T_{13}).[max(T_{24},T_{13})]} \quad (3.1.4\text{-}29)$$

$$\boldsymbol{E= E_{fqcw}(FPBP) = S_{qcw}(E_h , E_v)}$$

$$= \boldsymbol{E_h.E_v + (1- E_h.E_v).[max(E_h.E_v)]} \quad (3.1.4\text{-}30)$$

$$E_{fcombined}= E_{fcross}. E_{fdiagonal} +$$

$$= (1-E_{fcross}.E_{fdiagonal}).[max(E_{fcross} .E_{fdiagona})] \quad (3.1.4\text{-}31)$$

4. ***JK*-type 4** of generalized *FQCW-ECF* can be obtained by using the Table 10 and Equation (3.1.4-2) as follows.

$$S_{14}= S_{qcw}(D_1, D_4)= D_1+D_4 - D_1.D_4 +(1- D_1 - D_4 + D_1.D_4).[min(D_1, D_4)] \quad (3.1.4\text{-}32)$$

$$S_{23}= S_{qcw}(D_2, D_3)= D_2+D_3 - D_2.D_3 +(1- D_2 - D_3 + D_2.D_3).[min(D_2, D_3)] \quad (3.1.4\text{-}33)$$

$$\boldsymbol{E = E_{fqcw}(FPBP)} = T_{qcw}(S_{14} , S_{23}) = \boldsymbol{(S_{14} . S_{23}).[max(S_{14}, S_{23})]} \quad (3.1.4\text{-}34)$$

$$T_{12} = T_{qcw}(D_1, D_2) = (D_1.D_2).[max(D_1, D_2)] \quad (3.1.4\text{-}35)$$

$$T_{34} = T_{qcw}(D_3, D_4) = (D_3.D_4).[max(D_3, D_4)] \quad (3.1.4\text{-}36)$$

$$\boldsymbol{E_h = E_h(FPBP)} = S_{qcw}(T_{12}, T_{34})$$

$$= \boldsymbol{T_{12}+T_{34} -T_{12}.T_{34} + (1- T_{12} -T_{34}+T_{12}.T_{34}).[min(T_{12} ,T_{34})]} \quad (3.1.4\text{-}37)$$

$$T_{24} = T_{qcw}(D_2, D_4) = (D_2.D_4).[max(D_2, D_4)] \quad (3.1.4\text{-}38)$$

$$T_{13} = T_{qcw}(D_1, D_3) = (D_1.D_3).[max(D_1, D_3)] \quad (3.1.4\text{-}39)$$

$$\boldsymbol{E_h = E_h(FPBP)} = S_{qcw}(T_{24}, T_{13})$$

$$= \boldsymbol{T_{24} +T_{13} -T_{24}.T_{13} + (1-T_{24} -T_{13}+T_{24}.T_{13}).[min(T_{24} ,T_{13})]} \quad (3.1.4\text{-}40)$$

$$\boldsymbol{E} = E_{fqcw}(FPBP) = \boldsymbol{S_{qcw}(E_h , E_v)}$$

$$= \boldsymbol{E_h +E_v - E_h.E_v + (1-E_h -E_v + E_h .E_v).[min(E_h .E_v)]} \quad (3.1.4\text{-}41)$$

$$E_{fcombined} = S_{com}(E_{fcross}, E_{fdiagonal})$$

$$= (1- E_{fcross} -E_{fdiagona}+ E_{fcross} .E_{fdiagonal}).[min(E_{fcross} .E_{fdiagonal})] +$$

$$E_{fcross}+ E_{fdiagona} - E_{fcross} .E_{fdiagonal} \quad (3.1.4\text{-}42)$$

5. ***JK*-type 5** of generalized *FQCW-ECF* can be obtained by using the Table 10 and Equation (3.1.4-2) as follows.

$$S_{14} = S_{qcw}(D_1, D_4) = D_1 + D_4 -(D_1.D_4).(D_1 + D_4 - D_1.D_4) \quad (3.1.4\text{-}43)$$

$$S_{23} = S_{qcw}(D_2, D_3) = D_2+ D_3 -(D_2.D_3).(D_2+ D_3 - D_2.D_3) \quad (3.1.4\text{-}44)$$

$$E = E_{fqcw}(FPBP) = T_{qcw}(S_{14}, S_{23})$$

$$= (S_{14} . S_{23}).(S_{14} + S_{23} - S_{14} . S_{23}) \quad (3.1.4\text{-}45)$$

$$T_{12} = T_{qcw}(D_1, D_2) = (D_1.D_2).(D_1 + D_2 - D_1.D_2) \quad (3.1.4\text{-}46)$$

$$T_{34} = T_{qcw}(D_3, D_4) = (D_3.D_4).(D_3 + D_4 - D_3.D_4) \quad (3.1.4\text{-}47)$$

$$E_h = E_h(FPBP) = S_{qcw}(T_{12}, T_{34})$$

$$= T_{12} + T_{34} - (T_{12} . T_{34}).(T_{12} + T_{34} - T_{12} . T_{34}) \quad (3.1.4\text{-}48)$$

$$T_{24} = T_{qcw}(D_2, D_4) = (D_2.D_4).(D_2 + D_4 - D_2.D_4) \quad (3.1.4\text{-}49)$$

$$T_{13} = T_{qcw}(D_1, D_3) = (D_1.D_3).(D_1 + D_3 - D_1.D_3) \quad (3.1.4\text{-}48)$$

$$E_h = E_h(FPBP) = S_{qcw}(T_{24}, T_{13})$$

$$= T_{24} + T_{13} - (T_{24} . T_{13}).(T_{24} + T_{13} - T_{24} . T_{13}) \quad (3.1.4\text{-}50)$$

$$E = E_{fqcw}(FPBP) = S_{qcw}(E_h, E_v)$$

$$= E_h + E_v - (E_h . E_v).(E_h + E_v - E_h . E_v) \quad (3.1.4\text{-}52)$$

$$E_{fcombined} = S_{com}(E_{fcross}, E_{Diagonal}) \quad (3.1.4\text{-}53)$$

$$= E_{fcross} + E_{fdiagona} - (E_{fcross} . E_{fdiagonal}).(E_{fcross} + E_{fdiagona} - E_{fcross} . E_{fdiagonal})$$

3.2 Correlation of *FQCW* Pattern With Binary Edge Patterns

There is another method by which we can evaluate the *FQCW* pattern within A processing block *FB*. This method is similar to methods explained in section 2.2, but here we deal with fuzzy vector *FPBP* which compares with edge code word space *BEP*. Since we can consider binary values as a special case of fuzzy values 0 and 1 with associating membership degree 1, (1/0 or 1/1), this comparison is possible.

3.2.1 Distance Correlation of *FQCW* Pattern

Consider a *FQCW* within a processing block *FB* of an intensity image. Let *FPBP* be a the fuzzy vector characterizing the *FQCW* pattern, then the distances between *FPBP* vector and the BEP_p vectors are generally defined as Equation (2.2.1-1). This equation represents the correlation between processing block pattern *FB* and the binary edge patterns.

$$FDC_p = \| DV - BEP_p \| \qquad for\ j=1,2,3,\ldots 9 \qquad (3.2.1\text{-}1)$$

DV is a vector obtained by the conversion of the fuzzy vector *FPBP* to a crisp value vector as

$$DV = \left[\mu d_1 \cdot d_1, \mu d_2 \cdot d_2, \mu d_3 \cdot d_3, \mu d_4 \cdot d_4\right] \qquad (3.2.1-2)$$

Distance correlation results in a value denoting the degree of correspondence of the *FPBP* vector to the edge code word BEP_p. We are looking for the maximum degree of correspondence to the edge code word space *BEP*, then the minimum value of FDC_p meets our need. We can define the degree of edginess of *FPBP* by Equation (3.2.1-3). According to this definition, the closer the *FPBP* vector is to the edge pattern vector space, the greater is the degree of edginess E_{fdc} is in value.

$$E_{fdc} = 1 - \frac{\min\limits_p \left\{ \left\| DV - BEP_p \right\| \right\}}{\max\limits_p \left\{ \left\| DV - BEP_p \right\| \right\}} \quad for\ \ p = 1,2,3,4 \qquad (3.2.1-3)$$

3.2.2 Angular Correlation of *FQCW* Pattern

Consider a *FQCW* within a processing block *FB* of an intensity image and let *FPBP* be the characteristic vector of this *FQCW* pattern. Angular correlation is a proper measurement for degree of correspondence of *FPBP* to binary edge patterns BEP_p. That is to find the minimum angle (or maximum cosine angle) between *FPBP* vector and BEP_p vectors. The angular correlation between the processing block pattern and the binary edge patterns is generally obtained by

$$Cos(\Phi_p) = \left[\frac{< DV \cdot BEP_p >}{\|DV\| \cdot \|BEP_p\|} \right] \qquad for \quad p = 1,2,\ldots,9 \qquad (3.2.2-1)$$

DV is defined by Equation (3.2.1-2). This Equation results in a value within interval [0,1]. Therefore, for p=1,...9 , there are nine different values representing the degree of correspondence of *FPBP* vector to BEP_p vectors. The maximum value for the cosine angle between vector *DV* and edge code word space will be obtained if the vector *DV* is completely matched with one of the edge code words. That means the maximum degree of edginess 1 occurs if Cos(Φp) possesses the maximum value 1. Therefore, the degree of edginess based on the defined angular correlation in Equation (3.2.2-1) is defined by Equation (3.2.2-2).

$$E_{fac} = \max_p \left\{ Cos(\Phi_p), \right\} \qquad for \quad p = 1,2,\ldots,9 \qquad (3.2.2-2)$$

3.3 Tunable Edge Detector Based on *FQCW-ECF*

The edge detector based on *FQCW-ECF* can be designed using a fuzzy logic controller to extract the edge as desired. An edge detecting algorithm based on fuzzy logic with flexible rules as well as tunable membership functions would be an effective approach in edge detection. The Figure 35 illustrates a general idea of this edge detecting algorithm using the fuzzy logic controller for block processing of an image in order to detect the edge.

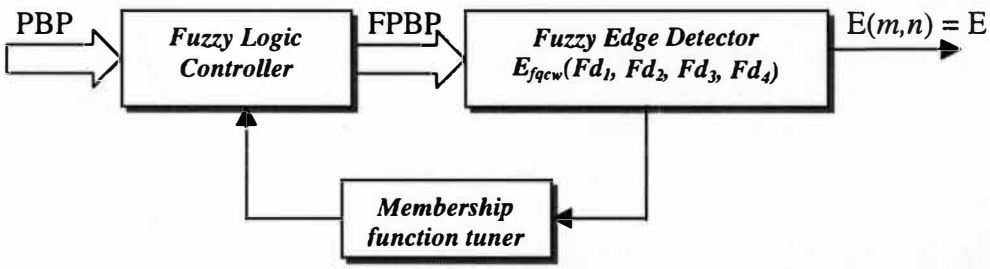

Figure 35. Illustration of Edge Detection Using Fuzzy Logic Controller.

The input is a processing block pattern (*QCW* intensity pattern of block *B*) denoted by vector *PBP*. This pattern is fuzzified by fuzzy logic controller to generate the *FQCW* intensity pattern, *FPBP* vector, as an input to fuzzy edge detector. While this fuzzy detector is defuzzifying the fuzzy vector *FPBP* to a crisp value, it is also generating the maximum degree of correspondence of pattern *PBP* to the binary edge patterns *BEP* or degree of edginess of the middle pixel (*m,n*) centered on the block *B*. The feedback is applied to tune the membership functions for gaining the appropriate membership degree μd_k for d_k (for k=1,2,3,4) based on the result *E* in output. The

design of an edge detector based on *FQCW-ECF* using fuzzy logic controller is explained in detail further in Chapter IV.

Edge detection algorithm based on *FQCW-ECF* algorithm can be summarized as follows:

1. Choose a proper size of block *FB*, *W*×*W*, with the middle fuzzy singleton indicating the intensity pixel FX_{mn}.

2. Do the *FQCW* within block *B* using the diagonal, cross, or/and other desired configurations (based on desired pixels neighboring the middle pixel), to find four child windows FB_1, FB_2, FB_3, FB_4.

3. Choose an appropriate aggregation operator *g* (averaging operator) and apply it over each child window to find four representative intensities FY_1, FY_2, FY_3, FY_4. It can be done by Equations (3.1.2-1), (3.1.2-2), (3.1.2-3). In case of noisy image, replace the fuzzy representative intensity pixel FX_{mn} with FX'_{mn} based on Equations (3.1.2-4) and (3.1.2-5).

4. Construct the fuzzy processing block pattern vector $FPBP=[\mu d_1/d_1, \mu d_2/d_2, \mu d_3/d_3, \mu d_4/d_4]$ using Equations (3.1.3-1), (3.1.3-2), (3.1.3-3).

5. Choose or derive a desired *t*-norm T_{qcw} and *t*-conorm S_{qcw} using Tables 2 and 10.

6. Apply the *JK*-type generalized *FQCW-ECF*, distance or angular correlation given respectively by Equations (3.1.4-2 or 3.1.4-5), (3.2.1-3), and (3.2.2-2) for each individual *FQCW* configuration (diagonally, crossly or any desired morphological structure), to find $E= E_{qcw}(FPBP)= E_{qcw}(\mu d_1/d_1, \mu d_2/d_2, \mu d_3/d_3, \mu d_4/d_4)$ the degree of

correspondence of vector *FPBP* to the binary edge pattern space *BEP* given by Table 8 (or degree of edginess of *FPBP* at middle pixel (m,n)). Since we applied the normalized gray scale indicating intensity within continuous interval [0,1]. Therefore, this degree of correspondence directly represents the intensity of edge pixel (if thresholding is not applied) and is replaced instead of middle pixel intensity X_{mn}.

7. If there are more than one configuration, combine the result of each pair of configurations obtained from step 6 using a proper t-conorm S_{fcom}, to find the $E_{fcombined} = S_{fcom}(E_{fcross}, E_{fcross})$.

8. Apply tuning of membership function to adjust $\mu d_1, \mu d_2, \mu d_3, \mu d_4$ till to obtain the desired output in edge detector (part 6 or 7), that is optimization of edge detection.

CHAPTER IV

SIMULATION AND MODELING

Generally speaking, there are the three facets to engineering systems: (1) input(s); (2) output(s); and (3) system itself. If input and output of system are known, then creating the system is a design problem. In a simple system design, the important factor is a precise mathematical description by which the relation between input and output is defined for that system. For modularity, a complex system consists of a set of sub-systems, each with their own input/output characteristics. However, each sub-system can be modeled by its own characteristic as a module to finally build up the main complex system model. Once modeling is completed, simulation can be done using computer software to demonstrate or to enhance the system performance, sensitivity and optimization.

4.1 Optimal Edge Detector System Using Fuzzy Logic System

In preceding chapter we attempted to find an appropriate characteristic function for edge extraction within a block B of an image. we now apply the obtained edge characteristic function (*ECF*) as a mathematical description of edge detector system. We are going to design a tunable edge detector system (*EDS*) which is controllable by a fuzzy logic controller system (*FLC*). The optimal edge is detected by means of multi-dimensional optimization module (*MOM*) which properly tunes the

membership functions of input/output variables of *FLC*. Fuzzy image processing module *F-IPM*, the controller *FLC*, and the optimizer system *MOM* are the fuzzy part of our *EDS* system. *F-IPM* provides the *FLC* and *MOM* with the necessary image data. The inter-module communication of *EDS* is represented in Figure 36.

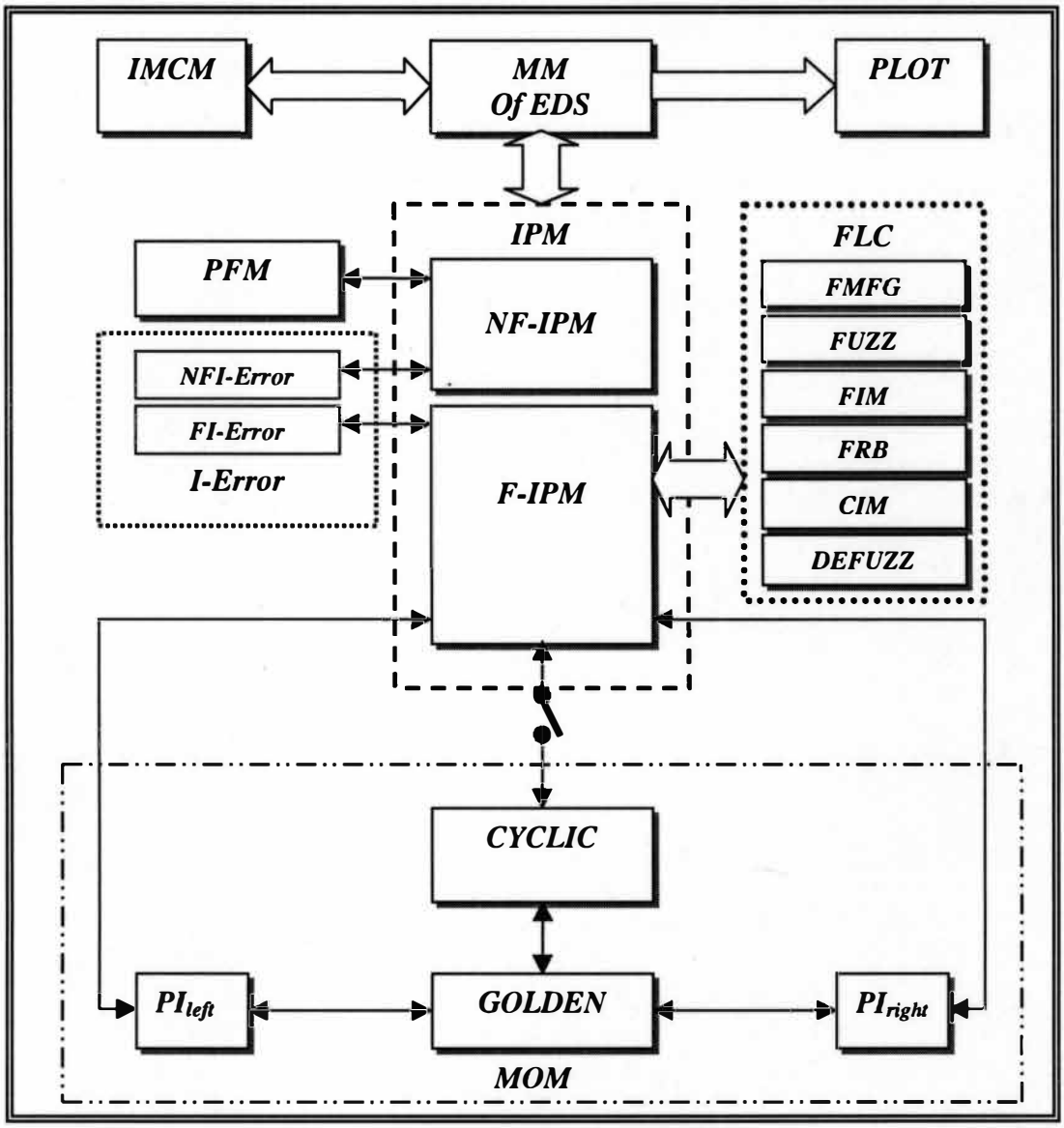

Figure 36. Optimal Edge Detector System (*EDS*) Using *FLC*.

4.1.1 Introducing *EDS* Modules

The designed and simulated *EDS* consists of 18 modules. *EDS* has been simulated according to the fuzzy and non-fuzzy algorithms which have been discussed in preceding chapters. Once modeling of *EDS* is completed and the tasks of *EDS* and its associated modules are specified, then the *EDS* can be simulated by individual simulation of each module and finally linking all modules together in order to obtain the desired task of the *EDS*. Here the simulation is done by *MATLAB* image processing and fuzzy logic tool box version 5.1. The simulation is capable of executing all defined algorithms simultaneously and making a comparison between algorithms. The simulated *EDS* modules are as follows:

1. ***IMCM***: Physical image to matrix conversion module. This module converts the given color or monochrome images to an intensity (monochrome) image matrix. Each component of this matrix represents the intensity of respective pixel in a physical image and has a value within interval [0,1] which is considered as the normalization of set {0,1,2,...L-1} with L gray levels.

2. ***MM***: Main module initializes parameters and provides interfacing or linking to the other modules. Also, it provides the desired information for displaying (monitoring).

3. ***IPM***: Image processing module consists of a fuzzy section *F-IPM* and non fuzzy section *NF-IPM*. This module is a base to provide other modules with the necessary data from the image matrix. This module applies the block processing method to properly modify the data for uses of the other modules (as you observe its

inter-communications with other modules in Figure 36). *NF-IPM* processes image data to make a suitable data for implementing the non-fuzzy algorithms. The *F-IPM* modifies image data to prepare the necessary data for implementing the fuzzy algorithms.

4. ***PFM***: Processing function module provides the non-fuzzy part of *EDS* with the *ECF* in order to implement the non-fuzzy algorithms for edge detection.

5. ***FLC***: Fuzzy logic controller is designed with the flexible fuzzy rules and tunable input/output membership functions to enhance the optimal edge trace. *FLC* consists of *fuzzification, FIM, FRB, CIF, defuzzification* and *MOM* modules.

6. ***FUZZ***: This fuzzification module is used to convert crisp data Y_1, Y_2, Y_3, Y_4, X_{mn}, (concerning *QCW*-pattern within block *B* of an intensity image *II*) respectively to the fuzzy singleton data FY_1, FY_2, FY_3, FY_4, FX_{mn}. The fuzzified data are processed in *FIM* to make the decision for he output of *FLC*.

7. ***FMFG***: Fuzzy membership function generator is used to produce the desired functions used in fuzzy plane *P* for fuzzification of image data. This module is able to generate triangular and trapezoid shaped functions (section 1.3.3) over the intensity interval [0,1] or gray scale {0,1,...*L*-1} as Figure 7. The membership functions are used in fuzzification of the input data to *FLC* and implicating the output membership degrees of the fuzzy inference machine *FIM*.

8. ***FRB***: Fuzzy rule base is the module where the knowledge concerning the performance strategy of *FLC* is linguistically stored in the form of fuzzy rules.

9. ***FIM***: Fuzzy Inference Module is used to implicate the membership degrees for output based on the fired fuzzy rules from the rule base. The input of *FIM* is fuzzy singletons FY_1, FY_2, FY_3, FY_4, FX_{mn} and the implicated output based on fuzzy rules are fuzzy singletons Fd_1, Fd_2, Fd_3, Fd_4.

10. ***CIM***: Contrast intensification module is used to intensify the membership degrees of fuzzy singletons in *FIM* outputs. The outputs of *FIM* are brought to this module for intensification of membership degrees by using the function T_s (section 1.4.2).

11. ***DEFUZZ***: This defuzzification module of *FLC* is applied to convert fuzzy singletons (intensified or not) Fd_1, Fd_2, Fd_3, Fd_4 to a crisp value E_{mn} which also indicates the degree of edginess of the middle pixel X_{mn}. This module is capable of implementing the fuzzification according to *COA*, *MOM*, *COM*, and all defined E_{fqcw} (defined in sections 1.3.7, 3.1.5, 3.2.1, 3.2.2).

12. ***MOM***: Multidimensional optimization module which is applied to tune input/output membership function(s) of *FLC* in order to optimize the edge trace in output of *EDS*. Cyclic coordinate algorithm (*CYCLIC*) along with the golden ratio line search algorithm (*GOLDEN*) are used to minimize the performance index $PI=\|e\|^2$. The term e is the error matrix between the desired edge matrix I_{Ed} and the actual edge trace matrix I_E in output of *EDS*. The vector V is constructed containing the overlap percentages and peak points of input/output membership functions of *FLC* as the tuning variables. 'V' is the input of *MOM* and the output is V^* indicating the optimal value for vector V, (section 1.5.5).

13. ***I-Error***: Image error module consists of two modules *NFI-Error* and *FI-Error* which are used to determine the cumulative error, cumulative square error, matrix square error (*SQE*), mean error (*ME*), and matrix correlation (*TDC*) for all explained non-fuzzy and fuzzy algorithms of edge detection (sections 1.6.4, 1.6.5).

4.1.2 *EDS* Task Descriptions

Figure 37 illustrates a tunable edge detector system (*EDS*) which is able to find edge based on the explained fuzzy and non-fuzzy algorithms in the preceding chapters. The optimal edge is detectable through a certain optimization algorithm. A simple feedback system is used to take the output of *EDS* towards an optimal point. The following block diagram gives the general idea about the inter-communications between the fuzzy logic controller *FLC*, fuzzy image processing module *F-IPM* and multi-dimensional optimization module *MOM*.

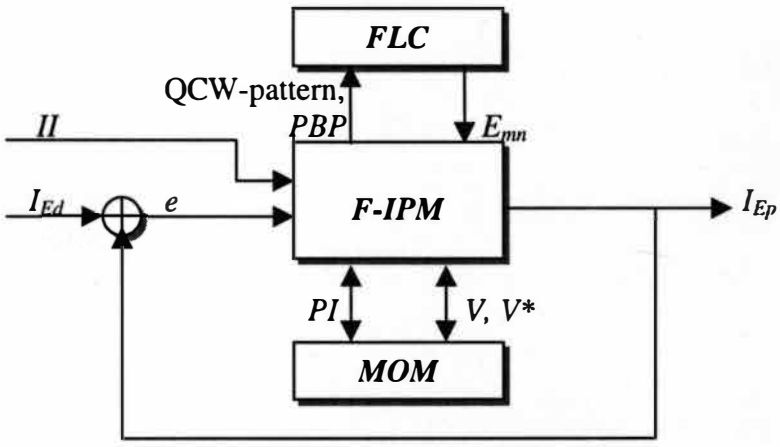

Figure 37. Inter-Communication of Fuzzy Part of *EDS*.

Child window filtering is properly implemented by *NF-IPM* for the non-fuzzy edge detection algorithm. Child window processing results in four representatives denoted by Y_1, Y_2, Y_3, Y_4. These four intensity representatives, as well as the middle pixel intensity X_{mn}, represent the *QCW*-pattern within block *B* and are also considered inputs to the *FLC* system. *NF-IPM* generates the proper *QCW* pattern(s) specified by its (their) patterning characteristic vector(s) *PBP* for the processing block *B* of the intensity image *II*. The *QCW* pattern(s) (Y_1, Y_2, Y_3, Y_4, X_{mn}) within the block *B* and its relevant vector(s) *PBP* are the input of *FLC*. The *FLC* output is the degree of edginess relating to the middle intensity pixel X_{mn} of the block *B*.

Multidimensional optimization based on the cyclic coordinate algorithm (explained in section 1.5.6) is adopted to minimize the desired error function as performance index *PI* (cost function) of *EDS* by tuning the input/output membership functions of *FLC*. This optimization is used just for fuzzy approaches to edge detection. Block processing technique is applied to find the edge pixels of the image by using *QCW* techniques which have been explained in chapter 2. As you observe in Figure 37, the error matrix $e = I_{Ed} - I_E$ (difference between the desired edge trace I_{Ed} and actual edge trace I_E) is used to derive performance index, $PI = \|e\|^2$, as an objective function in the optimization procedure for conducting the *EDS* system towards an optimal state. The output of multidimensional optimization module *MOM* is the vector *V* which contains the tuning variables of the input/output membership function of *FLC*.

The non-fuzzy part of *EDS* can be simply illustrated as Figure 38. The

input of *NF-IPM* is the intensity image *II*. After choosing proper *QCW* configuration(s) within block *B*, this module executes the suitable child window processing for the non-fuzzy algorithm and creates the *QCW* pattern(s) with its (their) relevant *PBP* as input to *PFM*. *PFM* which contains the functions relating to the non-fuzzy edge detection algorithms generates E_{mn}, the degree of edginess of the middle pixel intensity X_{mn}.

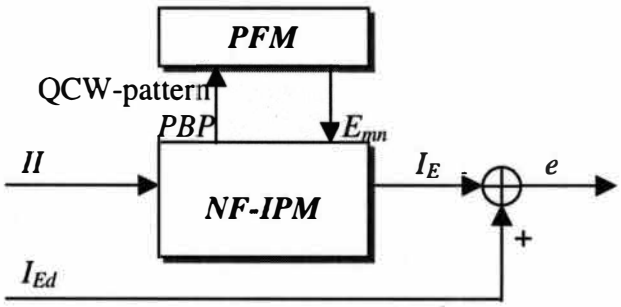

Figure 38. Inter-Communication of Non-Fuzzy Part of *EDS*.

Tasks of the optimal edge detector system (*EDS*) depicted in Figure 36 can be summarized as follows:

1. Converting the physical monochrome or color image to an intensity (monochrome) image matrix *II* with size $M \times N$ and *L* gray levels, section 1.2.3. Done by the module *IMCM*.

2. Constructing a movable block (window or mask) *B* with the selective size of block $W \times W$ and middle intensity pixel X_{mn}. Done by the module *IPM*.

3. Sliding the block *B* over the given image pixel by pixel from top to bottom to process all regions of the given image, section 1.2.6. Done by the module *IPM*.

4. Selecting and constructing the suitable *QCW* configuration(s) (cross, diagonal and combination of both), section 2.1.3. Done by module *IPM*.

5. Child window processing (filtering) using *median, min, max, mean* operators based on the inquiry of fuzzy or non-fuzzy algorithms to find representative pixels Y_1, Y_2, Y_3, Y_4, section 2.1.4. Done by the module *IPM*.

6. Constructing the processing block pattern vector $PBP=[\ d_1,\ d_2,\ d_3,\ d_4]$ which is defined as the patterning characteristic of *QCW* within the processing block *B*, Equation 2.1.5-7. Done by the module *IPM*.

7. Constructing the code words BEP_p for 9 classes of the defined binary edge patterns, Table 8. Done by the module *IPM*.

8. Detecting edge based on non-fuzzy algorithms within the processing block *B*, and individually storing the edge trace matrix I_E resulting from each algorithm, sections 1.2.10 (derivative methods), 2.1.6, 2.1.7, 2.2.1, 2.2.2 (*QCW- ECF* algorithms). Done by *PFM*.

9. Generating tunable membership functions, trapezoid and triangular shaped, over the gray level $\{0,1,2,\ldots,L\text{-}1\}$ or intensity interval [0,1], sections 1.3.3 and 1.3.8. Done by the module *FMFG*.

10. Fuzzification of *QCW* pattern (crisp values Y_1, Y_2, Y_3, Y_4, X_{mn}) within the block *B* in order to obtain *FQCW* pattern (fuzzy singletons FY_1, FY_2, FY_3, FY_4, FX_{mn}), section 3.1.2. Done by the *fuzzification* module in *FLC*.

11. Storing information or knowledge pertaining to the desired performance of *FLC* in the form of linguistic fuzzy rules, *IF-THEN*, in fuzzy rule base *FRB*.

12. Applying *Max-Min* fuzzy reasoning, to implicate the membership degrees of *FIM* outputs based on the fired control rules from *FRB*, done by the module *FIM*, (section 1.3.6). The inputs to *FIM* are fuzzy singletons FY_1, FY_2, FY_3, FY_4, FX_{mn} defining *FQCW* pattern. The implicated outputs are fuzzy singletons Fd_1, Fd_2, Fd_3, Fd_4, which are components of vector *FPBP*, section 3.1.3.

13. Defuzzifying the fuzzy vector $FPBP=[Fd_1, Fd_2, Fd_3, Fd_4]$ based on defuzzification methods *COA*, *MOM*, *COM* or *FQCW-ECF*, E_{fqcw}, section 3.1.4 (special cases of *QCW* edge characteristic functions *JK*-type1,2,3,4,5)). The value E_{mn} indicates the degree of edginess of vector *FPBP* at point (m,n) and is replaced instead of middle intensity value X_{mn} in processing block. Done by the defuzzification module.

14. Determining the error matrix e which is deference between desired edge trace I_{Ed} and the actual edge trace matrix I_E in output of *EDS* (for normalization of components, each edge trace matrix before calculation of error is divided by its maximum component). Also, calculating the commutative error and commutative square error in each middle pixel while block B is sliding over the image. This is computed simultaneously for all running algorithm during the process, section 1.6.4. Done by the *FI-Error* and the *NFI-Error* modules.

15. Determining the performance index (cost function) $PI = \|e\|^2$. This is used as an objective function to be minimized by *MOM* in order to optimize the *EDS* system, section 1.5-6. Done by PI_{left}, PI_{right} modules.

16. In case of optimization, optimizing the edge trace in *EDS* output based on minimizing the $PI=||e||^2$ as the objective function. The optimization is done by tuning the input/output membership functions of *FLC*. The overlap percentages and peak points (the components of vector *V*) of the membership functions are used as the tuning variables. The cyclic coordinate algorithm is applied to derive the result of defuzzification ($E_{mn}= E_{fqcw}$) in the *FLC* output toward an optimal value ($E^*_{mn}= E^*_{fqcw}$) by tuning μd_1, μd_2, μd_3, μd_4, section 1.5.6. Done by the *MOM* module.

4.1.3 Experimental Results

Due to different variation of intensities and also variety of objects from one image to the another one, an efficient edge detection algorithm must be such powerful to possess that flexibility to produce the proper edge traces for any type of images, disregards to the degree of smoothness, sharpness, noisiness, and pixel to pixel intensity transition. Also, it must generate the appropriate edge traces independent to the size of the objects and satisfactorily results in a same quality for small and big objects. Toward this purpose, To investigate the efficiency of the aforementioned algorithms, we find the experimental results through three examples over three types of $M\times M$ images as: (1) an image illustrating an small object in example one; (2) an image given in example two representing the similar foreground and background intensities (in some regions), smoothness, and various intensity transition in different regions; and (3) an image covered by Gussian and Salt & Pepper noises.

To judge about the obtained results, we compare the $M\times M$ edge trace matrix

resulted from each algorithm (without thresholding), denoted by *IE,* with a *M×M* ideal binary edge trace matrix, denoted by *Id.* For this purpose, we apply three kinds of measurements as the performance indexes as; (1) mean error, *ME*, and total mean error *TME* defined by Equations (1.6.5-2) and (1.6.5-3); (2) square error, *SQE*, defined by Equation (1.6.5-4), but multiplied by 100/(*M.M-NIEP*) such that *NIEP* is the number of ideal edge pixels; and (3) two dimensional correlation ,*TDC*, given by Equation (1.6.6-1), where *A=IE* and *B=Id* in all three cases.

The outputs, edge trace matrices *IE1, IE2, ...,IE21,* have been obtained without using thresholding technique. These matrices are respectively the results of the algorithm mentioned in the tables given in examples 1,2,3. The *IE1, IE2,* and *IE3* matrices are results of non-linear derivative algorithms. The *IE4, IE5,* and *IE6* matrices represent the results from simple intensity difference (classic) methods explained in section 1.4.4. The *IE7, ...,IE17* matrices are resulted from some special cases of generalized *QCW-ECF*. The *IE18* matrix is the optimal edge trace based on *FQCW-ECF* (*JK*-type1) generated by fuzzy logic system and optimized by the cyclic coordinate algorithm. The *IE19, IE21* are also edge matrices based on *FQCW-ECF* but not optimized. They are defuzzified in *FLC* respectively using *COA* and *MOM* methods. To obtain *IE20,* the membership degrees μ_{d1}, μ_{d2}, μ_{d3}, μ_{d4} resulting from *FLC* are intensified 7 times (*s*=7) by means of recursive Equation (1.4.2-2) before applying *COA* defuzzification method.

For *QCW* and *FQCW* within a block of 5×5, the morphological structure given in Figure 39 is applied. Also, for diagonal and cross *QCW* configurations (both

5×5 and 3×3), the structures represented in Figures 22 and 23 are applied.

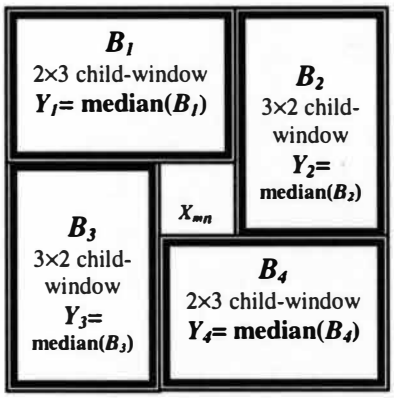

Figure 39. One Possible $(F)QCW$ Configuration Within a 5×5 Block B.

In case of noisy images in example 3, to remove the noises, the median filtering is applied within each child window B_k. Averaging operation is also used within the region B-$\{(m,n)\}$ and the result of this averaging (Equation 1.2.5-1) X'_{mn} is considered as the representative of entire block B. That is, $X_{mn} = X'_{mn}$.

The fuzzy logic rule base designed for edge detection algorithm contains the rules given by Figure 40.

Outputs d1,d2,d3,d4

MF of FLC for input Xmn	MF of FLC, for inputs Y1,Y2,Y3,Y4: D	DG	G	BG	B
D	Z	S	M	L	XL
DG	S	Z	S	M	L
G	M	S	Z	S	M
BG	L	M	S	Z	S
B	XL	L	M	S	Z

Figure 40. Fuzzy Rules Applied in *FLC* for Fuzzy Algorithms in Examples 1,2,3.

To find the optimal edge trace using fuzzy logic, we use cyclic coordinate algorithm to tune input/output membership functions of *FLC* in order to obtain the appropriate μ_{d1}, μ_{d2}, μ_{d3}, μ_{d4}. In this optimization, tuning the membership functions are done by adjusting the percentage of overlaps and peak points.

We consider one fixed percentage of overlap for input *MF*s, denoted by P_{ovlin}, and another fixed value for output *MF*s, denoted by P_{ovlout}. Five peak points, denoted by C_{in1}, C_{in2}, C_{in3}, C_{in4}, C_{in5}, for input *MF*s and five peak points, denoted by C_{out1}, C_{out2}, C_{out3}, C_{out4}, C_{out5}, for outputs are also considered along with mentioned percentage of over lap to adjust the *MF*s such that the performance index $SQE = [100/(M.M\text{-}NIEP)].\|Id - IE\|^2$ is minimized. The vector $V=[P_{ovlin}, C_{in1}, C_{in2}, C_{in3}, C_{in4}, C_{in5}, P_{ovlout}, C_{out1}, C_{out2}, C_{out3}, C_{out4}, C_{out5}]$ is considered for this multidimensional optimization using cyclic coordinate algorithm explained in 1.5.5 and 1.5.6.

Cyclic coordinate algorithm finds the optimal components for the vector V (containing the input/output *MF*s of *FLC*) by minimizing the *SQE*. That is, $V_{initial} \rightarrow V^*_{optimal}$.

For all three examples, the input and output membership functions of *FLC* are initialized symmetrically before optimization meaning that the vector V is initialized as $V_{initial}$=[0.5, 0.167, 0.333, 0.5, 0.667, 0.833, 0.5, 0.167, 0.333, 0.5, 0.667, 0.833].

Example 1. To represent the efficiency of *QCW-ECF* and its fuzzy associated *FQCW-ECF* against the other derivatives algorithm for small object edge detection, we have provided the first experiment as follows. A 8 × 8 intensity image matrix *II*1 (*L*=16) containing a small size object (ring) has been applied as an input to the *EDS*. The data and figures resulted from *EDS* are given in Table 11 and Figures 41 to 46.

Table 11

Comparison Table for Fuzzy and Non-Fuzzy Algorithms in Example 1

	Trace	Methods	Eq.	Block size	(F)QCW structure Fig.	Defuzzification	TME	SQE %	TDC
	IE1	**Roberts**	1.2.10-1	2×2			0.082	4.765	0.858
	IE2	**Sobel**	1.2.10-2	3×3			0.092	5.495	0.836
	IE3	**Wallis**	1.2.10-5	3×3			0.063	4.282	0.884
	IE4	**Classic**	1.4.4-1	5×5			0.250	30.76	-.124
	IE5	**Classic**	1.4.4-2	5×5			0.026	1.335	0.967
	IE6	**Classic**	1.4.4-3	5×5			0.063	7.692	0.832
	IE7	**Angular Corr.**	2.2.2-1	5×5	39		0.064	7.408	0.833
	IE8	**Distance Corr.**	2.2.2-2	5×5	39		0.012	0.077	0.998
	IE9	***JK*-type1**	2.1.7-7	5×5	39		0.018	0.654	0.984
	IE10	***JK*-type2**	2.1.7-14	5×5	39		0.013	0.129	0.997
	IE11	***JK*-type3**	2.1.7-21	5×5	39		0.013	0.129	0.997
Q	*IE12*	***JK*-type4**	2.1.7-32	5×5	39		0.025	0.328	0.993
C	*IE13*	***JK*-type5**	2.1.7-43	5×5	39		0.019	0.197	0.995
W	*IE14*	***JK*-type1**	2.1.7-10	5×5	23 (b)		0.005	0.053	0.999
	IE15	***JK*-type1**	2.1.7-11	3×3	22 (c)		0.036	0.617	0.936
	IE16	***JK*-type1**	2.1.7-11	5×5	23 (e)		0.018	0.654	0.984
	IE17	***JK*-type1**	2.1.7-11	5×5	23 (d)		0.018	0.654	0.984
F	*IE18*	***JK*-type1***(Fuzzy)*	3.1.4-9	5×5	39	*JK*-type1	0.000	0.000	1.000
Q	*IE19*	**Fuzzy model**	1.3.7-5	5×5	39	*COA*	0.034	0.706	0.984
C	*IE20*	**Fuzzy model**	1.3.7-5	5×5	39	*COA*, (*INT*)	0.022	0.369	0.988
W	*IE21*	**Fuzzy model**	1.3.7-4	5×5	39	*MOM*	0.034	0.706	0.984

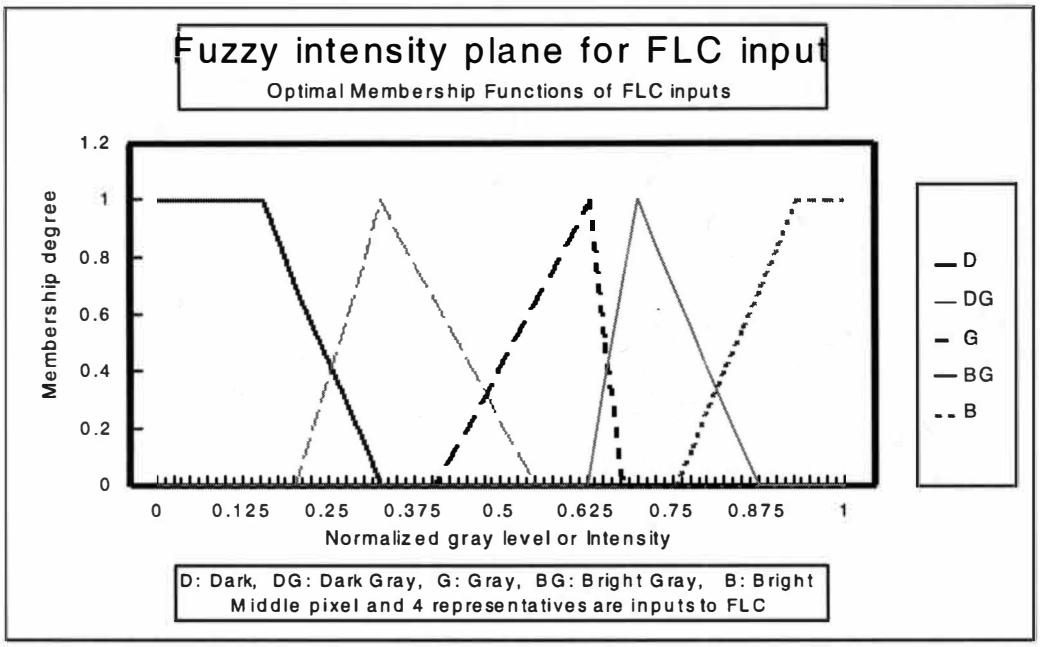

(a) Input *MF*s of *FLC* for Example1.

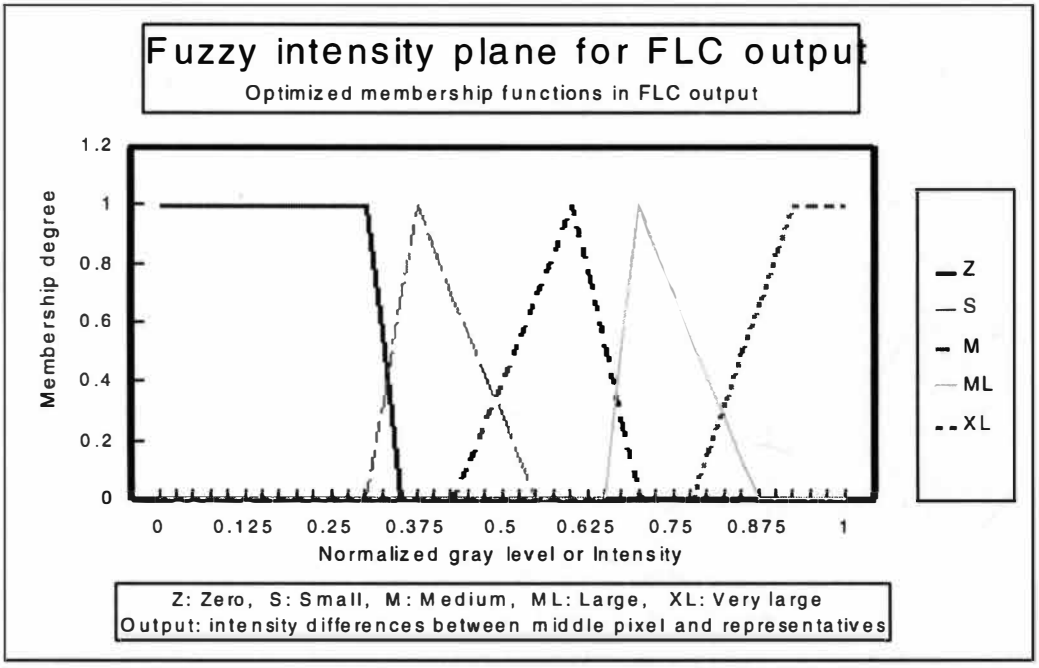

(b) Output *MF*s of *FLC* for Example 1.

Figure 41. Optimized Input/Output *MF* of *FLC* for Example 1 Obtained by *MOM*.

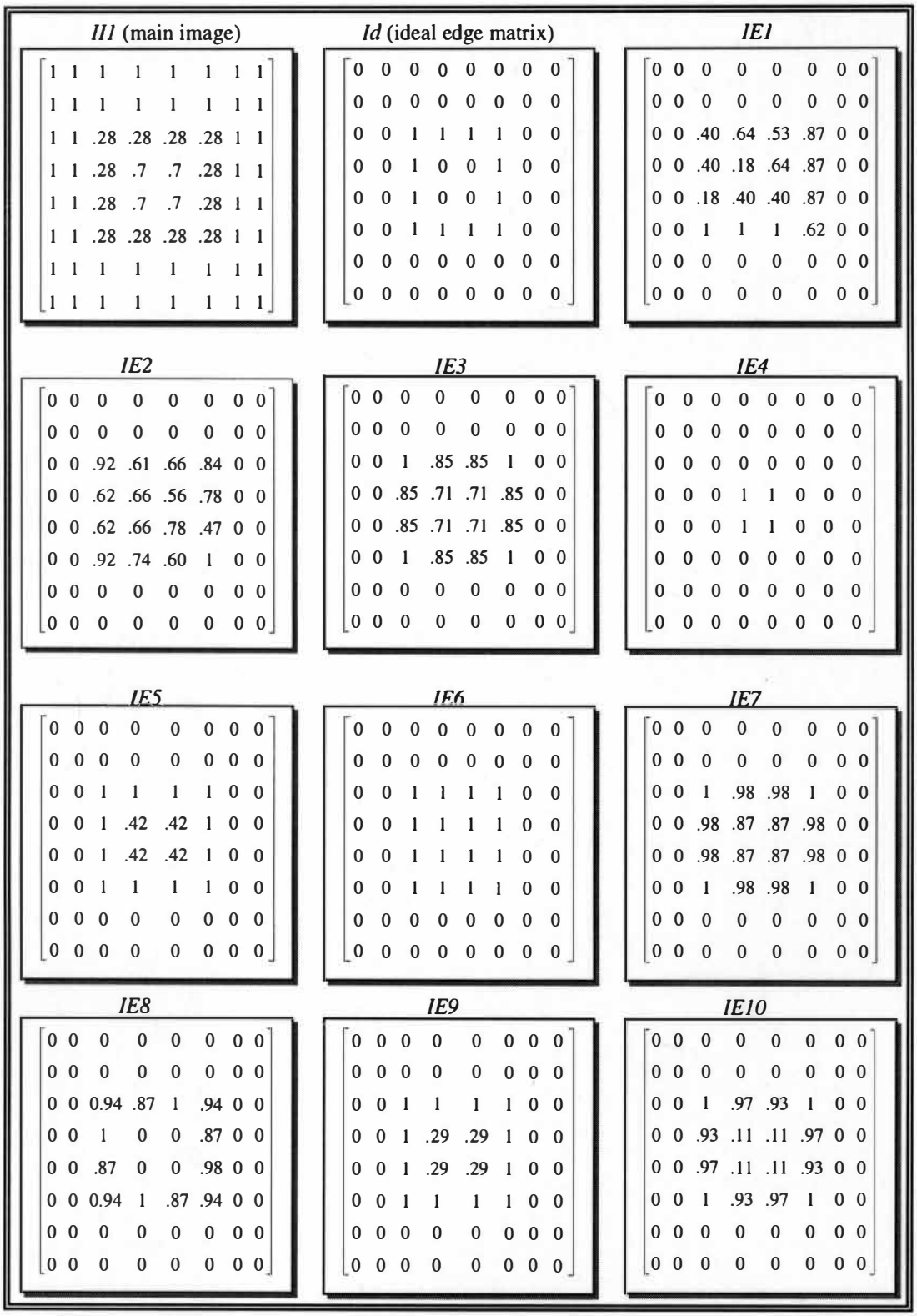

Figure 42. Illustration of Edge Trace Matrices Generated by *EDS* in Example1.

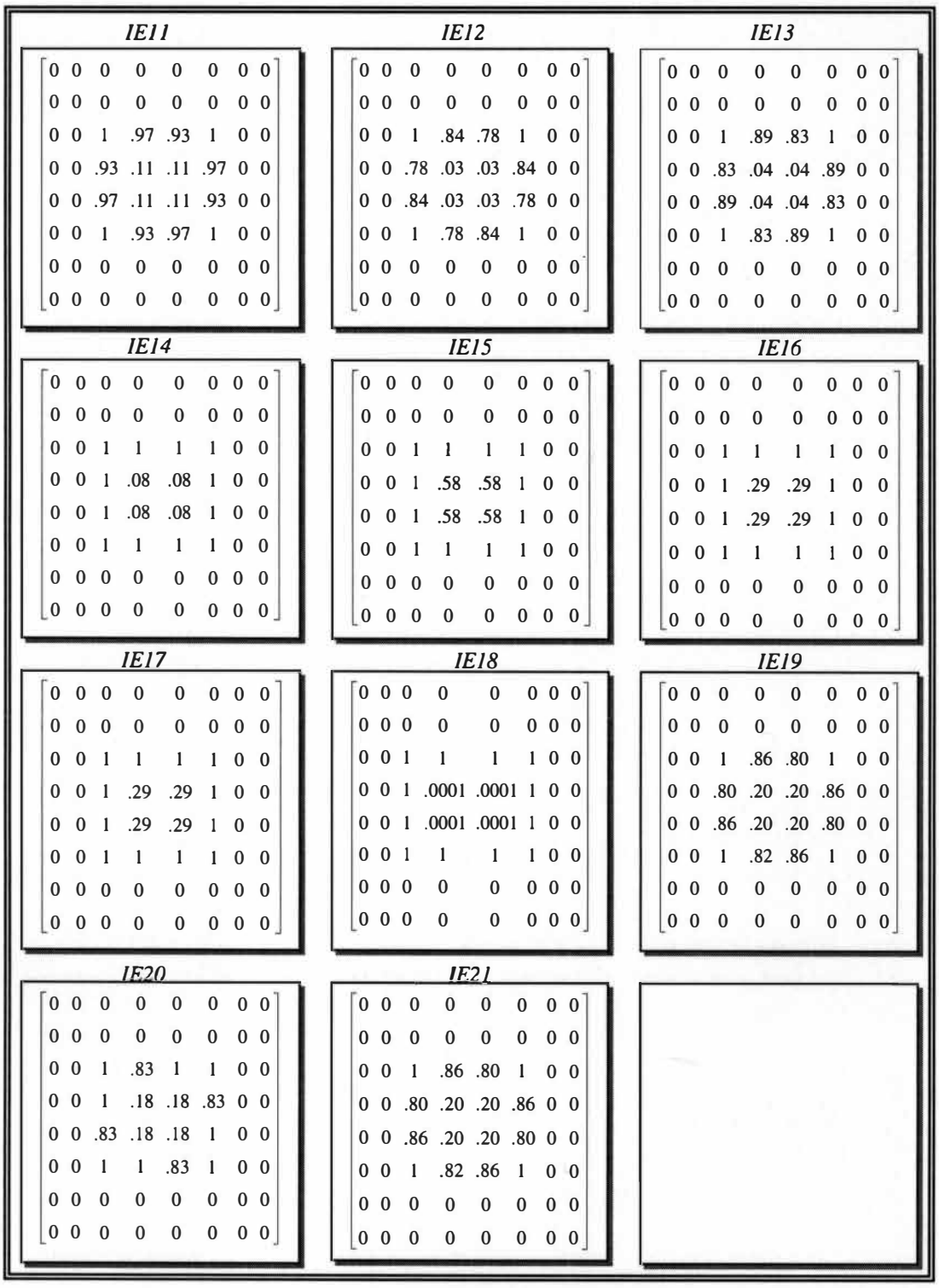

Figure 43. Illustration of Edge Trace Matrices Generated by *EDS* in Example 1.

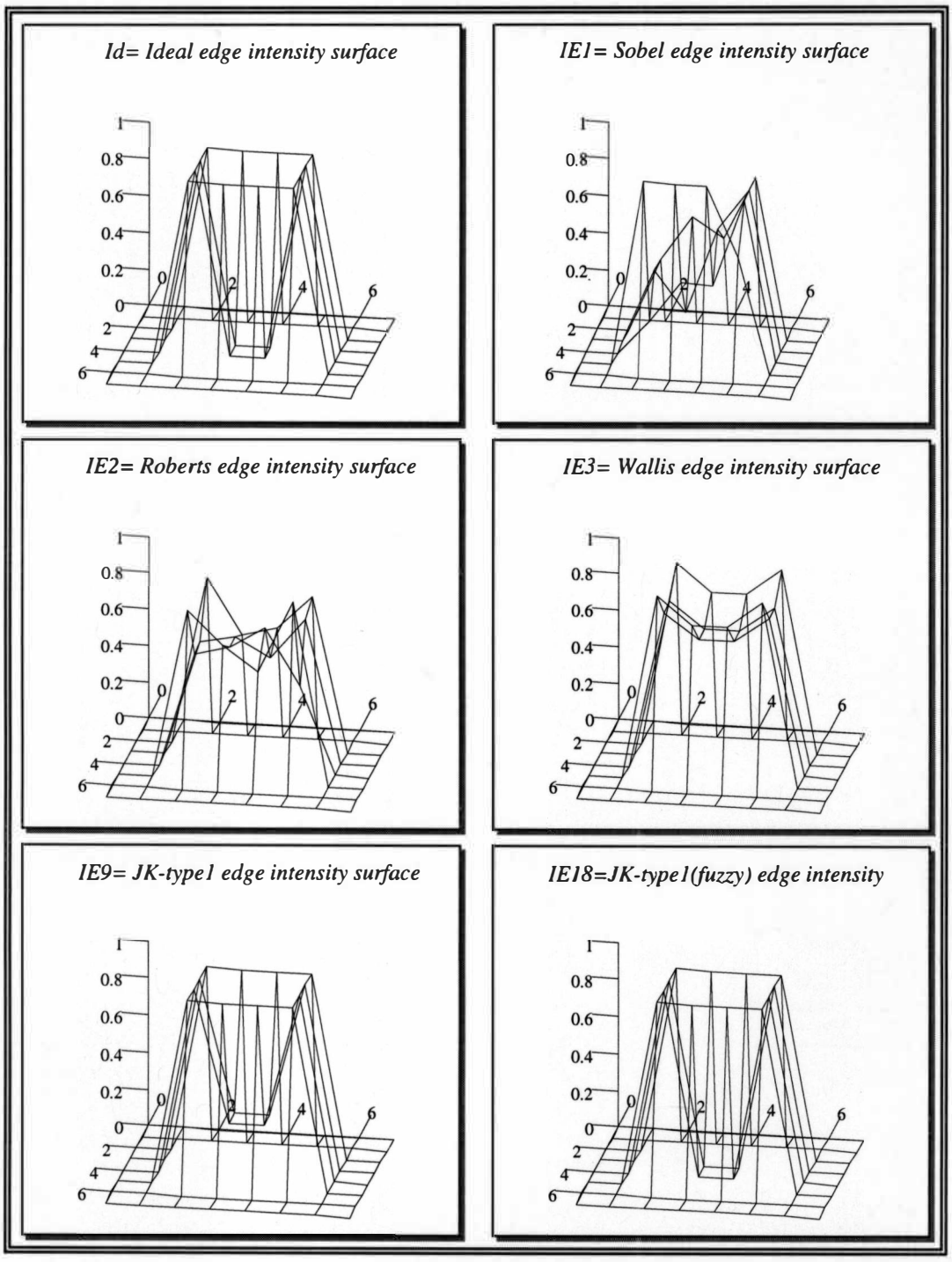

Figure 44. Illustration of Edge Intensity Surfaces for Comparison of Intensity Levels at Edge Points Between the Ideal Edge Trace and the Edge Traces Resulting From Some Algorithms in Example 1.

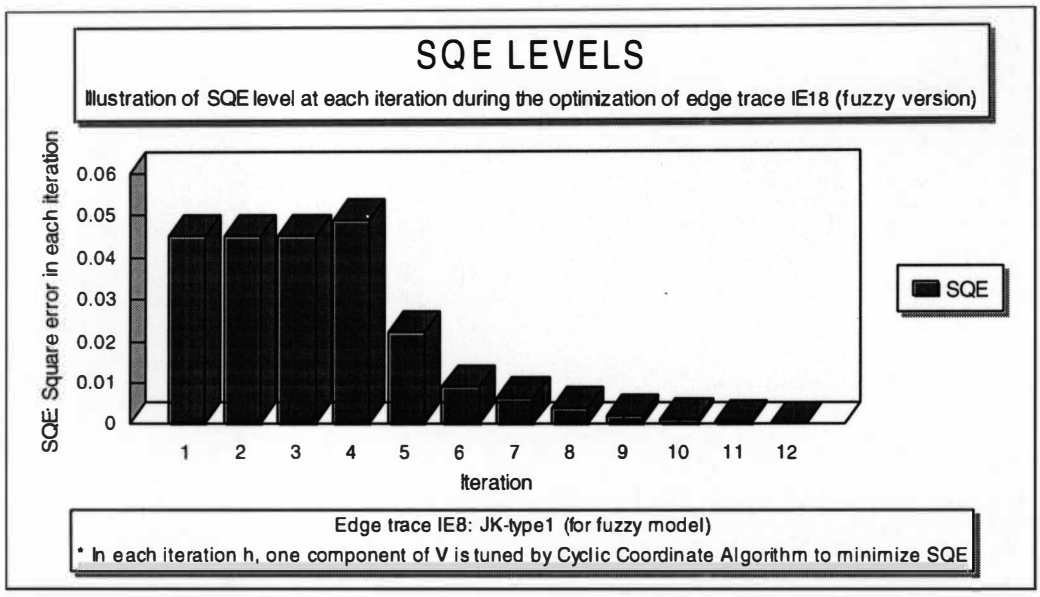

Figure 45. Illustration of *SQE* Trajectory (*SQE* Minimization) During the Optimization of Edge Trace *IE18* Using Cyclic Coordinate Algorithm to Tune the Input/Output Membership Functions of *FLC* Illustrated in Figure 41 (a), (b).

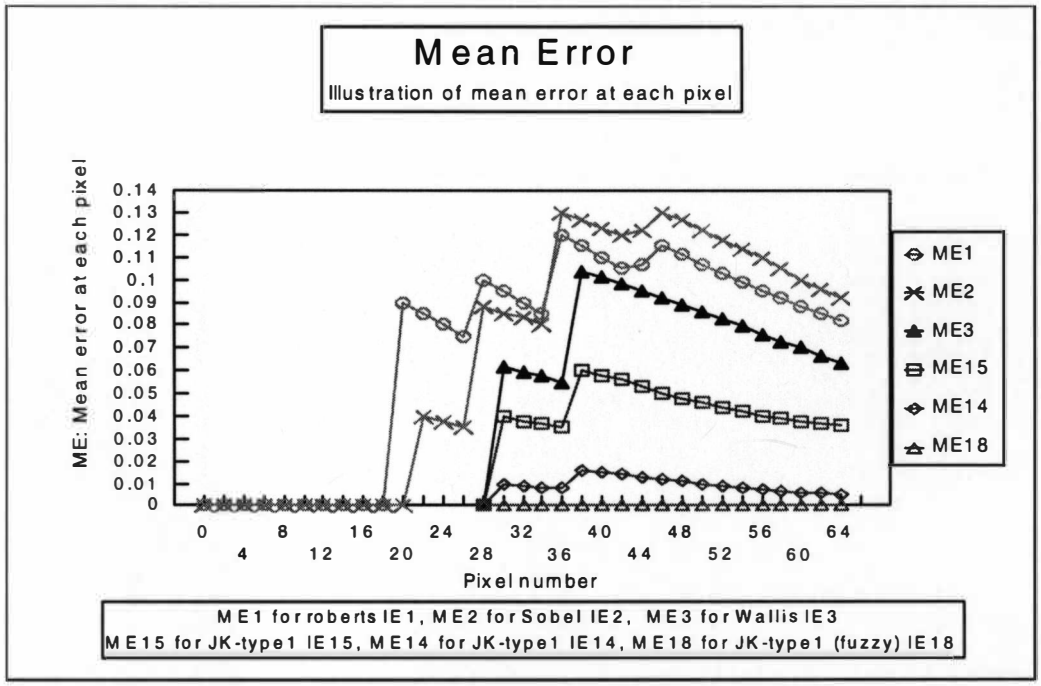

Figure 46. Illustration of Mean Error at Each Pixel for Fuzzy and Some Non- Fuzzy Algorithms Obtained by *EDS* in Example 1.

As observed from obtained edge trace matrices (Figures 42 and 43) and the illustrated edge intensity surfaces (Figure 44), obviously, in small images the derivative methods (Sobel, Roberts, and Wallis) creates the scattered data at edge points. This makes some difficulties in choosing an appropriate threshold levels T_L and T_H (T_L and T_H are illustrated in Figure 32), since the lower level and upper level thresholds can not be distinguished. In Roberts *IE1* and Sobel *IE2*, some edge points have the less intensity than some other points which are not supposed to be edge according to the ideal edge trace *Id*. That is, it is not possible to find T_L and T_H such that $T_L \leq T_H$. In Wallis edge trace *IE3*, the T_L and T_H are distinguishable, but difference between T_L and T_H is small and it causes the selection range of threshold levels to be so limited. On the contrary, the *QCW* (specially *FQCW* which is not dependent on thresholding) does not possess the above mentioned problem. All data concerning the edge points generated by the algorithms of *QCW-ECF* family are organized and not scattered. Consequently, distinguishing the appropriate lower level and upper level thresholds (T_L and T_H) is easy since we can easily find T_H and T_L such that $T_L \leq T_H$ and $T_H - T_L >> 0$.

Also a quick review on the Table 11 proves that generally the algorithms of *QCW* and specially *FQCW* families have three advantages in performances compare to the other derivative algorithms for small object edge detection as: (1) bigger correlation *TDC* (close to 1); (2) less total mean error *TME* (even mean error *ME* at each pixel, illustrated in Figure 46); and finally (3) less square error *SQE*.

One significant result, *IE18,* has been obtained by *FQCW-ECF* (*JK*-type1) (fuzzy approach to edge detection) and optimized by cyclic coordinate algorithm. The optimal edge trace, *IE18*, generated by *EDS* without using threshold technique has the best correlation to the ideal edge trace *Id* and the least *TME* and *SQE* comparing with the non-fuzzy algorithms.

The general conclusion of this example is that, for small object edge detection, the algorithms of *QCW-ECF* family (which are based on correlation or degree of correspondence to the binary edge patterns) performs better than the derivative algorithms such as Roberts, Sobel, and Wallis. They are all dependent on thresholding technique but implementation of thresholding for *QCW-ECF* family is much easier than the other compared algorithms. At the end, *FQCW-ECF* generates the better results without using threshold technique comparing to its non-fuzzy associates *QCW-ECF* and the other mentioned non-fuzzy algorithms.

Example 2. To represent the efficiency of *QCW-ECF* and its fuzzy associated *FQCW-ECF* against the other derivative algorithms for edge detection of an image with a similar foreground and background intensity, we have provided the second experiment as follows. A 130×130 intensity image matrix *II2* (L=256) has been applied as an input to the *EDS* system for edge detection without using thresholding technique. Some data and graphs resulted from *EDS* are given in Table 12 and Figures 47 to 51.

Table 12

Comparison Table for Fuzzy and Non-Fuzzy Algorithms Applied for 130×130 Pixels Image *II*2 in Example 2, Illustrated in Figure 48

	Trace	Methods	Eq.	Block size	(F)QCW structure Fig.	Defuzzification	TME	SQE %	TDC
	IE1	**Roberts**	1.2.10-1	2×2			0.273	9.039	0.186
	IE2	**Sobel**	1.2.10-2	3×3			0.171	5.388	0.276
	IE3	**Wallis**	1.2.10-5	3×3			0.117	3.873	0.128
	IE4	**Classic**	1.4.4-1	5×5			0.152	3.642	0.402
	IE5	**Classic**	1.4.4-2	5×5			0.227	9.186	-.124
	IE6	**Classic**	1.4.4-3	5×5			0.259	10.14	0.322
	IE7	**Angular Corr.**	2.2.2-1	5×5	39		0.121	3.391	0.372
	IE8	**Distance Corr.**	2.2.2-2	5×5	39		0.114	3.401	0.385
	IE9	***JK*-type1**	2.1.7-7	5×5	39		0.147	4.216	0.430
	IE10	***JK*-type2**	2.1.7-14	5×5	39		0.117	3.407	0.413
	IE11	***JK*-type3**	2.1.7-21	5×5	39		0.117	3.407	0.413
Q	*IE12*	***JK*-type4**	2.1.7-32	5×5	39		0.113	3.473	0.369
C	*IE13*	***JK*-type5**	2.1.7-43	5×5	39		0.112	3.411	0.381
W	*IE14*	***JK*-type1**	2.1.7-10	5×5	23 (b)		0.160	4.842	0.442
	IE15	***JK*-type1**	2.1.7-11	3×3	22 (c)		0.163	4.863	0.435
	IE16	***JK*-type1**	2.1.7-11	5×5	23 (e)		0.164	4.958	0.441
	IE17	***JK*-type1**	2.1.7-11	5×5	23 (d)		0.164	4.956	0.444
F	*IE18*	***JK*-type1***(Fuzzy)*	3.1.4-9	5×5	39	*JK*-type1	0.106	3.172	0.493
Q	*IE19*	**Fuzzy model**	1.3.7-5	5×5	39	*COA*	0.147	4.313	0.321
C	*IE20*	**Fuzzy model**	1.3.7-5	5×5	39	*COA*, (*INT*)	0.140	4.297	0.335
W	*IE21*	**Fuzzy model**	1.3.7-4	5×5	39	*MOM*	0.156	4.557	0.434

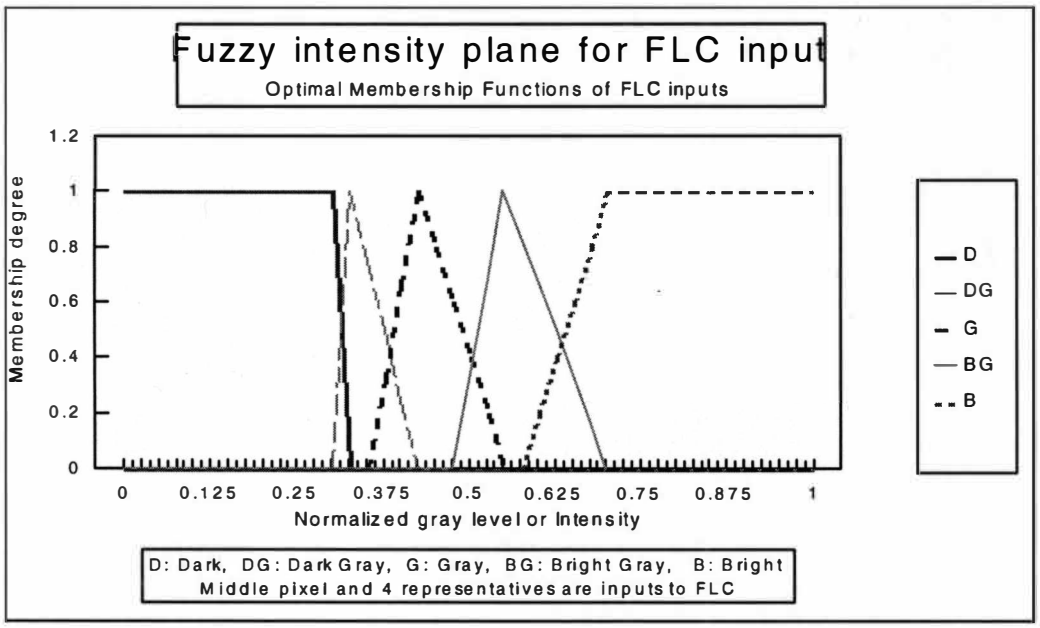

(a) Input *MF*s of *FLC* for Example2.

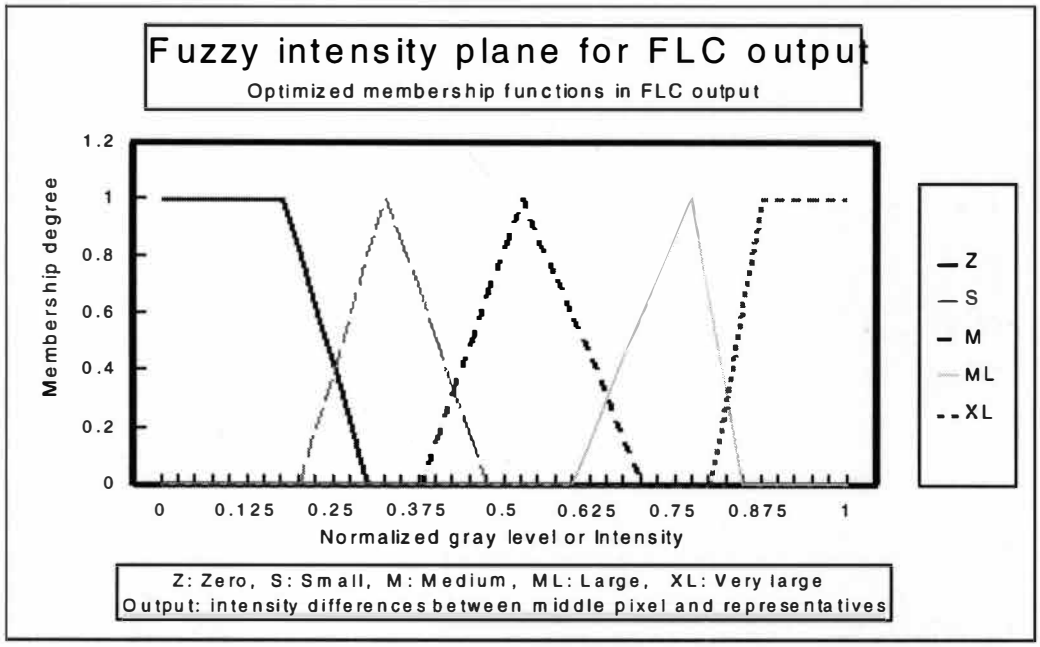

(b) Output *MF*s of *FLC* for Example2.

$V^*_{optimal}$ = [.5135, .294, .333, .4213, .5393, .706, .3989, .1667, .333, .5150, .7825, .8722]

Figure 47. Optimized Input/Output Membership Functions of *FLC* for Example 2.

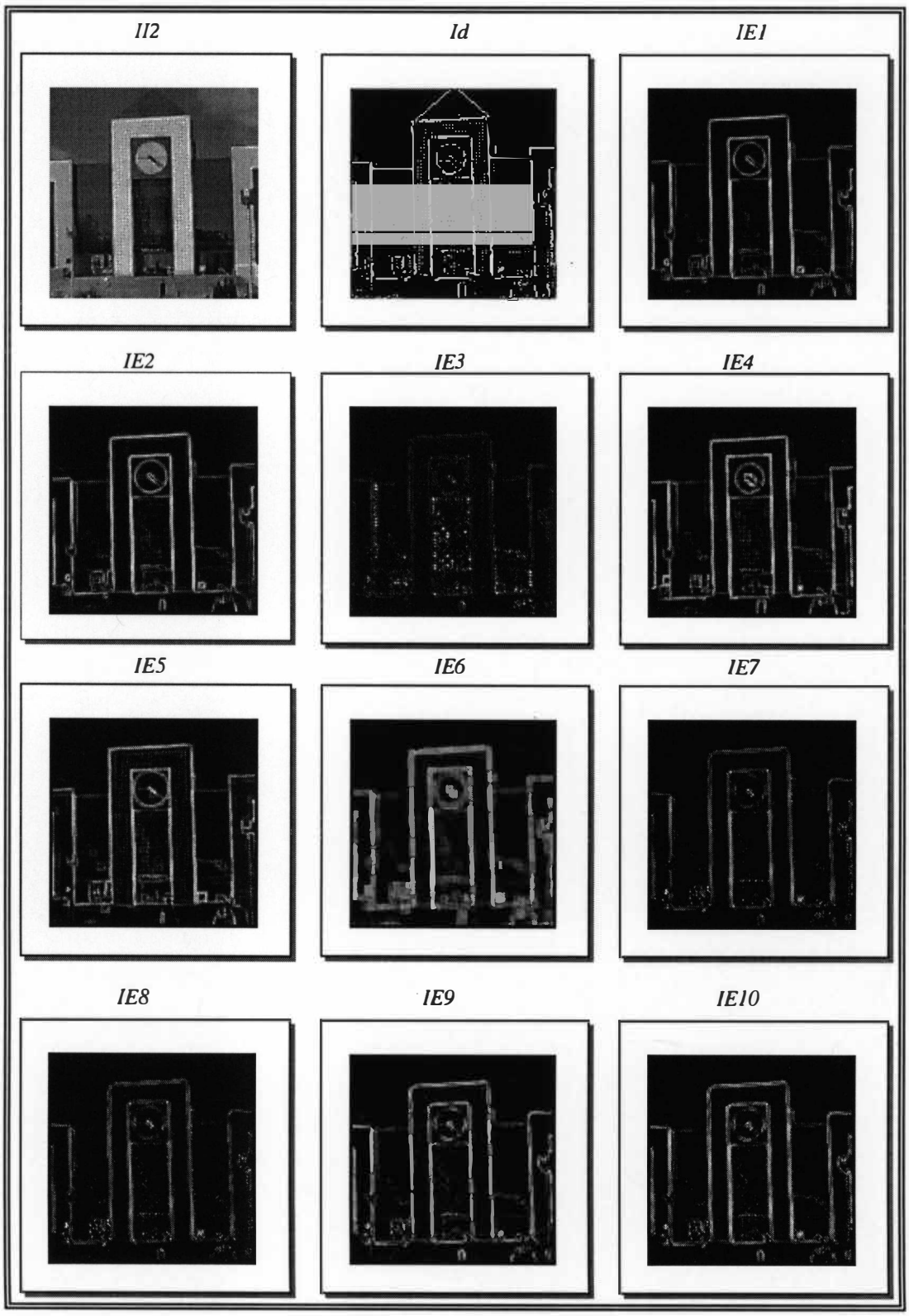

Figure 48. Illustration of Edge of Image *II*2 Generated by *EDS* in Example 2.

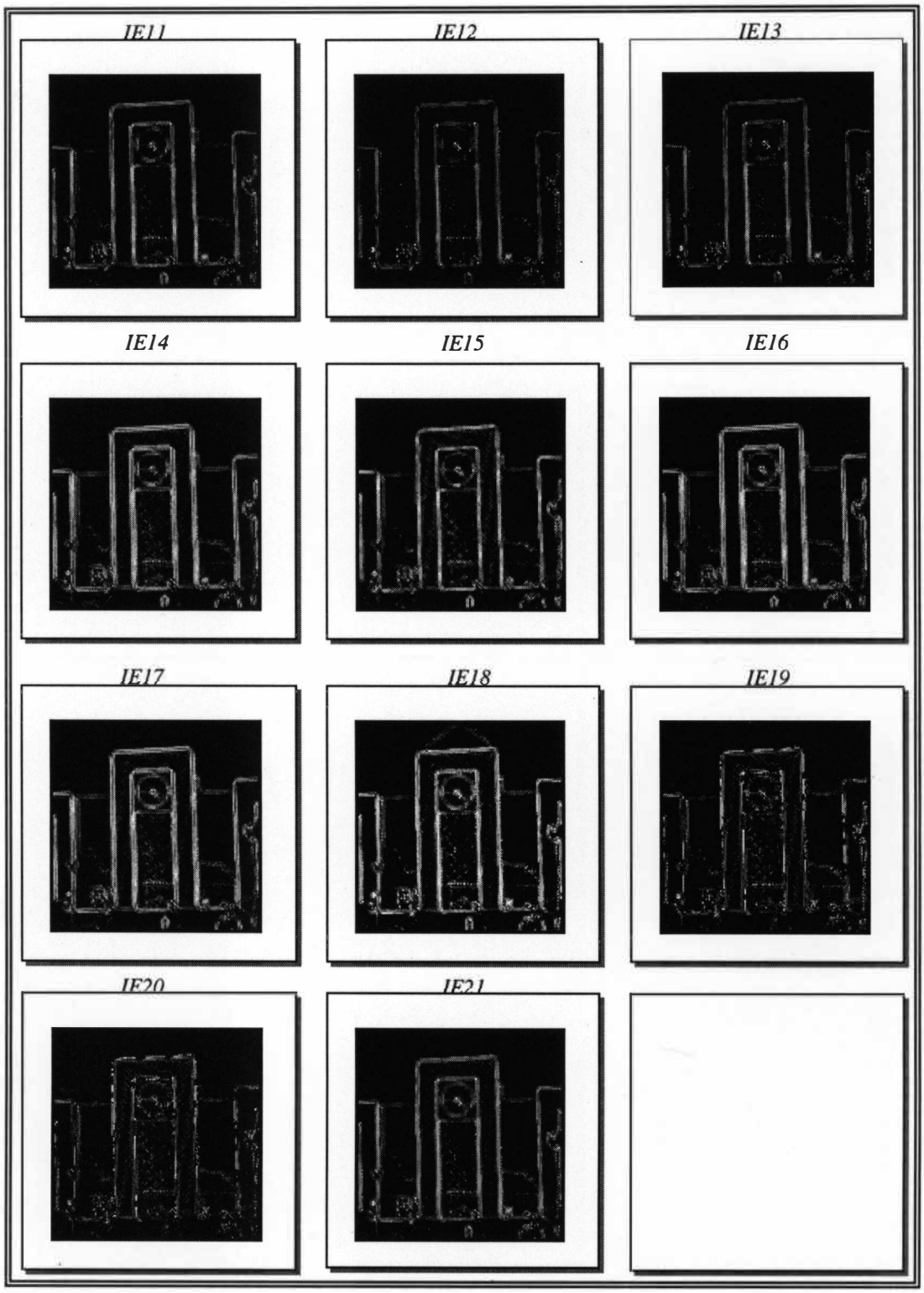

Figure 49. Illustration of Edge of Image *II*2 Generated by *EDS* for Example 2.

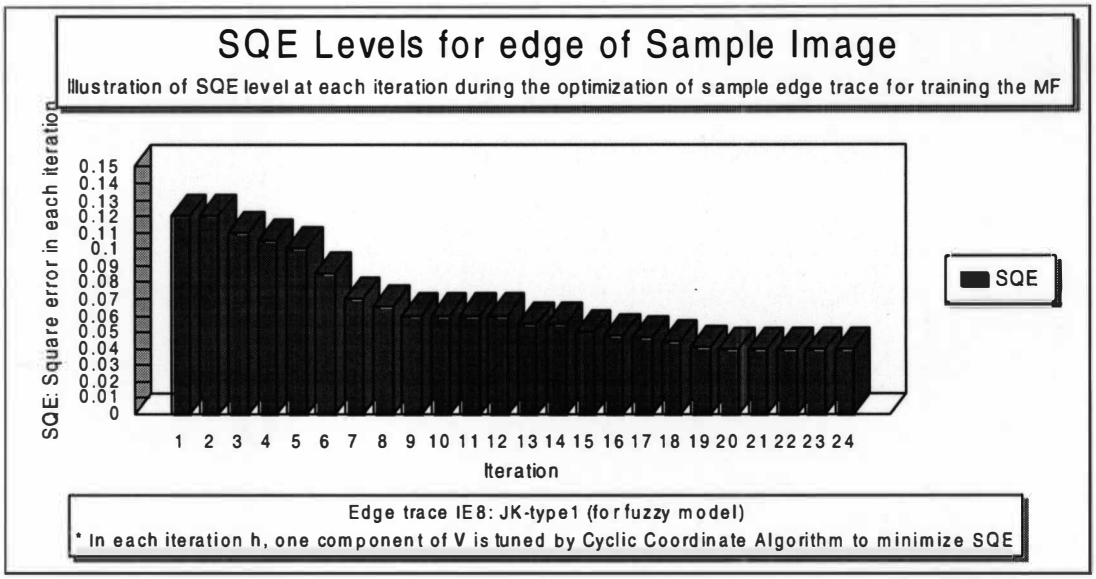

Figure 50. Illustration of *SQE* Trajectory (*SQE* Minimization) During the Optimization of Edge of Sample Image Using Cyclic Coordinate Algorithm to Tune the Input/Output Membership Functions of *FLC* Illustrated in Figure 47 (a), (b), for Example 2.

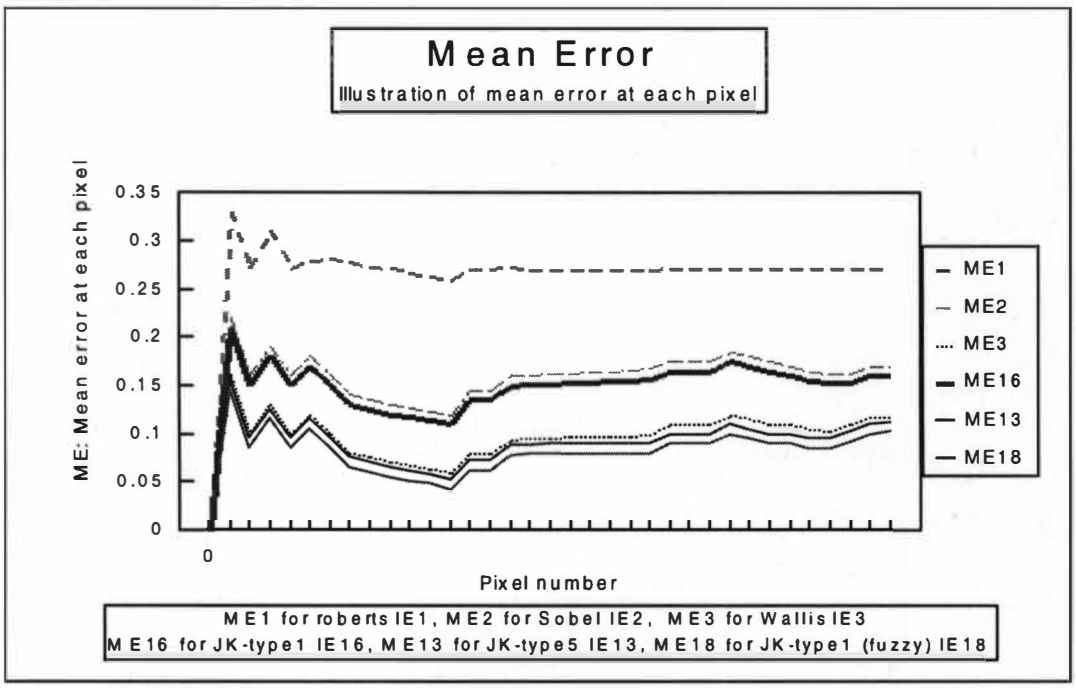

Figure 51. Illustration of Mean Error at Each Pixel for Some (Fuzzy and Non-Fuzzy) Algorithms for Edge Detection of Image *II*2 in Example 2.

The image *II*2 displays a perspective of a building with different intensity of regions. All algorithms applied in example 1 have been reused to detect the edge of image *II*2. Table 12 contains the data resulting this experiment and helps to analyze the edge trace images *IE*1,…,*IE2*1 and the efficiencies of the given algorithms. Edge trace *Id* is a desired binary images (ideal) chosen as an comparison base for the other obtained traces.

All *QCW-ECF* result in edge traces with a (a) less total mean error *TME* (even pixel by pixel mean error *ME* as illustrated in Figure 51), (b) less mean square error *SQE*, and (c) bigger correlation, comparing to the Sobel and Roberts algorithms. Comparing to the *QCW-ECF*, Wallis algorithm produces an edge trace *IE*3 with the competitive *TME* and *SQE,* but the low correlation *TDC*. As observed in Figure 48, the Wallis algorithm results in a low intensity edge trace *IE*3. The edge trace *IE*16 resulting from *JK*-type1 possesses the maximum *TME*= 0.164 and *SQE*= 4.95 among the other *QCW-ECF,* but it has a high correlation *TDC*= 0.441 to ideal edge trace *Id.* The edge trace *IE*16 is illustrated in Figure 49 and obtained by combining of diagonal and cross *QCW* configuration (illustrated in Figure 23 (*e*)) within a block of 5×5 using the Equation (2.1.7-11). *JK*-type1 generates a higher intensity edge among the other types, *JK*-type2,3,4 of *QCW-ECF*. Also, edge trace *IE*13 resulting from JK-type5 possesses the minimum *TME*= 0.112 and competitive *SQE*= 3.401 among the other *QCW-ECF* but has a less correlation *TDC*= 0.441 to ideal edge trace *Id*. The edge trace *IE*13 is illustrated in Figure 49 and obtained by *QCW* configuration

(illustrated in Figure 39 (a)) within a block of 5×5 using the Equation (2.1.7-42). *JK*-type5 generates a lower intensity edges among the other types of *QCW-ECF*.

As you see all above algorithms do not have enough sensitivity to detect the edges of an object which has similar intensity with background. Fuzzy logic algorithm with flexible rules and tunable membership functions (in inputs/output of *FLC*) is a significant approach in this regard. As a part of experiment 2, we apply the *JK-type*1 of the proposed *FQCW-ECF* to remove the above mentioned problem.

Edge traces *IE*18, *IE*19, *IE*20, and *IE*21 are resulted from fuzzy logic algorithms for edge detection. *IE*18 is resulted from *JK*-type1 of *FQCW-ECF* (given by Equation (3.1.4-9))which functions as an edge characteristic function and the defuzzificator in *FLC*. *IE*18, *IE*19 are the edge traces obtained respectively by *COA* and *MOM* defuzzification methods in *FLC*. *IE*20 is an edge trace resulted from *COA* defuzzification method in which the membership degrees μ_{d1}, μ_{d2}, μ_{d3}, μ_{d4} (output of inference machine of *FLC*) are intensified (s= 7 times) before defuzzification. *IE*21 resulted from *MOM* defuzzification possesses bigger *TME*, *SQE*, and even higher *TDC* comparing to those of *IE*20 and *IE*19. The edge trace *IE*21 resulted from fuzzy algorithm of *JK*-type1 in which the membership functions (*MF*) of *FLC* have been trained in advance. The *MF*s are trained such a way to make the fuzzy edge detector system sensitive to those part of image which have similar intensity in foreground and background (like roof of the building in image *II*2). For this purpose, a 10×10 block of image is cut from top of the image *II*2 where the roof of the building has very similar intensity to the background (both dark gray *DG*). Then, like example 1, we

tune the membership functions using cyclic coordinate algorithm regarding the minimization of performance index *SQE* (for 10×10 image sample illustrated in Figure 50). The optimal membership function resulted from this optimization using cyclic coordinate algorithm is depicted in Figures (a) and (b) of Figure 47. These membership functions tuned optimized for a desired part of the image *II*2 have been applied for edge detection of entire images. This is illustrated as edge trace *IE*18 in Figure 49. As seen in this edge trace, the edges of the roof of the building are appeared, but in other edge traces which the *MF* are not trained the edges are not detected. We can tune the membership functions to obtain the optimal edge trace for whole image *II*2. But, this example shows the flexibility of fuzzy algorithm for edge detection of desired part of an image.

Example 3. In third example, we attempt to investigate the sensitivity of aforementioned edge detection methods against two types of noises, Gaussian and Salt & Pepper covering all over an image. we have provided the third experiment in two sections as follows.

Example 3*a*. A 130×130 intensity image matrix *NI3a* (*L*=256), covered by Gaussian noise with zero mean and 0.005 variance, have been applied as an input to the *EDS* system for edge detection without using thresholding technique. Data obtained from this experiment are given in Table 13. Some relevant images and graphs are also represented in Figures 52 t0 55.

Table 13

Comparison Table for Fuzzy and Non-Fuzzy Algorithms Applied for 130×130 Noisy Image (Gussian Noise σ^2=0.005) *NI*3a

	Trace	Methods	Eq.	Block size	(F)QCW structure Fig.	Defuzzification	TME	SQE %	TDC
	IE1	**Roberts**	1.2.10-1	2×2			0.271	8.913	0.135
	IE2	**Sobel**	1.2.10-2	3×3			0.208	6.277	0.229
	IE3	**Wallis**	1.2.10-5	3×3			0.121	3.502	-.035
	IE4	**Classic**	1.4.4-1	5×5			0.295	10.58	0.329
	IE5	**Classic**	1.4.4-2	5×5			0.315	12.45	0.124
	IE6	**Classic**	1.4.4-3	5×5			0.387	18.14	0.247
	IE7	**Angular Corr.**	2.2.2-1	5×5	39		0.126	3.492	0.230
	IE8	**Distance Corr.**	2.2.2-2	5×5	39		0.119	3.580	0.261
	IE9	***JK*-type1**	2.1.7-7	5×5	39		0.182	5.222	0.302
	IE10	***JK*-type2**	2.1.7-14	5×5	39		0.125	3.600	0.273
	IE11	***JK*-type3**	2.1.7-21	5×5	39		0.125	3.600	0.273
Q	*IE12*	***JK*-type4**	2.1.7-32	5×5	39		0.119	3.575	0.227
C	*IE13*	***JK*-type5**	2.1.7-43	5×5	39		0.117	3.484	0.226
W	*IE14*	***JK*-type1**	2.1.7-10	5×5	23 (b)		0.186	5.564	0.300
	IE15	***JK*-type1**	2.1.7-11	3×3	22 (c)		0.258	8.573	0.238
	IE16	***JK*-type1**	2.1.7-11	5×5	23 (e)		0.188	6.120	0.313
	IE17	***JK*-type1**	2.1.7-11	5×5	23 (d)		0.195	6.115	0.307
F	*IE18*	***JK*-type1***(Fuzzy)*	3.1.4-9	5×5	39	*JK*-type1	0.116	3.251	0.432
Q	*IE19*	**Fuzzy model**	1.3.7-5	5×5	39	*COA*	0.176	5.313	0.244
C	*IE20*	**Fuzzy model**	1.3.7-5	5×5	39	*COA*, (*INT*)	0.165	4.822	0.229
W	*IE21*	**Fuzzy model**	1.3.7-4	5×5	39	*MOM*	0.187	5.559	0.298

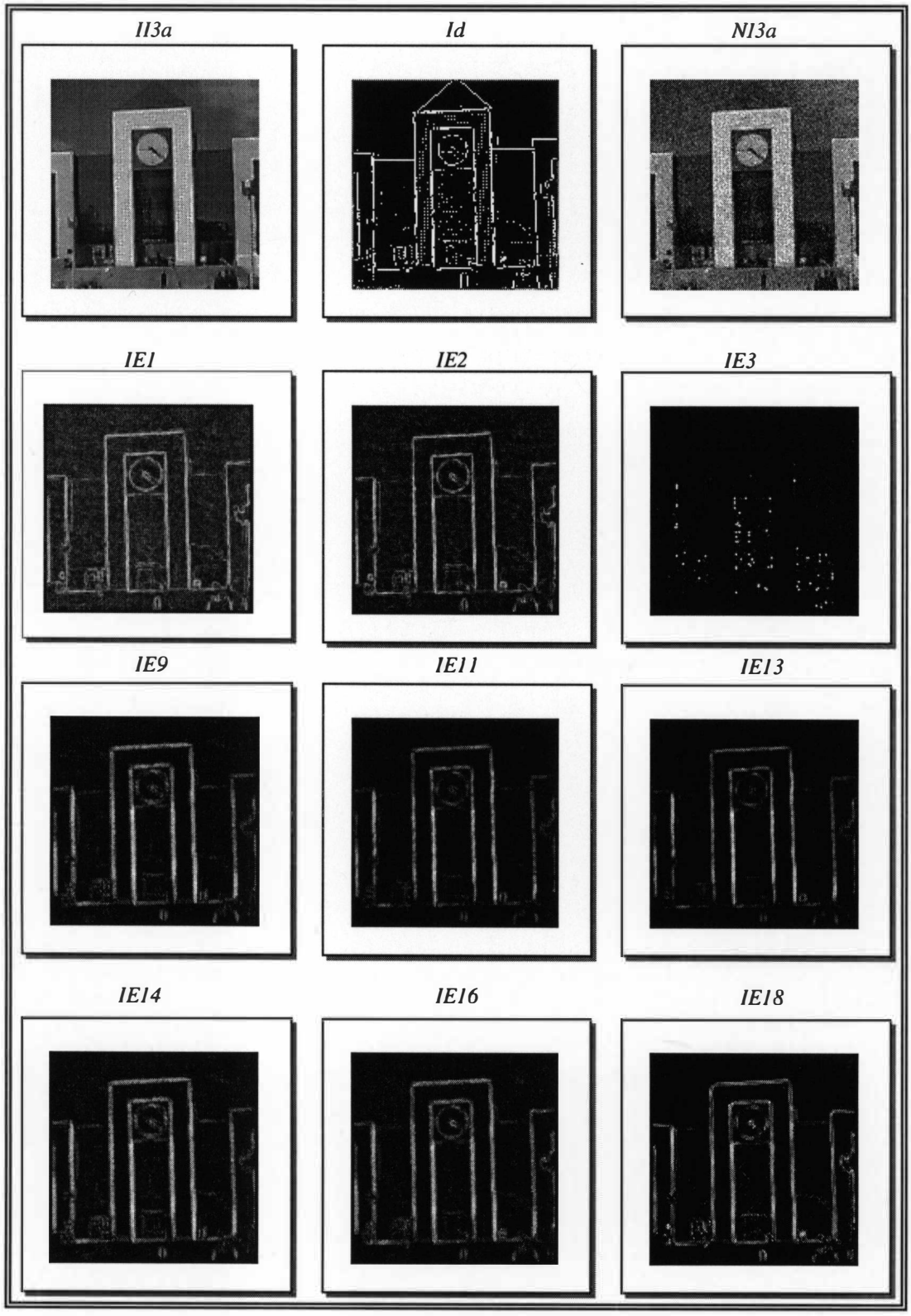

Figure 52. Illustration of the Edge of a Noisy Image, *NI*3a, in Example 3a.

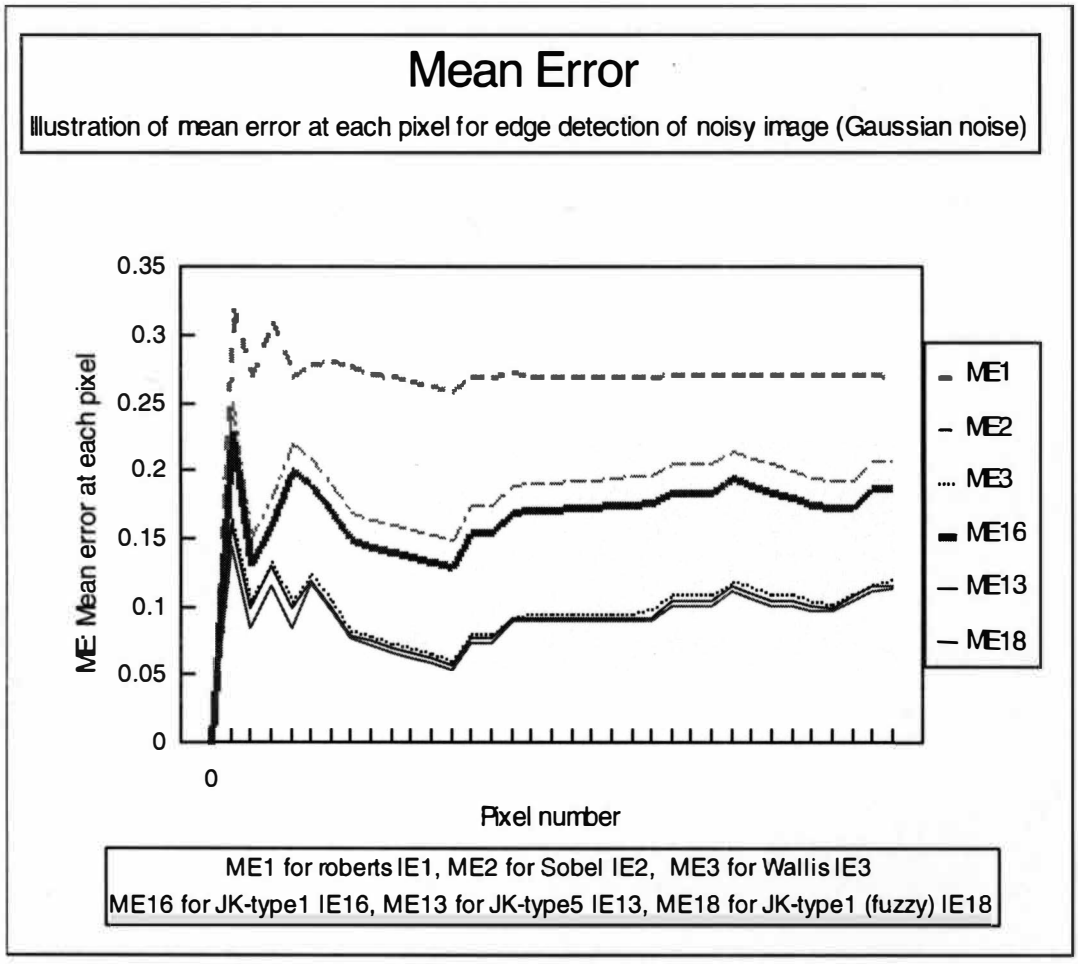

Figure 53. Illustration of Mean Error at Each Pixel for (Fuzzy and Non- Fuzzy) Algorithms Concerning Edge Detection of Noisy Image *NI*3a in Example 3a, the Guassian Noise With Variance $\sigma^2 = 0.005$.

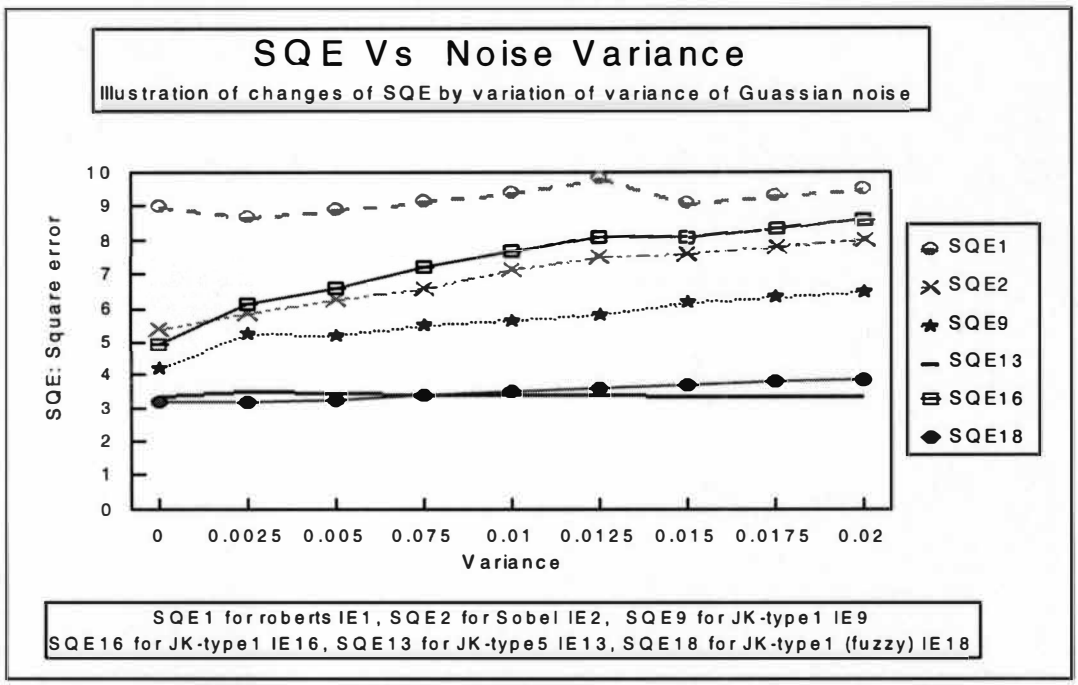

Figure 54. Illustration of *SQE* Versus σ^2 of a Noisy Image *NI3a* for Example 3a.

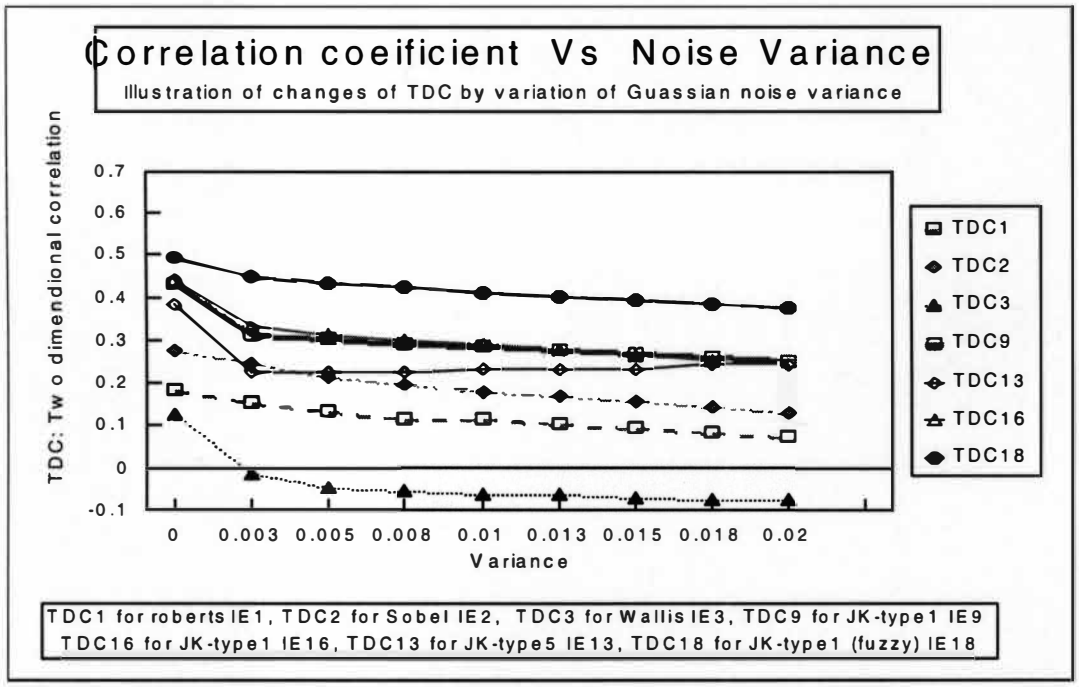

Figure 55. Illustration of *TDC* Versus σ^2 of a Noisy Image *NI3a* for Example 3a.

Example 3*b*. A 130×130 intensity image matrix *NI3b* (*L*=256), covered by Salt & Pepper noise with 0.02 density, have been applied as an input to the *EDS* system for edge detection without using thresholding technique. Data obtained from this experiment are also given in Table 14. Some relevant images and graphs are also illustrated in Figures 56 to 59.

Table 14

Comparison Table for Fuzzy and Non-Fuzzy Algorithms Applied for 130×130 Noisy Image (Salt & Pepper Noise *d*=0.02) *NI3b*

	Trace	Methods	Eq.	Block size	(F)QCW structure Fig.	Defuzzification	TME	SQE %	TDC
	IE1	**Roberts**	1.2.10-1	2×2			0.265	8.577	0.130
	IE2	**Sobel**	1.2.10-2	3×3			0.194	5.910	0.223
	IE3	**Wallis**	1.2.10-5	3×3			0.121	3.423	0.014
	IE4	**Classic**	1.4.4-1	5×5			0.271	6.850	0.193
	IE5	**Classic**	1.4.4-2	5×5			0.291	11.92	0.045
	IE6	**Classic**	1.4.4-3	5×5			0.407	20.41	0.154
	IE7	**Angular Corr.**	2.2.2-1	5×5	39		0.128	3.262	0.225
	IE8	**Distance Corr.**	2.2.2-2	5×5	39		0.121	3.273	0.337
	IE9	***JK*-type1**	2.1.7-7	5×5	39		0.170	3.797	0.317
	IE10	***JK*-type2**	2.1.7-14	5×5	39		0.124	3.256	0.278
	IE11	***JK*-type3**	2.1.7-21	5×5	39		0.124	3.256	0.278
Q	*IE12*	***JK*-type4**	2.1.7-32	5×5	39		0.121	3.324	0.230
C	*IE13*	***JK*-type5**	2.1.7-43	5×5	39		0.119	3.274	0.228
W	*IE14*	***JK*-type1**	2.1.7-10	5×5	23 (b)		0.172	4.245	0.306
	IE15	***JK*-type1**	2.1.7-11	3×3	22 (c)		0.158	4.667	0.293
	IE16	***JK*-type1**	2.1.7-11	5×5	23 (e)		0.184	4.385	0.331
	IE17	***JK*-type1**	2.1.7-11	5×5	23 (d)		0.189	4.419	0.332
F	*IE18*	***JK*-type1***(Fuzzy)*	3.1.4-9	5×5	39	*JK*-type1	0.120	3.006	0.426
Q	*IE19*	**Fuzzy model**	1.3.7-5	5×5	39	*COA*	0.160	3.848	0.262
C	*IE20*	**Fuzzy model**	1.3.7-5	5×5	39	*COA*, (*INT*)	0.159	4.829	0.251
W	*IE21*	**Fuzzy model**	1.3.7-4	5×5	39	*MOM*	0.179	3.828	0.313

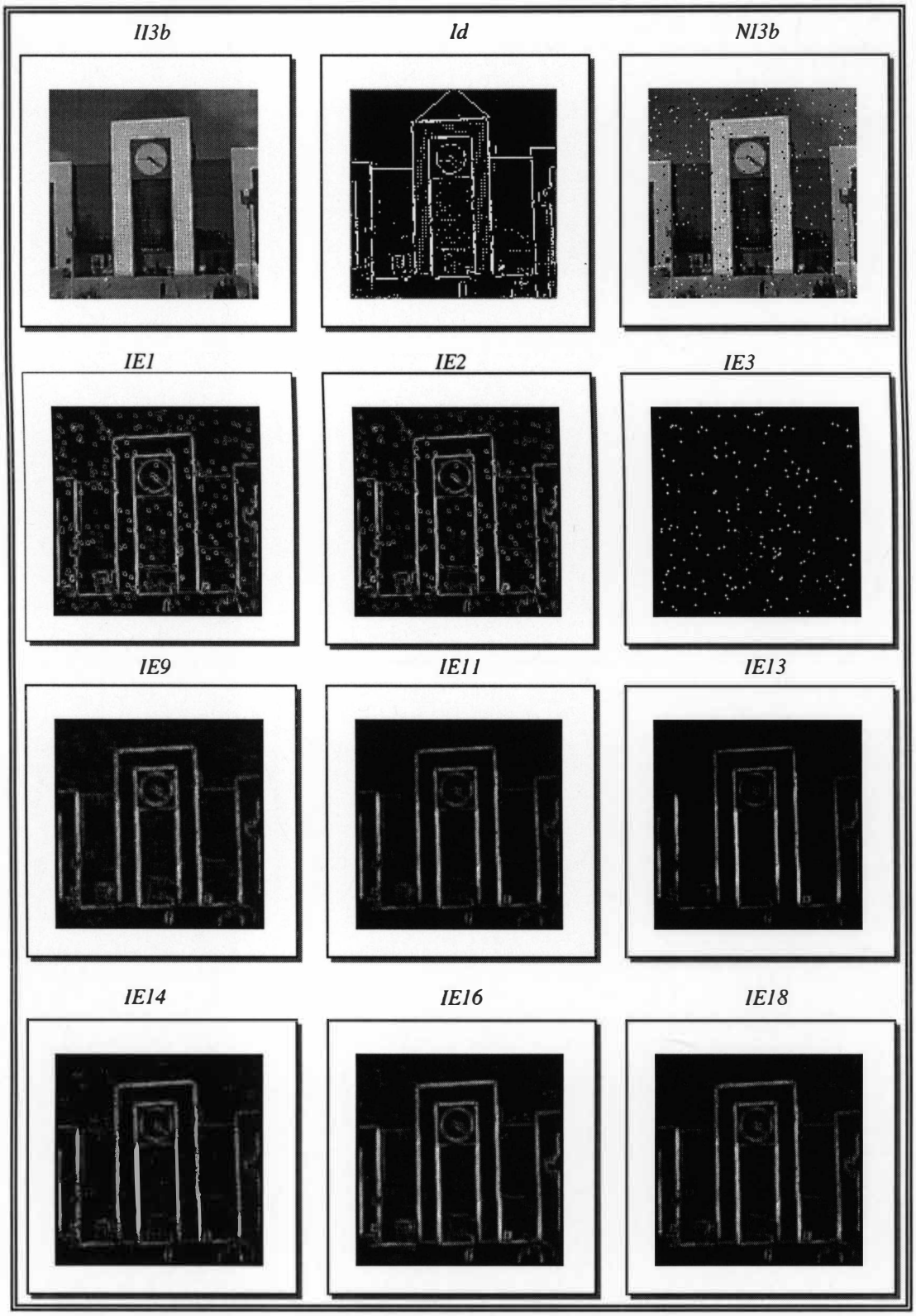

Figure 56. Illustration of Edge of Image *NI3b* Generated by *EDS* in Example 3b.

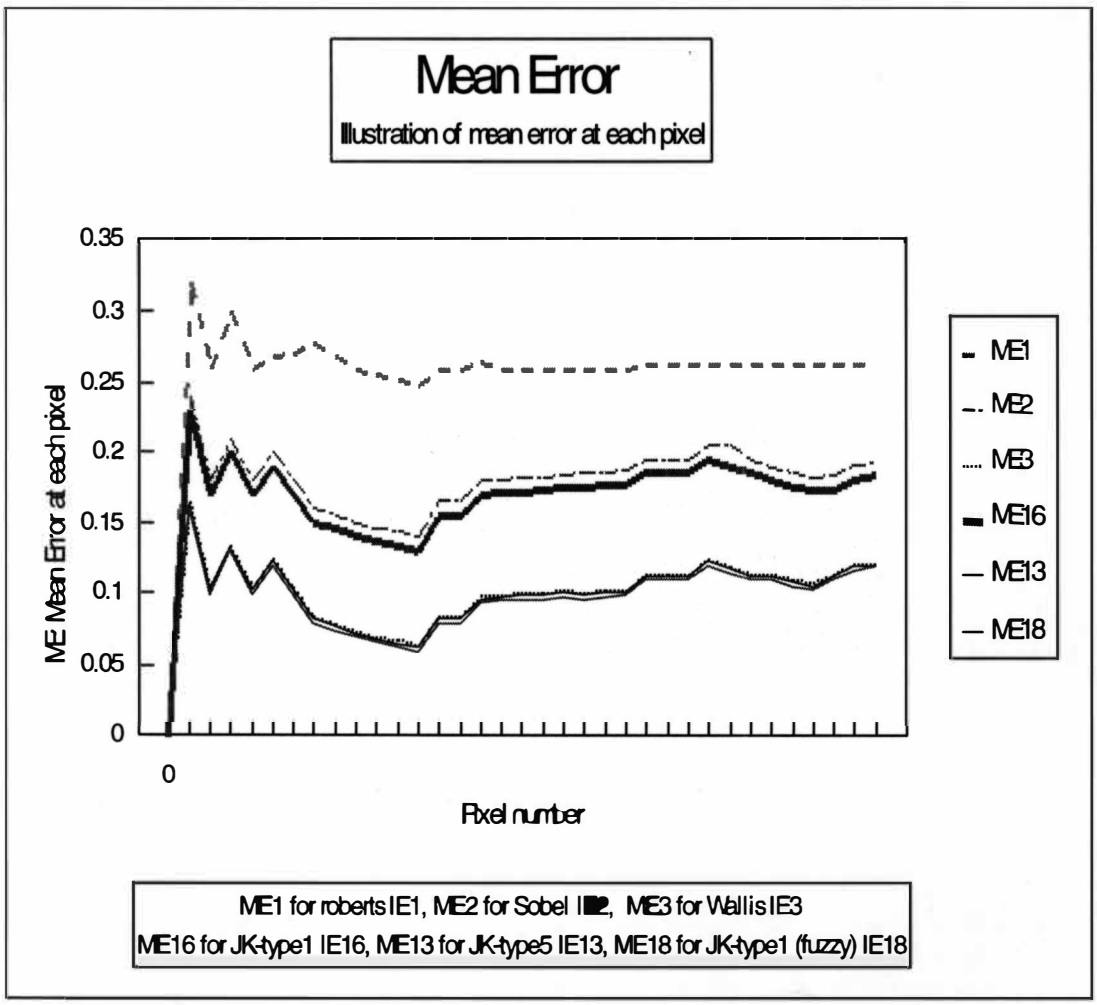

Figure 57. Illustration of Mean Error at Each Pixel for (Fuzzy and Non-Fuzzy) Algorithms Concerning Edge Detection of Noisy Image *NI3b* in Example 3b, Salt & Pepper Noise With Density d=0.02.

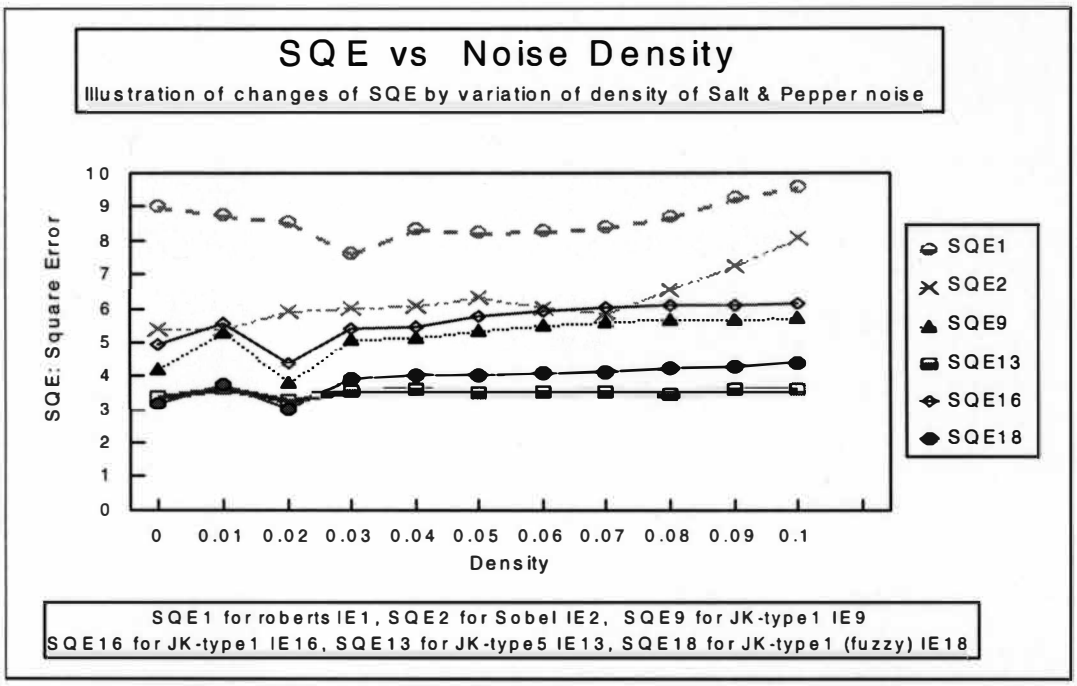

Figure 58. Illustration of *SQE* Vs. Density *d* of a Noisy Image *NI3b* in Example 3b.

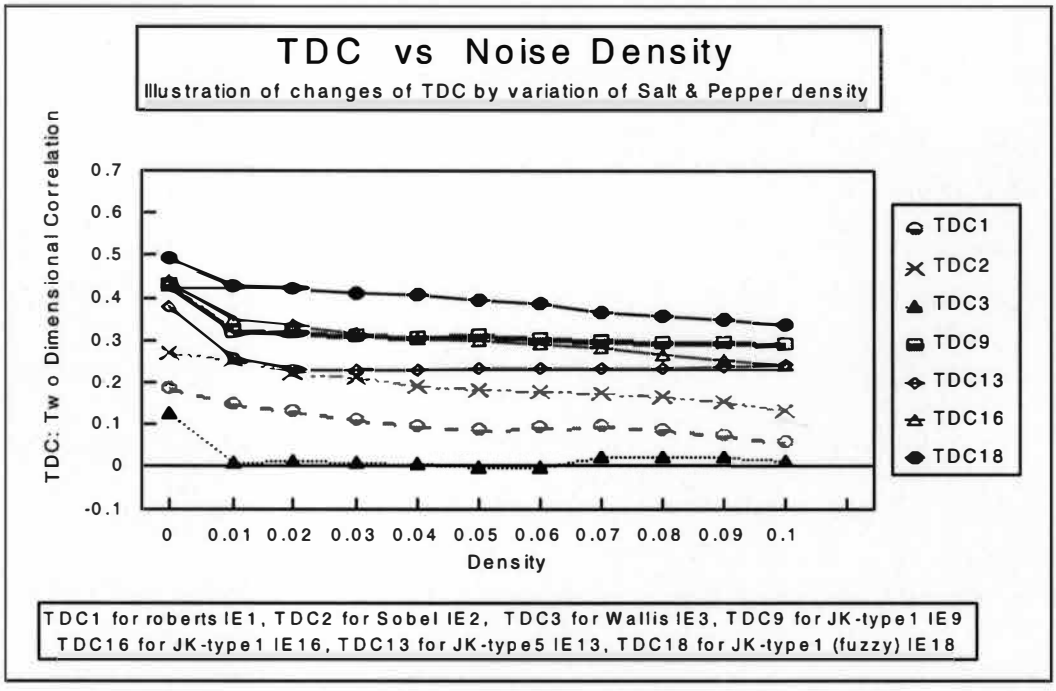

Figure 59. Illustration of *TDC* Vs. Density *d* of a Noisy Image *NI3b* in Example 3b.

As observed in Figures 52 and 53, the derivative algorithms Roberts , Sobel, and Wallis algorithms are strongly sensitive to the noises. Wallis algorithm which generates very low intensity edge *IE*3 as seen in example 2 Figure 47, can not detect edge points properly since noises are brighter than image pixels. On the contrary, all methods derived from generalized *QCW-ECF* (such as *JK*-type1,2,...) possess much less sensitivity to the noises comparing with derivative methods. This is because of using median filtering within each child window B_k and averaging operation within the main block B-$\{(m,n)\}$. In fact, these two operations are noise removal tools applied in *QCW-ECF* algorithms for edge detection of noisy images.

As seen in Tables 13 and 14, in case of noisy images, all of *QCW-ECF* significantly generate edge traces with a (a) less total mean error *TME* (even mean error at each pixel as illustrated in Figures 53 and 57), (b) less mean square error *SQE*, and (c) bigger correlation, comparing with the Sobel and Roberts algorithms. Comparing with the *QCW-ECF*, Wallis algorithm produces an edge trace with the competitive *TME* and *SQE*, but with negative or almost zero correlation *TDC*. The mean error at each pixel *ME* is illustrated in Figures 53 and 57 for both type of noises, Gaussian and Salt & Pepper. In these figures, the upper-bound and lower-bound of mean error curves (generated by *QCW-ECF* family) are illustrated.

Figures 54 and 58 illustrate the changes of *SQE* respect to the changes of noise variance σ^2 (for Guassian noise) and density d for (for Salt & Pepper noise). As seen, the *QCW-ECF* family has the least *SQE* comparing to the derivative algorithms. Also Figures 55 and 59 represent the changes of *TDC* respectively by changes of

noise variance σ^2 and noise density *d*. As seen, the *QCW-ECF* family has also the least *TDC*.

As seen in Figures 52 and 56, some noise pixels on edge traces *IE*1 and *IE*2 resulting from derivative algorithms are brighter than edge pixels. Thus, the thresholding technique does not help to eliminate these noise spots from edge traces. In spite of using noise removal operations in *QCW-ECF*, there are still some unwanted noise spots on some edge traces, specially on *IE*9 and *IE*16 (*JK*-type1). But these noise spots have very low intensity and are easily removable by thresholding.

FQCW-ECF (*JK-type*1) is trained by tuning the membership functions (*MF*) of *FLC* to be sensitive to the noises. For this purpose, a 10×10 block of image is individually cut from a part of the image *II*3*a* and *II*3*b* where the noise spots are on the images. Then, like example 1 and 2, we tune the membership functions using cyclic coordinate algorithm through the minimization of performance index *SQE*. The optimal vector $V^*_{optimal}$ containing the membership function parameters resulted from optimization using cyclic coordinate algorithm are (a) $V^*_{optimal}$ = [.527, .303, .356, .445, .548, .715, .413, .167, .333, .518, .793, .862] for example 3*a*, and (b) $V^*_{optimal}$ = [.518, .299, .333, .4310, .547, .719, .403, .166, .333, .528, .791, .868] for example 3*b*. In both case of noisy image, membership functions are tuned such that *FQCW-ECF* (*JK-type*1) results in edge traces *IE*18 illustrated in Figures 52 and 53 with a minimum *SQE* and maximum correlation *TDC* to the ideal edge trace *Id*. On the other hand, Figures 54, 55, 58, and 59 prove that, for edge detection of a noisy image, *FQCW-ECF* (*JK*-type1) is a reliable tool in generating the edge traces with a least *SQE* and

highest correlation to the ideal one without using thresholds. It has the tuning flexibility to be adjusted for edge detection of any kind of noisy images.

4.1.4 Summary of Experimental Results

Most edge extraction techniques based on derivative approximation such as Sobel, Roberts, and Wallis methods possess the disadvantages of, (a) sensitivity to noise; (b) dependency to the size of object on image; (c) inflexibility to the size of the block for block processing; (d) insensitivity to all combinations of the edges (diagonal, horizontal and vertical); and (e) difficulties in thresholding, specially in noisy images.

But the proposed edge characteristic functions based on quadruple child windowing, *QCW-ECF,* possess the advantage of, (a) less sensitive to the noise comparing to the above mentioned; (b) independent to the size of object for edge detection; (c) flexible in size of block for block processing; (d) sensitivity to all kinds of edges, diagonal, vertical and horizontal; and (e) easy to use thresholding technique, thresholding sometimes is not needed.

For many cases, the intensity edge detection techniques depend on the appropriate choice of thresholds. Thus, finding the edge in intensity images at those pixels which have the same intensity with background. Edge detecting algorithms based on fuzzy logic with tunable membership functions are an effective solution to remove the above mentioned problems. The proposed *FQCW-ECF* is an effective tool in fuzzy image processing for edge detection. *FQCW-ECF* possesses the

advantages of, (a) having the same advantages as *QCW-ECF*; (b) being double purpose tool for both edge detection and defuzzification method in *FLC*; (c) independent of the threshold; (d) sensitive to similar foreground and back ground intensities; (e) tunable membership degree provides a significant tool in training algorithms; (f) very low sensitivity to the noises; and (g) being an explicit edge detection function which can be easily applied in optimization.

The Cyclic Coordinate Algorithm is straight-forward approach to tuning the membership function in *FLC* and optimization of edge detection. This optimization algorithm provides significant results.

CHAPTER V

SUMMARY AND CONCLUSION

Most derivative edge extraction techniques such as Sobel, Roberts, Prewitt, and Wallis methods are limited to making some non-linear manipulation of pixels over a 2×2 or 3×3 block as a means of edge enhancement before thresholding. All these mentioned methods possess the disadvantage of sensitivity to noise and dependency on the size of the block in block processing. Their efficiency depend on the size of object on image and have problem in small object edge detection. Finding the edge in an image in which the foreground object and its background are of similar intensity is difficult, especially in case of noisy images.

Most of the edge detection techniques also depend on thresholds. Since choosing an appropriate thresholds is very difficult in case of a noisy and smoothed image, an edge detection algorithm based on fuzzy logic with tunable membership functions is an effective approach. The efficiency can be also improved by training an edge determination algorithm to be sensitive to edges in a consistent manner. The *FQCW-ECF* introduced in this paper is an effective tool in fuzzy image processing for edge detection. *QCW-ECF* and its fuzzy extension *FQCW-ECF* are flexible and can be applied to blocks of any size. The *(F)QCW-ECF* results in a degree of edginess concerning the middle pixel of the processing block. In other words, it indicates the maximum degree of correspondence of the processing block pattern to

the binary edge patterns. Also the *FQCW-ECF* is a double-purpose function used as both an edge detection tool and a defuzzification method in fuzzy logic system. They are also sensitive to the diagonal, vertical and horizontal edges. Due to tuning flexibility, the *FQCW-ECF* provides an ability to train the edge detection algorithm toward an optimal result by minimizing the performance index. This improves the efficiency of the edge detection. Flexibility in deriving the desired edge characteristic function from the proposed general *QCW-ECF* and its fuzzy associate *FQCW-ECF* makes these algorithms powerful in using for any kind of application of edge detection. I also developed other methods to estimate edge trace using distance and angle correlation between the processing block pattern (within a block of binary or intensity or fuzzy intensity image) and the binary edge patterns.

Multidimensional optimization using the cyclic coordinate algorithm is a straightforward approach for edge detection optimization based on minimizing the desired performance index. The optimization is done by tuning the input/output membership functions of the Fuzzy Logic Controller (*FLC*) in order to adjust the membership degrees (as weights) of *FQCW-ECF*.

5.1 Future Research

We extended the binary *QCW-ECF* to the intensity *QCW-ECF* and its fuzzy version, *FQCW-ECF*, by employing the operator conversions (.), ($\wedge$) to (t-norm) and also (+),($\vee$) to (t-conorm). We also derived some special cases of *QCW-ECF* and

FQCW-ECF using the *t*-(co)norm operators given by Table 10. Deriving *QCW-ECF* using some other *t*-(co)norm may improve the performance.

We also employed multidimensional optimization method, cyclic coordinate algorithm, to tune the membership functions in *FLC* (or the membership degrees μ_{d1}, μ_{d2} , μ_{d3} , μ_{d4} as weights in *FQCW-ECF*) and train the edge detection algorithm toward optimal result. Using neural network to train the *FQCW-ECF* for optimal edge detection can be effective approach for improving the results.

REFERENCES

[1] *Fuzzy Mathematical Approach to Pattern Recognition*, S.K. Pal, D.K. Dutta Majumder.

[2] *Fundamentals of Digital Image Processing*, Anil K. Jain, Prentice Hall, 1989.

[3] *Fuzzy Techniques in Pattern Recognition*, A. Kandel, Addison Wesely, 1989.

[4] Using Fuzzy Logic, Jun Yan, Michael Ryan, James Power, Prentice Hall, 1992.

[5] Y.W.Lim and S.U.Lee, *on the Color Image Segmentation Algorithm Based on the Thresholding and Fuzzy c-means Techniques*, Pattern Recognition, Vol.23, pp935-952, 1990.

[6] T.Peli and D. Malah, *A Study of Edge Detection Algorithms*, Computer Graphics and Image Processing, V0l.20, pp1-21, 1982.

[7] *Image Processing and Understanding Based on the Fuzzy Inference Approach*, Chen, Chen & Hsu, the Third IEEE Conference on fuzzy Systems, pp254-259, 1994.

[8] *Effective Fuzzy Logic Approach to Image Enhancement*, Xhao Li, Cheng, The International Society for Optical Engineering, Vol.2094, No.1, pp244-251, 1993.

[9] *Fuzzy Rule Based Approach for Edge Detection of Color Image*, N. Kamekura, R. Tashiro, H. Yokoyama, International Conference on Fuzzy Theory and Technology , Vol.2, pp67-69, 1993.

[10] *Image Processing Using Fuzzy Clustering Algorithms*, Maged S. Riad, The university of Wisconsin-Milwaukee Master thesis, 1995

[11] *Image Processing Analysis and Machine Vision*, M. Sonka, V. Hlavac and R. Boyle, Chapman & Hall, Cambridge, UK, 1993.

[12] *Edge Detection and Image Enhancement Using Neuron-like Networks and Fuzzy Rules*, Woon-Tack Woo, International Neural Network Society Annual Meeting, Vol.1, pp I-738-I-742, 1994.

[13] *Digital Image Processing*, Pratt w. k., Willey-interscience, 1978.

[14] *MATLAB Image Processing Toolbox*, Clay M. Thompson and Loren Shure, The MathWorks Inc., 1993.

[15] *Fuzzy Sets and Fuzzy Logic Theory and Applications*, George J. Klir and Bo Yuan, Prentice Hall PTR, 1995.

[16] *Simulation and Modeling*, F. Severance, Electrical & computer Engineering Department, Western Michigan University.

[17] *Modern Control Systems; A Manual of Design Methods*, John Borrie, Prince Hall International, 1986.

[18] *Pictorial Representation of Fuzzy Connectives, PartII: Cases of Compensatory Operators & Self Dual Operators*, Masaharu Mizumoto, 1987.